Advanced Fiber Materials (2022) 4:631–682
https://doi.org/10.1007/s42765-022-00134-x

REVIEW

Carbon-Based Fibers: Fabrication, Characterization and Application

Kunming Li[1] · Xuepeng Ni[1] · Qianqian Wu[1] · Chunshun Yuan[1] · Changlei Li[3] · Dong Li[1] · Huifang Chen[1,2] · Yonggen Lv[1] · Anqi Ju[1,2]

Received: 17 September 2021 / Accepted: 9 January 2022 / Published online: 28 March 2022

Abstract
In recent years, the carbon-based fibers (CBFs) including carbon fibers, carbon nanotube fibers and graphene fibers have received extensive attention due to excellent thermal, electrical and mechanical properties. Here, the current status of CBFs is reviewed from the following aspects: sprecursors, preparation, performance and application. The precursor systems including acrylonitrile copolymers, pitch, cellulose and lignin, carbon nanotube, graphene and other rare synthetic polymeric precursors. The relationship of preparation method and performance of CBFs is presented. In addition, this review gives the overview of application and future development of CBFs.

Keywords Carbon-based fibers · Carbon fibers · Carbon nanotube · Graphene

Introduction

Carbon-based fibers (CBFs) with high carbon content possess excellent mechanical, electrical, thermal and other intrinsic properties, which are useful in various fields, such as aerospace, military, automobiles, biomedicine, energy, construction, and sports [1]. The precursor of CBFs mainly include polymers and carbon units. Polyacrylonitrile (PAN), pitch, cellulose and lignin are the representive polymer precursor for CBFs. CBFs are typically prepared in four stepes: polymer preparation or polymerization, spinning, pre-oxidation and carbonization. At present, the carbon nanotube (CNT) and graphene are the main precursors which are used for carbon unit-based CBFs, and the preparation process includes the construction of carbon unit and subsequent spinning. Among them, PAN, pitch, cellulose, lignin, CNT and graphene are mainly introduced in this review. In addition, other rare precursors are also introduced briefly.

As early as the late 1870s, Joseph Swan and Thomas Edison trial-produce carbon yarn with cotton and other materials, which was used as filament for electric bulb. Then viscose-based CBFs were developed by the U.S. Air Force Base-Wright Patterson in 1950 and successfully produced by the U.S. Union Carbide Corporation company in 1959. PAN-based CBFs were first prepared by Shindo in 1959 and successfully produced by Japan Nippon Carbon Co., Ltd in 1962. The pitch-based CBFs were invented by Sugirou Otani in 1965 and first produced by Japan Kureha Chemical Company in 1970. After decades of development, the PAN-based CBFs accounts for more than 90% of the global CBFs markets and the total production was 167.90 kiloton in 2020 [2]. Generally, the mechanical performances are the significant evaluation factors in producing PAN-based CBFs. The theoretical tensile strength and tensile modulus of PAN-based CBFs calculated by the interatomic bonding force can reach 180 GPa and 1020 GPa, respectively. However, the actual maximum tensile strength and elastic modulus of PAN-based CBFs are only 7.15 GPa and 600 GPa at present, which makes more efforts to narrow the gap. With the rapid development of the modern industries, such as aerospace transportation, and military industries, the demand for CBFs is growing quickly. Therefore, the low-cost, easy-to-obtain, high-efficiency and simple-to-process are important factors in industrial production. In addition,

✉ Anqi Ju
anqiju@163.com

[1] College of Materials Science and Engineering and State Key Laboratory for Modification of Chemical Fibers and Polymer Materials, Donghua University, Shanghai 201620, China

[2] Key Laboratory of High-Performance Fibers and Products, Ministry of Education, Donghua University, Shanghai 201620, China

[3] Weifang Xinlong Biomaterial Co., Ltd., Weifang 261000, China

with the over-exploitation of oil resources, the search for new alternative renewable precursors is never stopping. As an example, lignin has been studied as precursor for polymers-based CBFs.

The CNTs-based CBFs have potential application in sensors, supercapacitors (SCs) and batteries due to high strength and good conductivity [3]. CNTs, a new kind of fullerene, were first reported by Iijima in 1991 [4]. CNTs can be classified into single-walled (SWCNTs), double-walled (DWCNTs) and multi-walled (MWCNTs) according to the number of graphite layers, the diameter of CNTs ranges from a few nanometers to tens of nanometers. The tensile strength, elastic modulus, conductivity, ampacity and thermal conductivity (room temperature) of CNTs can achieve 50 GPa, 1 TPa, 10^6 S/m, 10^9 A/cm^2 and > 3000 W/m·K, respectively, because of the nearly perfect graphene network structure [5–7]. CNTs-based CBFs were first fabricated by Vigolo et al. using the coagulation spinning method in 2000 [8]. The elastic modulus was only ~ 15 GPa, which was much less than the theoretical value of individual CNT due to the introduction of unavoidable defects during the CNTs assembling process. In recent years, many technologies have been developed to fabricate CNTs-based CBFs, including solution spinning [9], CNT arrays [10], chemical vapor deposition (CVD) [11], as well as twisting/rolling of CNT Films [12]. However, these technologies are not mature enough to large-scale industrial production.

Graphene is a unique two-dimensional honeycomb monolayer crystal material with sp^2 hybridization of carbon atoms, which was proposed by Brodie in 1859 [13] and was prepared by Andre Geim and Konstantin Novoselov using the micromechanical exfoliation method in 2004 [14]. The thinness of graphene is only one carbon atom, which breaks the thermodynamical concept that the two-dimensional crystal structure can not exist stably under normal temperature and pressure. Actually, the appearance of corrugation structure in free graphene may be the reason for the stable existence according to Meyer et al. [15]. Incredibly, graphene possesses unprecedented comprehensive performance: tensile strength, elastic modulus, carrier mobility, thermal conductivity (room temperature) and transmittance are 130 GPa, 1.0 TPa, 200,000 cm^2/Vs, 5000 W/mK and 97.7% [16–20], respectively. However, graphene is hard to form uniform dispersion owing to the intermolecular forces between graphene sheets, it can not be arranged uniformly and orderly along the fiber axis [21]. Graphene oxide (GO), as an intermediate substance, can be dissolved in water and other "similar-water" solvents because of abundant oxygen functional groups on GO sheets [22]. In 2011, Gao et al. first prepared GO-based fibers by traditional wet-spinning of GO liquid crystals (LCs) [23], then successfully obtained graphene-based CBFs after reduction, which show tensile strength of 140 MPa and elastic modulus of 7.7 GPa. In recent years, various technologies have been developed to prepare graphene-based CBFs through GO self-assembly, such as microfluidics [24], dimensionally confined hydrothermal [25], CVD [26], GO films twisting [27], electrophoretic [28] and dry-spinning [29], which endow graphene-based CBFs with excellent comprehensive performance. Therefore, graphene-based CBFs have great potential application in many fields, such as aerospace, electronics and chemical industries.

Among all CBFs materials, the natural CBFs including cellulose and lignin-based CBFs are mainly used to produce ablation-resistant and thermal insulation materials. Pitch-based CBFs are mainly used as reinforce composite materials, high-temperature ablation materials, high-temperature structural materials and high-thermal-conductivity materials in the fields of aerospace, energy and construction. PAN-based CBFs have large-scale application in aerospace, national defense, military industry, energy, construction, biomedicine, environment and sporting goods. However, CNTs and graphene-based CBFs are in the initial stage of development, which need more exploration in practical application. In this review, the CBFs prepared from different precursor mainly including acrylonitrile copolymers, pitch, cellulose and lignin, carbon nanotube, graphene, and their processing, properties, application are presented. Some terms from the original paper are used in this review.

PAN-Based CBFs

Polymerization

PAN is a main precursor to prepare CBFs, which accounts for more than 90% of the entire global fiber market [2]. Shindo et al. first adopted PAN as a precursor to prepare PAN-based CBFs with the elastic modulus of 140 GPa in 1961 [30]. Subsequently, some improvements including the tension and length retention were introduced in the stabilization and carbonization process to increase the mechanical properties of PAN-based CBFs [31]. The elastic modulus of PAN-based CBFs is 414 GPa after carbonization at 2500 °C [31]. Generally, PAN precursor is fabricated by the copolymerization of AN and another monomer or more than two monomers, such as methyl acrylate, acrylic acid, methyl methacrylate, methacrylic acid, itaconic acid, maleic acid, sodium propylene sulfonate, vinyl acetate vinyl bromide and acrylamide (Fig. 1) [32, 33]. The comonomers should maintain suitable copolymerization parameters with PAN, resulting in the comonomer evenly distributed along the main chain to obtain ideal copolymer. Meanwhile, the content of comonomer is also an important consideration that can affect the properties of the fibers, which is generally ≤ 5 mol% [34]. The introduction of comonomers into

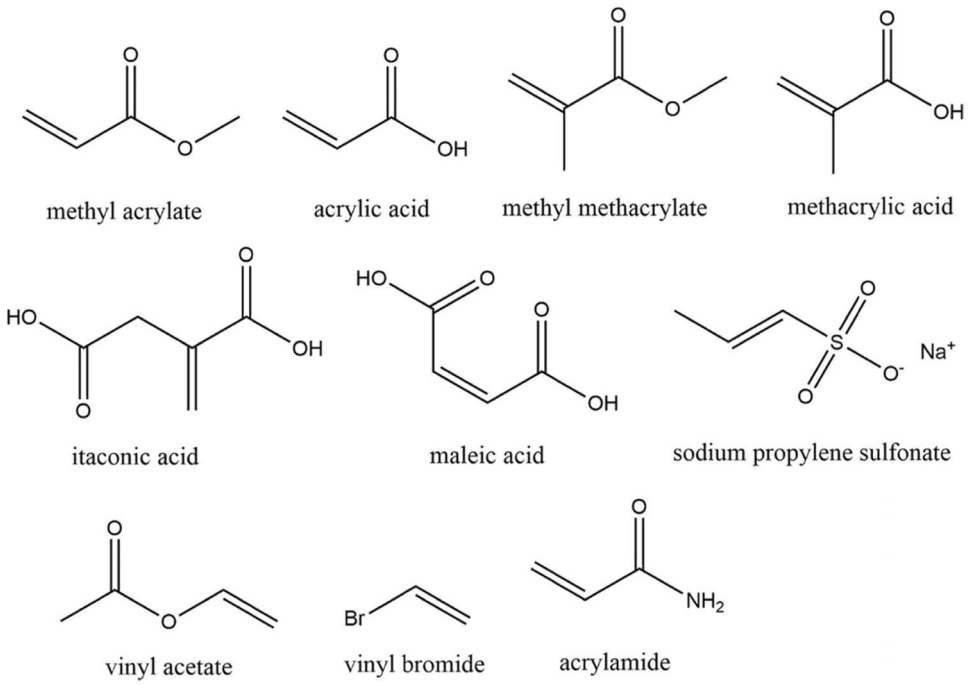

Fig. 1 Several types and structures of copolymer for PAN precursor

the PAN chains can reduce the activation energy in the late cyclization reaction process and broaden the exothermic peak, which improved the performance of the fibers [35]. Many technologies were used for the synthesis of PAN precursor, such as suspension polymerization, solution polymerization, emulsion polymerization, bulk polymerization, ion polymerization, etc. Among them, solution polymerization, emulsion polymerization and suspension polymerization are main methods for the processing of PAN precursor in recent years. Many solutions are adopted to dissolve PAN prepolymer, such as dimethylformamide (DMF), dimethylacetamide (DMA), dimethylsulfoxide (DMSO), propylene carbonate and sodium thiocyanate (NaSCN) aqueous solution. These solutions can endure the polymerization reaction proceeding smoothly and make the solution spinnable after polymerization [36]. The solution polymerization is suitable for the continuous processing of PAN precursor, while the lower concentration of polymerization solution, high transfer constant of traditional solvent systems and limited-molecular weight products are not conductive to the development in the industrial production [37]. In comparison, the suspension polymerization is used to prepare PAN precursor with negligible by-products, and the molecular weight can be adjusted to an extremely high range. The polymer yield can reach 90% since the exothermic nature of polymerization is well controlled during the discontinuous processes of suspension polymerization [38]. Moreover, the reactants need to be treated before the spinning process including ishing, filtration, drying, milling and redissolving processes. Initiators, such as persulfate salts and iron salts, are also used for polymerization. However, the initiator remaining in the spinning solution will cause defects in the fiber, and then lower the mechanical properties. Various measures have been developed to improve the purity of spinning solutions. As an example, the modified initiators are introduced into reaction systems to decrease or even extinguish the metal impurities [34]. Therefore, as mentioned above, the composition of the PAN precursor and polymerization process are the significant factors to fabricate the high mechanical performance of PAN-based CBFs. In addition, the polymerization method and initiator are necessary factors to achieve high mechanical performance.

Processing

The spinning methods of PAN-based CBFs mainly include dry spinning, wet spinning, melt spinning, electrostatic spinning. Melt spinning is not suitable for PAN-based copolymer because the decomposition temperature of PAN is lower than that of the melting temperature, so that it has to introduce suitable plasticizers, solutions or copolymers to decrease the melting temperature of PAN [39]. Moreover, the PAN precursor obtained by melt spinning possesses solvent residue affecting the performance of the final fibers. In dry spinning, a suitable solvent is also demanded to dissolve PAN precursor, it has to maintain stability with PAN copolymers when the temperature reaching the boiling point. Therefore, the

choice of solvent is limited to a certain extent, usually, DMF or DMAc is feasible.

Wet spinning is the main technology for the processing of PAN precursor in industrial production, which is generally divided into wet spinning, dry-jet wet spinning and gel spinning. The traditional wet spinning process is to extrude the spinning solution directly through the spinneret into the coagulation bath, followed by stretching and winding to form the birth fibers (Fig. 2a). In comparison, in the process of dry-jet wet spinning, the spinning solution will pass through a period of air after being extruded by the spinneret, and then enter the coagulation bath (Fig. 2b). The gel spinning process is similar to dry-jet wet spinning in that there is also an air section during the processing, while the spinning liquid is cooled in the air to form a pre-gel, and then form the gel in a low-temperature coagulation bath (Fig. 2c). The fibers prepared by gel spinning possess ultra-high mechanical properties since the high molecular weight PAN-based copolymer and high spinning solution concentration are adopted. Chae et al. used the PAN/methacrylic acid copolymer with high molecular weight ($M\eta = 513{,}000$ g/mol) to prepare CBFs precursor by gel spinning technology, as well as a low temperature (− 50 °C) methanol bath was used to condense the spinning liquid into the gel state [40]. After carbonization, the tensile strength and elastic modulus were 5.5–5.8 GPa and 354–375 GPa, respectively [40]. Morris et al. adopted PAN/methyl acrylate (97/3 wt%) copolymer with the M_w of 1.7×10^6 g/mol and the polydispersity of 1.7 to prepare CBFs precursor with small filament diameters of 5 μm by gel spinning technology [41]. The CBFs precursor showed that the average tensile strength and elastic modulus were 954 MPa and 15.9 GPa, respectively [41]. After carbonization, PAN-based CBFs with smaller diameters of ~ 2.5 um showed that the tensile strength and elastic modulus were 4.3 ± 1.0 GPa and 361 ± 45 GPa, respectively [42]. In addition, there are also some works to prepare CBFs with a high mechanical performance by using high molecular weight PAN-based copolymer that the tensile strengths and elastic modulus can reach 1.8 GPa and 35 GPa, respectively [43].

During the wet spinning process, various conditions can influence the performance of CBFs precursors, such as solvents, spinnerets and coagulation bath. The polar solvents are used to dissolve PAN-based copolymer because of the dipole–dipole interaction between the polar nitrile groups of PANs, such as DMF, DMSO, DMAc, zinc chloride, nitric acid, NaSCN and ionic liquids [44]. Moreover, the amount of solvent depends on the parameters of the copolymer including contents, molecular weight and PDI, ensuring the copolymer solution has suitable viscoelastic behavior for the spinning. The topography of spinneret and the number and size of the aperture have great influence on the performance of PAN-based CBFs precursor. Generally, the shape of the spinneret hole is designed to be round, and the number of the holes is $100–5 \times 10^5$ with a diameter of 40–100 μm. The spinneret hole is designed to other shapes to adjust the shape and the performance of CBFs precursor, such as conical, square and trilobal, etc. The composition of the coagulation bath is a significant factor that can affect the internal structure of the fiber, such as the hole and skin core structure. Usually, water, ethanol, ethylene glycol and acetone are used as coagulation baths which possess a certain velocity to promote uniformly relative diffusion between the solvent and the coagulation bath in the spinning solution and reduce the voids and defects inside the fiber. In addition, the pre-fiber is stretched during the spinning process to increase the orientation of the polymer chain along the stretching direction and reduce the diameter of the precursor fibers, thereby reducing the gaps and improving the mechanical performance. The stretching temperature can be combined with the stretching rate to synergistically enhance the mechanical properties of CBFs precursor. In the post-treatment process, the precursor is also stretched at a suitable velocity to further improve the regularity, density and orientation of the polymer chains, generally including water bath stretching and steam stretching. After spinning process, the oils are used to inhibit the binding of precursor and keep it stable during the stabilization process, such as polyester of long-chain fatty acid and polyol, ethylene oxide adducts of long-chain fatty amides, and modified polydimethylsiloxane. However, the processing of PAN-based

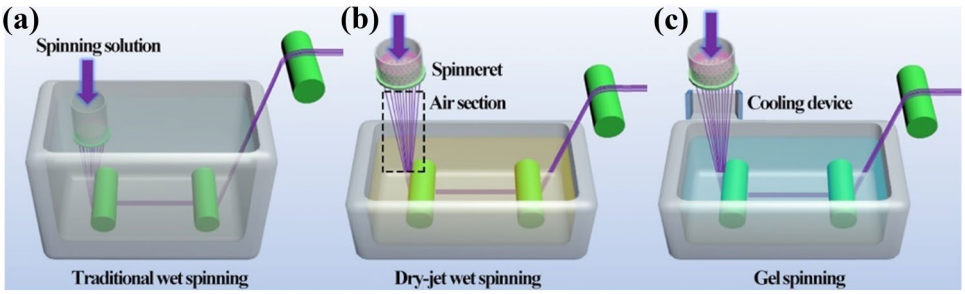

Fig. 2 Schematic of three species of wet spinning. **a** Traditional wet spinning. **b** Dry-jet wet spinning. **c** Gel spinning

CBFs will be influenced. In addition, drying, relaxation drying and heat setting treatment are performed at post-processing to remove the moisture and increase the density of the fiber. Finally, PAN-based CBFs precursor is twisted on a spool for further heat treatment.

Heat Treatment of PAN-Based CBFs Precursor

The heat treatment of PAN-based CBFs precursor is generally divided into three species: oxidation, carbonization and graphitization (Fig. 3) [34]. The temperature ranges of oxidation, carbonization and graphitization are 200–300 °C, 1000–1700 °C and 2500–3000 °C, respectively [45]. During the oxidation process, a precursor is oxidized to N-containing ladder-type polymers, which endure higher temperature processing. The structure of fibers is further transformed into a turbostratic carbon structure in the carbonization process performed in an inert atmosphere. The graphitization process is also carried out under inert gas conditions, and the graphite crystals inside PAN-based CBFs are further

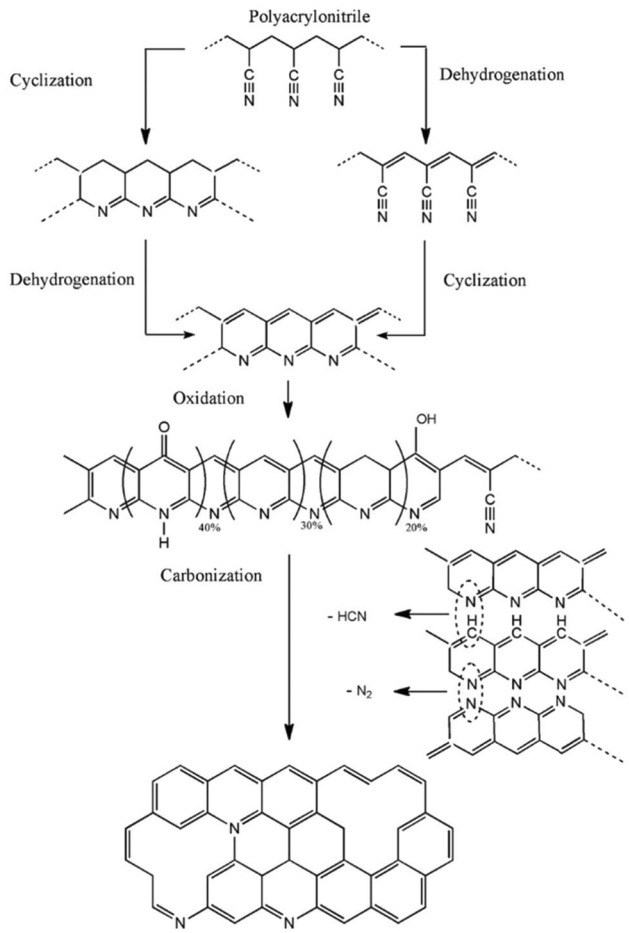

Fig. 3 Schematic of the reaction process from PAN to carbon phase [34]. Reproduced with permission from ref. 34. Copyright 2012, WILEY–VCH

oriented and arranged along the axis of the fiber. The tensile modulus of PAN-based CBFs can be adjusted by graphitization. In addition, the precursor is drawn to ensure the arrangement and orientation of the structure during the whole heat treatment process.

Initially, PAN-based CBFs precursor is oxidized at 200–300 °C. PAN polymer possesses an extremely strong, concentrated exothermic reaction that is hard to control during the oxidation process, resulting in the formation of internal and surface defects in CBFs. Since the functional groups in the comonomer may cause side reactions during the polymerization and spinning process, the specific comonomer is introduced into PAN polymer to reduce the activation energy of the oxidation reaction and broaden the temperature range of the exothermic reaction [46]. The oxidation process is performed in an oven with a series of different air heating zones ensure the temperature of PAN-based CBFs precursor increase gradually. The exothermic reaction is strictly controlled during the process to avoid local overheating, and the fiber is stretched to prevent fiber from shrinking and to increase the tensile modulus [47]. Moreover, the hot gas stream is passed into the oven to achieve the purpose of heating, supplying oxygen, and removing reaction gas and excess reaction heat. The polymer chain will undergo complex reaction processes including reorganization and oxygen cross-linking during this process [48]. The reaction rate of the cyclization reaction of the polymer under the oxygen condition is higher than that of the inert gas condition, and the final PAN-based CBFs show a higher yield and better performance. Meanwhile, the cyclization rate is also influenced by the properties of the copolymer. Therefore, the density of PAN-based CBFs increases as the polymer chains transform into the heteroaromatic structure after oxidation treatment. In addition, there are some technologies to reduce the stabilization time and energy consumption, such as thermal and environmental treatment [49], microwave-assisted plasma treatment [50] and electron-beam-assisted cyclization [51].

After oxidation, the precursor with heteroaromatic structure is carbonized and graphitized at a higher temperature and inert gas conditions (Fig. 3). When the temperature is heated to 400–600 °C, the hydroxyl groups in the oxidized fibers will undergo a cross-linking condensation reaction, leading to the reorganization and coalescence of the cyclized cross-section. The dehydrogenation reaction occurs with the cyclization reaction, resulting in a graphite-like structure fixed by nitrogen atoms [52]. Subsequently, the denitrification will happen at a higher temperature to form a normal graphite layer [53]. In the initial stage of carbonization, the heating rate is controlled to protect the internal structure of PAN-based CBFs from being destroyed by the gas compounds formed during the reaction, simultaneously, the nitrogen atoms are removed more thoroughly and CBFs

with high mechanical performance. However, the structure of PAN-based CBFs will be influenced by the high heating rate, resulting in a decrease of the final mechanical performance. The gaseous compounds formed at 200–1000 °C mainly included water, oxygen, hydrogen, carbon monoxide, ammonia, methane, hydrogen cyanide, tars and other high molecular weight compounds [54]. PAN-based CBFs include more than 90% carbon and a very small amount of nitrogen and hydrogen after the non-carbon elements were removed. The polymer will undergo further condensation reaction to form the turbostratic carbon phase when the temperature is heated to 1600 °C [55]. This structure is oriented in the direction of the external force to endow the high tensile properties for PAN-based CBFs. Moreover, the orientation and size of the crystallites are greatly increased during the carbonization process [56]. The tensile strength and elastic modulus of PAN-based CBFs were improved by increasing the carbonization temperature and the tensile strength will reach the maximum value of 1500 °C [57]. The elastic modulus will increase in the higher temperature due to the formation of more ordered crystals, while the tensile strength decreased slightly.

Finally, PAN-based CBFs undergo a graphitization process at 2500–3000 °C. The crystals in fibers are further arranged and oriented, which thereby improving the tensile modulus. However, the tensile strength will decrease accordingly since the void inside fibers will increase with the process of graphitization (Fig. 4) [58]. The graphitization process is also performed under inert gas conditions and the processing is seriously controlled to prevent the graphite structure in PAN-based CBFs from damage. In addition, the surface oxidation treatment is performed to increase the surface adhesion of PAN-based CBFs. And then a small amount of thermoplastic/thermosetting polymer is applied on the surface to improve the processing performance of fiber-based composites and enhance the interface adhesion with matrix substances. Finally, PAN-based CBFs products are classified and collected according to different mechanical performances.

Pitch-Based CBFs

The pitch is a suitable raw material to prepare CBFs, which is the most widely used substance in the industrialization of CBFs except PAN. The pitch is obtained from petroleum byproducts, coal istes, tar, pyrolysis of polymers and some pure raw materials (Fig. 5). Generally, the pitch is divided into two species: isotropic pitch and anisotropic pitch (mesophase pitch). Otani first prepared pitch-based

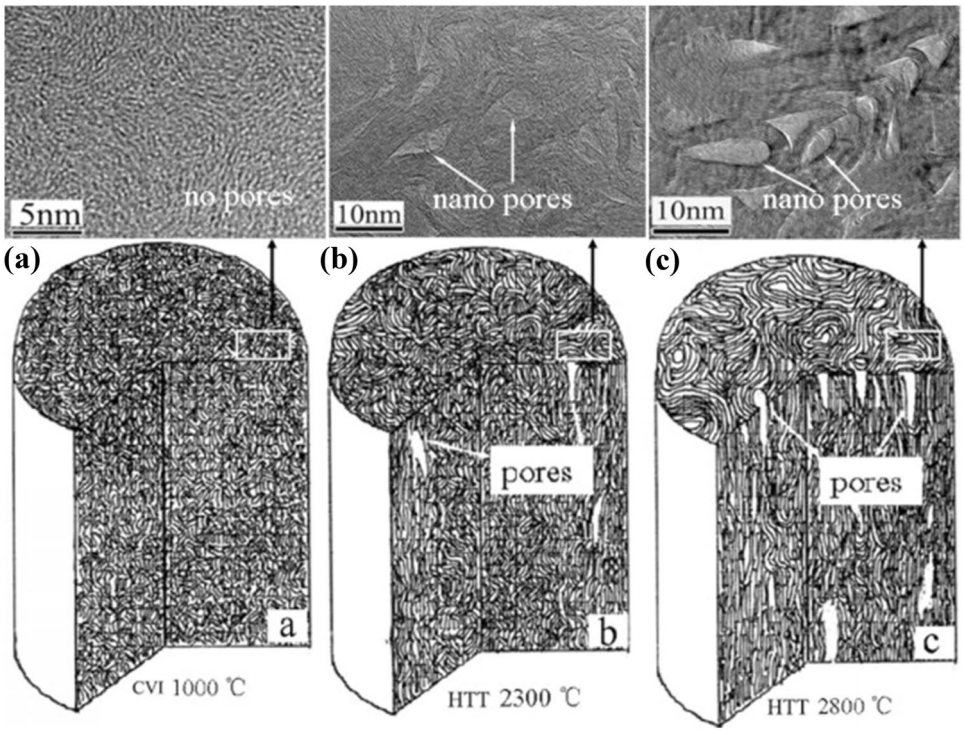

Fig. 4 High Resolution Transmission Electron Microscope (HRTEM) images and schematic of PAN-based CNFs with chemical vapor infiltration at **a** 1000 °C, **b** 2300 °C, and **c** 2800 °C. The above pictures show the actual pores (arrows) in the fiber [58]. Reproduced with permission from ref. 58. Copyright 2011, Elsevier Ltd

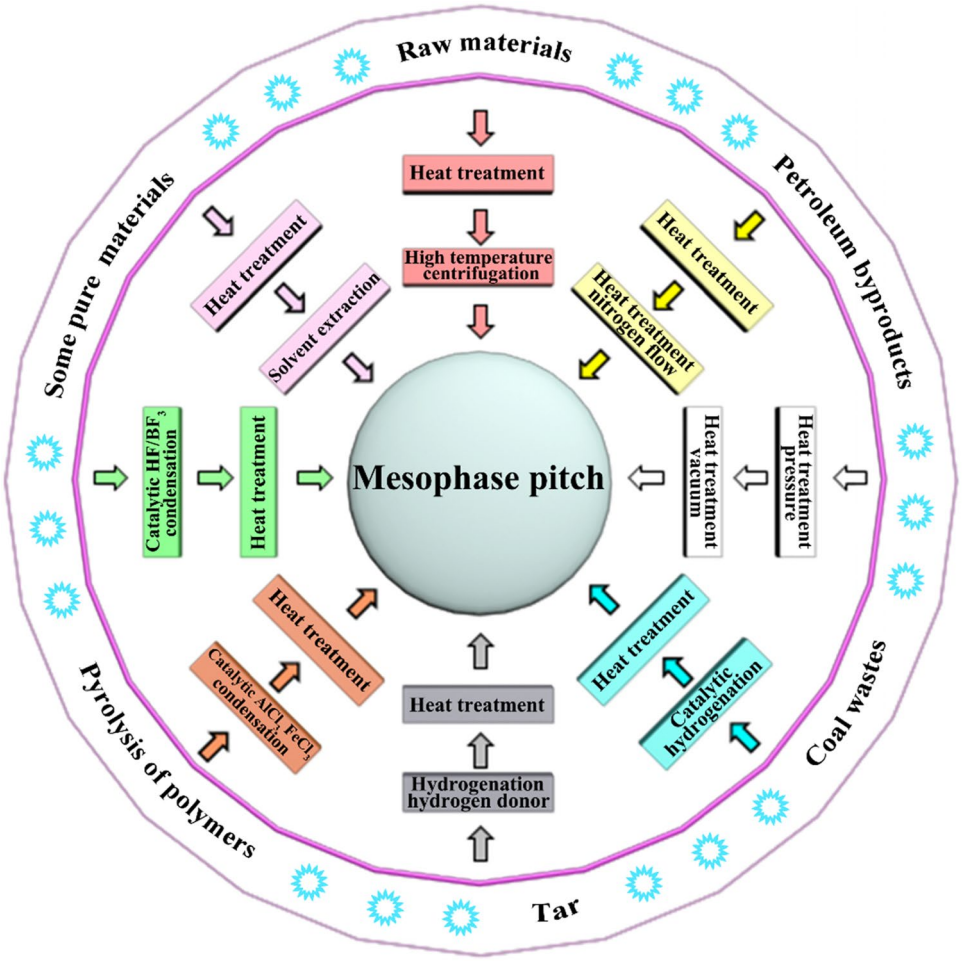

Fig. 5 The processing of mesophase pitch

CBFs by isotropic pitch obtained from the pyrolysis of polyvinyl chloride (PVC) in 1965 [59]. In the same year, Brooks et al. discovered mesophase pitch by polarizing microscope during the processing of isotropic pitch [60]. Since then, many studies on mesophase asphalt had been carried out [61]. Compared with isotropic pitch, mesophase pitch possesses more excellent intrinsic properties, such as high molecular weight, graphitization, aromaticity and high crystallinity, which thereby endowing better mechanical performance for pitch-based CBFs. According to the research, the tensile strength, elastic modulus and elongation of pitch-based CBFs could reach 3.8 GPa, 965 GPa and 0.9%, respectively [62]. Even if isotropic pitch-based CBFs are disadvantageous in mechanics, the better elongation and the intrinsic nature will improve the development in many applications, such as chemical resistance, toughening and heat resistance [63].

Pitch Preparation

The performance of the pitch is significant for the quality of the final CBFs. Generally, petroleum byproducts and coal residue are the main raw materials to prepare the pitch precursor since they are inexpensive and ubiquitous in industrial production. The various aromatic polymers are simply obtained from these istes, followed by heat-treating in a harsh environment to obtain pitch precursor [64]. The properties of the prepared pitch precursor can not be predicted and controlled since the raw materials are impure and the complex chemical reactions happened during the preparation of the precursor. Moreover, the pitch precursor obtained from petroleum byproducts and coal residue is often isotropic [65]. To obtain high mechanical performance of pitch-based CBFs, some methods are performed to convert isotropic into mesophase, such as hydrogenation, pyrolysis, catalyst and solvent extraction [66–69]. In addition, high-temperature centrifugation, high-pressure condition and heat treatment are also conducive to the formation of mesophase pitch [70–72].

The relatively pure raw materials are used to prepare the pitch precursor. Otani firstly used PVC to fabricate the pitch precursor that was simple converted from polymer chains to pitch structure through heat treatment at different temperature [59]. The PVC will undergo cyclization, aromatization and condensation to form the pitch structure during the heat treatment process, while it has some disadvantages, such as the long processing time and low yield which limit the development in industrial production [73]. In addition, some researchers used polymer and petroleum byproducts or coal istes mixtures to prepare the pitch precursor, and the processing parameters were adjusted to improve the mechanical performance of CBFs [74, 75].

The pure raw materials are also suitable to prepare the pitch precursor, such as anthracene, naphthalene, poly(methyl vinyl ketone) and polyolefin [76–79]. Generally, these raw materials possess low reactivity which demand harsh reaction conditions during the processing, including high temperature and high pressure [80]. Moreover, the catalysts are also used to promote the reaction, such as ferric chloride and aluminum chloride [81]. However, these catalysts will remain in the system after processing, resulting in the reduction of the processing performance of the pitch precursor, especially in spinnability. Therefore, the hydrofluoric acid/boron trifluoride (HF/BF_3) was developed to overcome the catalyst legacy so as to obtain pitch-based CBFs with excellent performance [80], while the strong acidity of the HF/BF_3 possessed extremely high requirements for production equipment which limits the development of the industry.

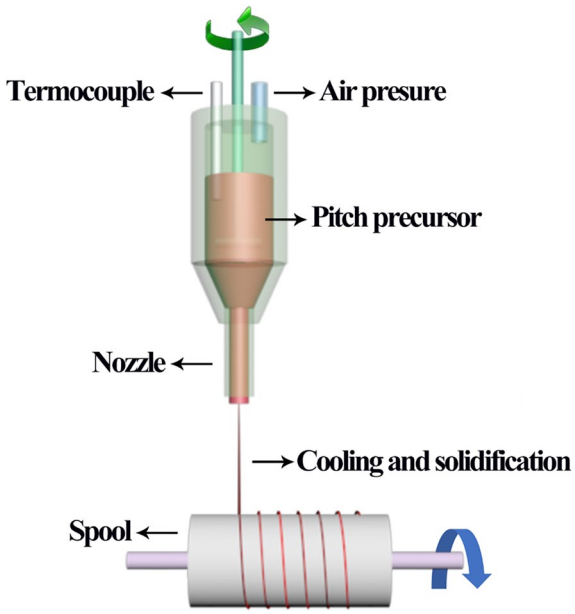

Fig. 6 Schematic of melt spinning process

Melt Spinning

The melt spinning is a suitable technology to prepare pitch-based CBFs precursor due to its high molecular weight, high viscosity and complete solid. During the melt spinning process, the pitch precursor is heated to a molten state under inert gas conditions, and then the molten body is extruded from the nozzle by applying air pressure to form nascent fibers (Fig. 6). The pitch-based CBFs precursor is quickly cooled and solidified in the air, and finally wound on a spool.

The design of the melt spinning process is an extremely complicated procedure. The properties of pitch-based CBFs precursors are influenced by numerous factors, including melting temperature, air pressure parameters, viscosity, collecting speed, stirrer and nozzle shape [82, 83]. The viscosity of pitch precursor is the key factor for spinning which is determined by the processing temperature. It is necessary to maintain a certain viscosity while ensuring the melting of the pitch precursor, therefore, the temperature is generally controlled slightly above the softening point. Meanwhile, the spinning process is carried out continuously through suitable air pressure [84, 85]. The fiber precursor is difficult to spin no matter the viscosity of the precursor is too high or too low, which will affect the performance of the fibers. Generally, both pitches of isotropic and mesophase structures have spinnable properties, and their viscosity exhibits similar variation trends during the spinning process which may be related to air pressure. The diameter of pitch-based CBFs can be adjusted by air pressure and collection speed [83, 86]. The topography of the nozzle is also a decisive factor for the shape and diameter of the fibers, which is usually designed as Y-shape, triangle, square and other shapes. The parameters of the nozzle, including length, diameter and angle, are designed to improve the spinnability of pitch precursor and the mechanical performance of the fibers. In addition, the nozzle is designed as non-circular to prepare pitch-based CBFs with specific shapes, which is used in composite materials [87].

Heat Treatment of Pitch-Based CBFs Precursor

The processing of pitch-based CBFs precursor is similar to that of PAN-based CBFs which are mainly divided into three processes: stabilization, carbonization and graphitization. The stabilization process is performed at air conditions and the temperature below the softening point of the pitch fiber precursor (250–350 °C). The complex physical and chemical reactions occured in this process include oxidation, condensation and dehydration, thereby promoting the transition of pitch fibers from a

thermoplastic state to a thermoset state [88, 89]. However, a disadvantage that the stabilization process will take a lot of time and energy to make the fiber withstand a higher temperature in the subsequent heat treatment. Therefore, many oxidizing agents are used to replace air to shorten oxidation time and reduce energy consumption, such as pure oxygen, nitric acid and iodine but these oxidizing agents are expensive and complicate to operate, which are not suitable for the fabrication of pitch-based CBFs in actual production. Some surface treatment technologies also improve the efficiency for oxidation including plasma, electromagnetic field and mechanical compression, while these process require additional energy.

Similar to PAN-based CBFs, during the carbonization process under inert gas conditions, pitch-based CBFs undergo a complicated removal reaction of non-carbon elements, such as dehydrogenation, deoxygenation, denitrification and condensation. Thus, the carbon content is increased and improve the arrangement and orientation structure of the crystals inside fibers. For pitch-based CBFs, carbonization is generally divided into two steps: low-temperature carbonization (300–500 °C) and high-temperature carbonization (500–1400 °C). At 300–500 °C, the non-carbon elements are beginning to disappear through the evaporation process of small molecule gases, such as ammonia, carbon monoxide and methane, resulting in the improvement of the aromatic structure [90]. As the non-carbon elements are almost removed at 500–1400 °C, the aromatic structure is transformed into a denser structure [91]. The orientation and arrangement of the molecular structure and the aromaticity are further improved, thereby greatly improving the mechanical properties of pitch-based CBFs [92].

The aromaticity, molecular weight, and crystallinity of mesophase precursor are better than that of the isophase pitch precursor, significantly, only the mesophase pitch fiber precursor can be graphitized at higher temperature [93]. The graphitization is performed at 2000–3000 °C, and the elastic modulus of fibers will be greatly improved due to the formation of more regular graphite crystal regions [94], while the tensile strength increases slightly [57]. Importantly, the precise control and inert gas conditions are required in graphitization to avoid the sublimation of graphite and the destruction of the crystal structure. Although the carbon loss can not be avoided during processing, the carbon yield is generally > 80% after graphitization [57].

Cellulose-Based CBFs

Cellulose is the most widely distributed polysaccharide in nature, which is mainly from plants. In recent years, cellulose has attracted widespread attention since it satisfies the requirements of the era, such as environmental protection, low cost and easy availability. However, for cellulose-based CBFs, Thomas Edison used cotton and other plant fibers to prepare CBFs as early as the 1880 [95]. In the following decades, rayon-based CBFs had achieved commercial production by Union Carbide through the hot stretching technology [96]. However, compared with PAN-based CBFs and pitch-based CBFs, cellulose-based CBFs have less industrial development. Because the disadvantages in the preparation of cellulose-based CBFs, such as cumbersome process, high cost, low efficiency, and low performance. Recently, with the rise of sustainable, degradable and recyclable raw materials, cellulose has received renewed attention in the preparation of CBFs. Moreover, the high cost of PAN-based CBFs and the over-exploitation of petroleum resources are significant reasons to drive the continued development of cellulose in the preparation of CBFs. Therefore, as one of the raw materials for CBFs, cellulose possesses a promising prospect in the current market.

Cellulose Precursor

Cellulose must be separated and extracted before fabricating CBFs because there are other biomass materials in the crude extract of cellulose, such as hemicellulose, lignin, etc. The discontinuity of cellulose is the shortcoming to prepare high mechanical performance of CBFs. Therefore, the regenerated cellulose (artificial cellulose) with specific dimensions and extremely high purity has been developed to improve the mechanical performance of CBFs [97]. The morphology and structure of cellulose are important parameters to achieve high performance. Northolt et al. proposed two different molecular chain conformations and the crystal structure of cellulose: cellulose I and cellulose II, which represented nature cellulose and regenerate cellulose, respectively [98]. It was obvious that the molecular chains of the two celluloses were arranged in parallel, while the arrangement of cellulose II was antiparallel,which was not as regular as that of cellulose I (Fig. 7a). Meanwhile, the content of hydrogen bonds in cellulose I were larger than that of cellulose II, so the naturally formed crystal structure was tighter (Fig. 7b). and the elastic modulus of cellulose I was higher than that of cellulose II.

Generally, artificial cellulose mainly includes viscose rayon, lyocell, tire cord, cotton, cupro, fortisan, bocell, etc. [99]. Among them, viscose rayon and lyocell are the representative candidates to prepare cellulose-based CBFs (Fig. 8). Generally, the traditional viscose is dissolved in an alkaline solution, such as sodium hydroxide and sulfonated with carbon disulfide (CS_2), followed by spinning in the coagulation bath including sulfuric acid and sodium sulfate to remove the excess CS_2 [99]. Moreover, zinc salts are introduced into a coagulation bath to control the formation of a skin/core structure during the spinning process, resulting in

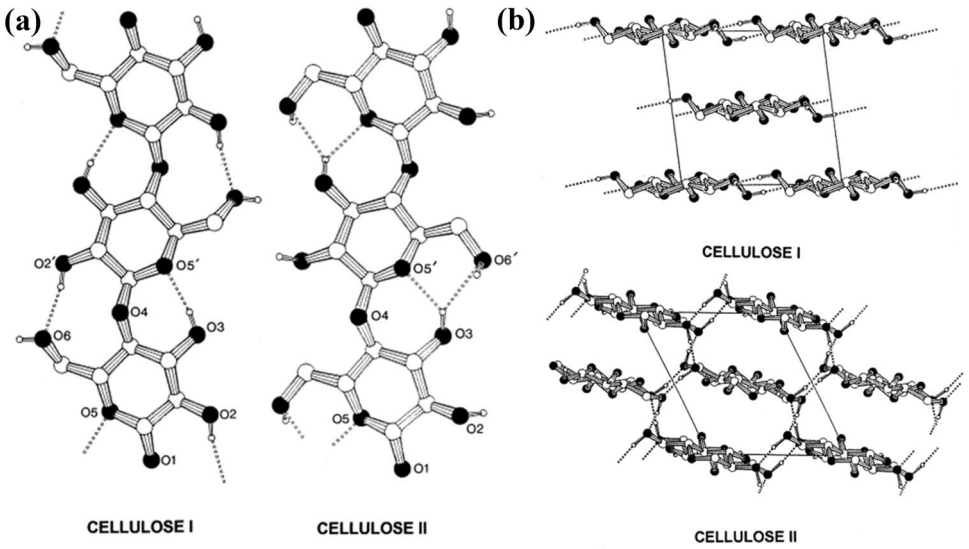

Fig. 7 Schematic of **a** the molecular conformation and **b** the crystal structure of two different cellulose: nature cellulose (cellulose I) and regenerated cellulose (cellulose II) [98]. Reproduced with permission from ref. 98. Copyright 2001, Elsevier Ltd

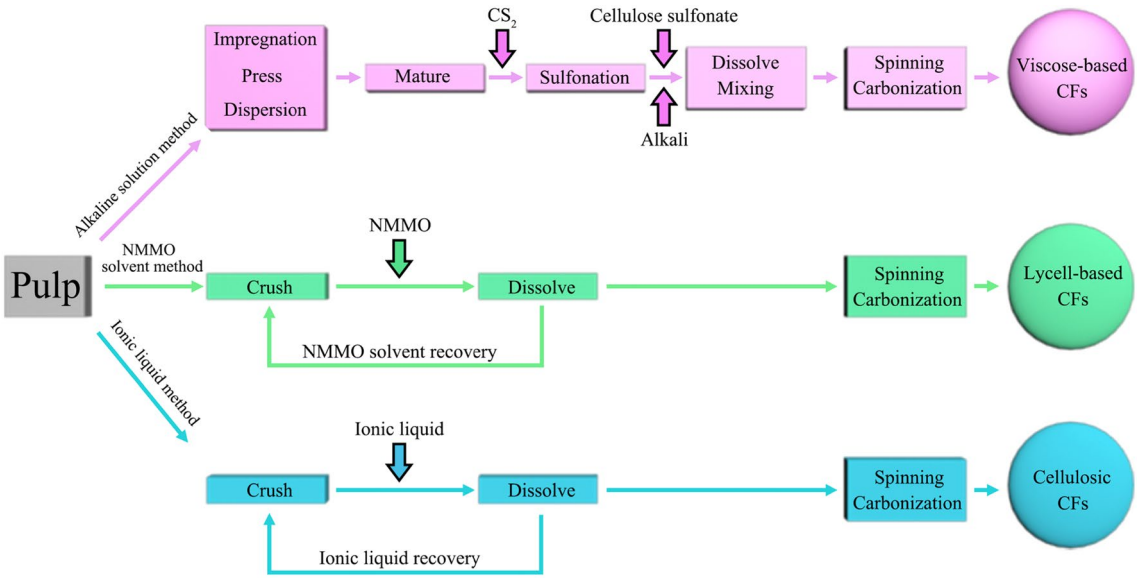

Fig. 8 Schematic of the preparation process of several different cellulose-based CBFs

the high mechanical performance of CBFs. But the complex production process and the large consumption of CS_2 with high pollution limit the development of viscose-based CBFs.

The dry-jet spinning is performed to prepare lyocell. The preparation process of viscose-based CBFs precursor is improved by replacing the traditional solutions with quaternary amine oxide N-methylmorpholine-N-oxide (NMMO), therefore the cellulose is directly dissolved and forms a spinnable solution. Moreover, the stabilizing agents are introduced into solution to prevent side reactions [100]. Compared with viscose, lyocell possesses various advantages, such as the ultra-high solvent recovery rate (≥99.9%), pollution-free emissions, simple operation and environmental protection. Significantly, the lyocell precursor has better cross-sectional morphology, sheath-core structure, higher orientation and crystallinity than that of viscose precursor, which benefits from the removal of the oxidative degradation process. The crystallinity of lyocell precursor is two times more than that of viscose precursor, resulting in the higher performance of the final CBFs. However, there is little

lateral interaction among the fibers, which may adversely affect performance.

Heat Treatment of Cellulose-Based CBFs Precuersor

The stabilization process of cellulose will undergo pyrolysis at 100–400 °C, and the precursor is further stabilized at [101]. The complex chemical reactions occur during the pyrolysis process due to the complexity of the internal structure of cellulose, which can be roughly divided into dehydration and dehydrogenation. The carbon-based covalent bonds are partially destroyed, such as carbon–oxygen bonds, carbon–carbon bonds. The main pyrolysis products include water, carbon dioxide, carbon monoxide, ethylene, L-glucose, and other small molecule compounds. However, the loss of carbon during the pyrolysis process is not conducive to the preparation of CBFs, which has prompted some effective methods to delay the carbon loss. In order to minimize the formation of L-glucose, there are several methods to promote the dehydration of cellulose-based CBFs precursor, such as reducing the heating rate, utilizing the flame retardant, pyrolysis in a reaction atmosphere, and impregnation of the precursor with organosilicon compound [102, 103]. It is beneficial to promote dehydration with the combination of at least two or more measures. As an example, Brunner found that the carbon yield was 11% when the heating rate was 70 °C/h, and it achieved 28% at 0.03 °C/h [103]. The burnt manifestation disappears at low heating rates, thereby increasing the carbon yield. Meanwhile, the low heating rate can promote the formation of the regular structure (density, specific surface area and micropore volume), while it will consume plenty of energy which is not conducive to the industrial production. For reactive atmosphere, although HCl vapor is the effective conditions to promote dehydration, it is impractical in actual product due to the strong corrosiveness of HCl vapor. A small amount of flame retardant can remove hydroxyl from cellulose, such as urea, Lewis bases and Lewis acids [52, 104]. In addition, the impregnation of fiber precursors by organosilicon compounds can effectively improve the mechanical properties of cellulose-based CBFs, which tensile strength and elastic modulus reach 1.8 GPa and 100 GPa, respectively [105].

The pyrolysis reaction is completed at 400 °C, then the temperature is increased to 900–1500 °C through faster heating rates for further carbonization. Under inert gas conditions, the carbon content continually increases with the release of non-carbon atoms, which will exceed 95% after carbonization. There are many complex reactions in the carbonization process due to the diversity of the structure of cellulose precursor, such as rearrangement, cyclization and aromatization, resulting in the shrinkage of the volume and the increase of the density. Eventually, the mechanical performance of fibers is improved after the formation of the graphite-like layer and the appearance of a microcrystalline structure.

The graphitization of cellulose-based CBFs is performed under inert gas conditions at 1500–3000 °C. The carbon content exceeds 99% and the graphite layer structure grows during this process. It is worth mentioning that, the drafting process runs through the entire heat treatment process to increase the regularity of the molecular structure along the longitudinal axis, thereby improving the tensile property. In addition, the time of graphitization is a significant parameter for the performance of the final fiber. Although the time is short, it is enough to change the graphite structure in a few seconds under the action of ultra-high temperature.

Lignin-Based CBFs

Lignin is the second-largest green and renewable carbon resource. Moreover, lignin possesses rich aromatic ring structure aliphatic group, aromatic hydroxyl group and quinone group, which can be used as a precursor to prepare CBFs [106]. Generally, lignin possesses an amorphous and disordered structure with phenylpropane as the basic structural unit (Fig. 9a) [107, 108]. It is derived from p-coumaryl alcohol, coniferyl alcohol and sinapyl alcohol, which are corresponding to p-hydroxyphenyl lignin, syringyl lignin and guaiacyl lignin, respectively (Fig. 9b). According to the different basic unit content, lignin is classified into softwood lignin and hardwood lignin. The softwood lignin consists of guaiacyl lignin and traces of syringyl lignin and p-hydroxyphenyl lignin, while the hardwood lignin possesses both guaiacyl lignin and syringyl lignin. It is worth noting that plant lignin includes the above three units, which promotes large-scale industrial production. In recent years, hardwood lignin and softwood lignin have been used to produce carbon nanofibers [109, 110]. The processing technology and properties of softwood and hardwood lignin in the preparation of carbon nanofibers demand to be further investigated.

Lignin Preparation

The lignin can be separated and extracted from trees as a sustainable green industrial materials (Fig. 10) [111]. The paper/pulp production processes, such as alkaline pulping, are also commonly technologies to obtain lignin. However, a large amount of impurities, such as salt, ash, sulfur-based compounds, etc., are produced during the papermaking process, resulting in impure lignin [112]. Besides, biomass conversion technology has been developed to prepare lignin. The sulfur-free technology is performed and the

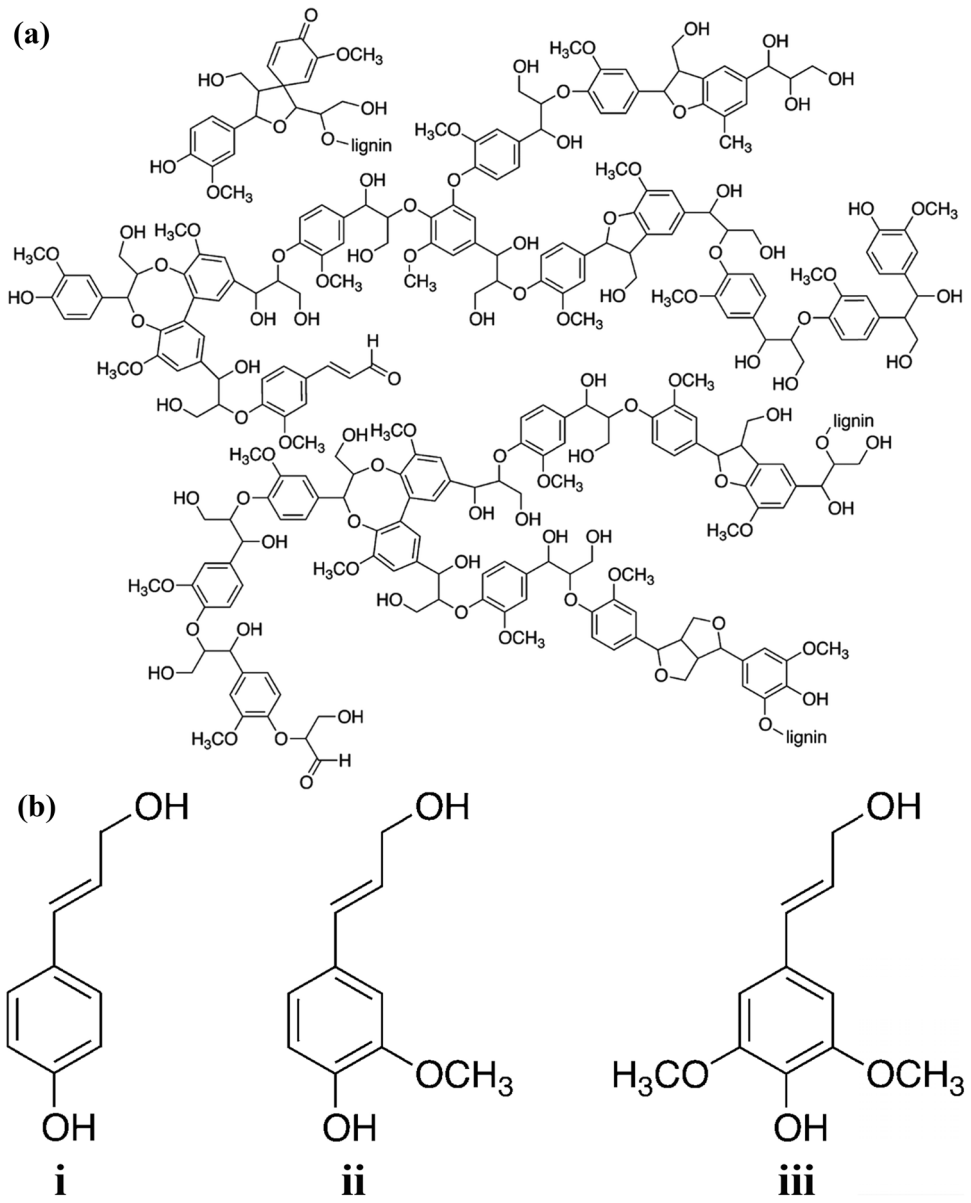

Fig. 9 **a** The molecular structure of softwood lignin [107]. Reproduced with permission from ref. 107. Copyright 1980, Springer-Verla. **b** The molecular structure of three aromatic alcohol precursors: (i) p-coumaryl alcohol, (ii) coniferyl alcohol and (iii) sinapyl alcohol [108]. Reproduced with permission from ref. 108. Copyright 2015, American Chemical Society

characteristics of lignin are controlled by process parameters and intrinsic properties of biomass [113].

Lignin-Based CBFs Processing

As early as the 1960s, Otani et al. first published a patent for the preparation of CBFs with lignin as a precursor [114]. Briefly, the technical lignin were pre-treated, such as purification and refining, followed by spinning to prepare precursor (Fig. 11) [115]. Many methods are used to spin lignin including dry spinning, wet spinning, melt spinning and electrostatic spinning [116, 117], but dry spinning and wet spinning technologies almost disappeared in the 1970s [118]. The melt spinning is the most common technology for preparing lignin-based CBFs in recent years [119, 120]. The spinnability of lignin can be improved by controlling the lignin parameters (molecular weight and polydispersity index) in the melt spinning process. The atmospheric acetic acid method can effectively remove insoluble impurities in lignin raw materials, thereby turning it into a meltable spinning dope [121]. The melt viscosity is a significant factor in determining the spinnability of lignin, therefore, the system temperature should be precisely controlled during processing. The spinning equipment parameters also affects

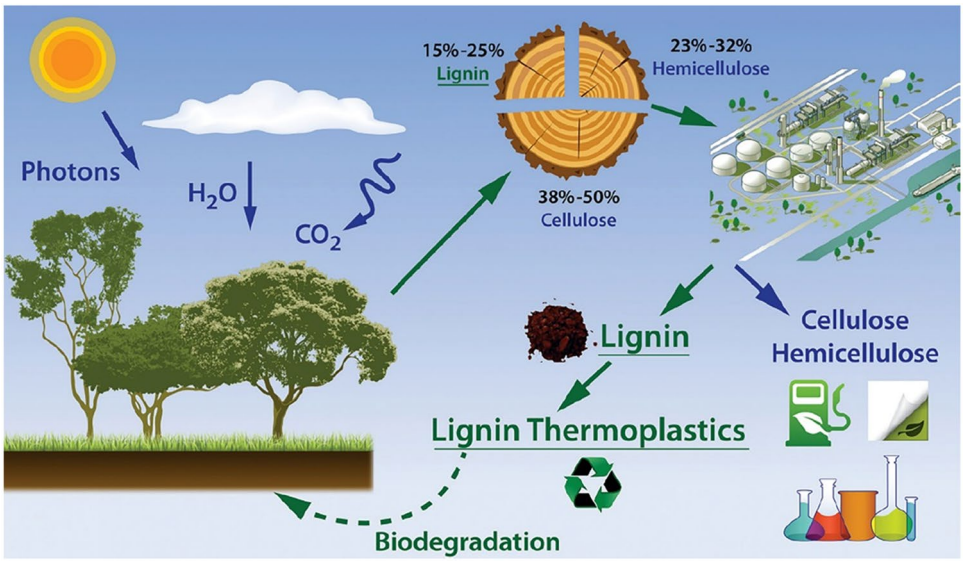

Fig. 10 Schematic of lignin and lignin-based polymers preparation and their recycling [111]. Reproduced with permission from ref. 111. Copyright 2012, The Royal Society of Chemistry

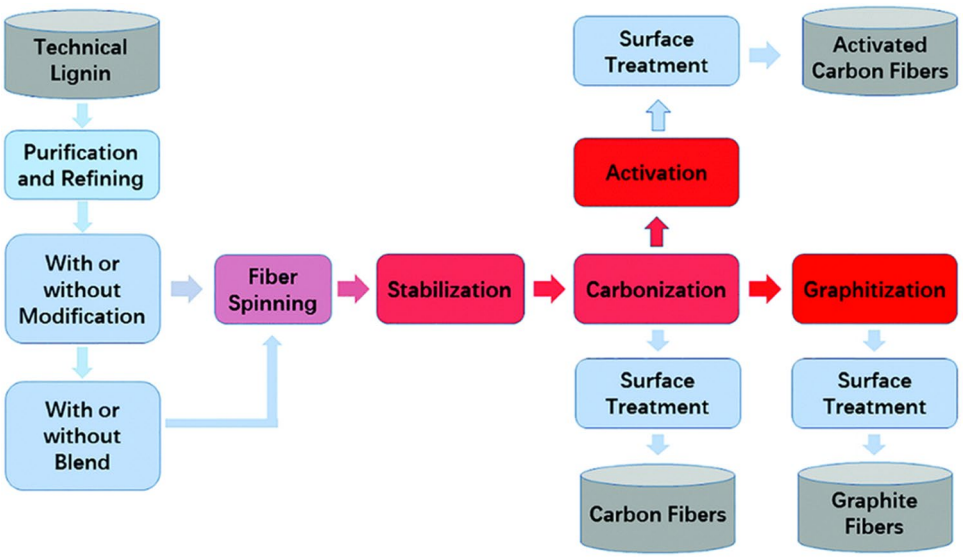

Fig. 11 Schematic of the fabrication process of the lignin-based CBFs [115]. Reproduced with permission from ref. 115. Copyright 2017, The Royal Society of Chemistry

the melt spinning process of lignin, which is similar to the pitch-based CBFs as mentioned above. In addition, heat treatment of the lignin precursor before melt spinning can effectively improve the spinnability and porosity.

Heat Treatment of Lignin-Based CBFs Precursor

The precursor stabilization process is heating and oxidation under air or oxygen conditions at 200–280 °C. The complex chemical reactions occur in this process including oxidation, condensation, cross-linking, and recombination, which ensure that the precursor can be carbonized at higher temperatures. Normally, the purpose of stabilizing is achieved by heat treatment, while it will take much time and energy. The oxidation treatment process can greatly shorten the stable time of the precursor and reduce energy consumption [122]. Moreover, the pre-treatment of the lignin precursor before stabilization like iodine treatment can improve

thermodynamic stability and reduce energy consumption [123]. Interestingly, Kubo et al. prepared cellulose spinning dope by atmospheric acetic acid pulping method, and the fiber precursor obtained by the melt spinning method was carbonized directly without stabilization [121]. The hardwood lignin exhibited excellent melting properties due to partial acetylation, while the softwood lignin was hardly transformed into the meltable spinning dope. Therefore, the melt spinning temperature of hardwood lignin and softwood lignin were 210 °C and 350–370 °C, respectively. Although the thermal stabilization process is omitted and the preparation process is simplified, the higher temperature will damage the surface structure, resulting in a decline in mechanical performance.

The carbonization process is carried out under inert gas conditions at 800–1400 °C. Similar to the carbonization process of other materials, most of the non-carbon elements in the system are removed and the carbon content is greatly increased. The carbon layer structure is arranged more neatly and tightly, which improves the mechanical properties of lignin-based CBFs. Besides, the graphitization is performed at a higher temperature to further improve the mechanical properties, while the lignin-based CBFs precursor can not achieve the expected effect. The modulus of the fibers will not increase or even decrease in the graphitization, which is inconsistent with industrial CBFs [124]. Therefore, the graphitization of lignin-based CBFs demands further in-depth research.

PAN, Pitch, Cellulose and Lignin-Based CBFs Applications

As early as the 1960s to the 1970s, CBFs have already realized industrial production, and its precursors mainly include PAN, pitch and viscose. The viscose-based CBFs are only used to produce ablation-resistant and thermal insulation materials due to its low carbonization yield, high technical difficulty, complex equipment and high cost. Although pitch-based CBFs have abundant resources and high carbon production, the complex raw materials and poor product performance hinder large-scale development. PAN-based CBFs have a simple production process, excellent mechanical properties and wide-range in application, which occupy more than 90% of all CBFs markets in industrial production. Nowadays, CBFs with ultra-high mechanical properties are widely used in aerospace, national defense, military industry, energy, construction, biomedicine, environment, sporting goods and other fields.

In recent years, the representative companies that produce CBFs mainly include Toray, Mitsubishi, DuPont, SGL, Hexcel, Cytec and Zoltek. Among them, Toray is in a leading position in the research and development of PAN-based CBFs. According to the standard proposed by Toray, CBFs can be divided into "T" (meaning tensile strength) and "M" (meaning tensile modulus) series, such as T300, T700, T1000, M35J, M40J, M60J, etc. In addition, according to the number of fiber filaments, CBFs are divided into small tows (< 48 K) and large tows (≥ 48 K). The small tows, such as 14 K and 21 K, which are mainly used in the high-tech fields such as national defense and military industry, and the large tows including 48 K, 60 K, 120 K, 360 K and 480 K are utilized in textile, medicine, electromechanical, civil engineering, transportation and other civil industries.

In addition to pure CBFs, there are also CBFs composites in industrial production. The mechanical properties of the matrix materials can be adjusted by CBFs, such as PEEK, CTBN, epoxy resin, etc. As an example, CBFs were sized by PEEK-1, 3-dioxolane to enhance the interface bonding force, so that the interfacial shear strength of the PEEK composites was increased from 43.42 to 83.13 MPa [125]. Although many researches have been carried out on the thermodynamic and electrical properties of CBFs in devices such as batteries and SCs [126–129], the rise of materials with excellent electrical properties including CNT and graphene has gradually diverted researcher's attention. As for green materials, although cellulose and lignin have great potential as CBFs raw materials, however, in-depth research is urgently demanded to improve production technology and mechanical properties in the future. Eventually, the various parameters of CBFs prepared by PAN, pitch, cellulose and lignin are shown in Table 1.

CNT-Based CBFs

CNT-Based CBFs Fabrication

CNT Solution Spinning

Solution spinning technology has been used to fabricate various CBFs with outstanding performance, such as PAN-based CBFs and acrylic acid-based CBFs. There are two main solution spinning methods for preparing CNT-based CBFs including surfactant suspension CNTs spinning and liquid crystal spinning of CNTs in superacid. Vigolo et al. first prepared CNT-based CBFs by CNT solution spinning in 2000 [8]. During the processing, sodium dodecyl sulfate (SDS) was used as a surfactant to make SWCNTs uniformly dispersed in the aqueous solution, then the dispersions were injected into coagulation liquid with polyvinyl alcohol (PVA, 5 wt%) through a syringe (Fig. 12a). According to the analysis of X-ray scattering, PVA was adsorbed onto CNTs to replace some SDS molecules due to the amphiphilic character, and then forms a CNT ribbon [9]. CNT-based CBFs were prepared by twisting a

Table 1 The various parameters of CBFs prepared by PAN, pitch, cellulose and lignin

Ref	Precursors	Processing/modification technology	Tensile strength (GPa)	Elastic modulus (GPa)	Applications
[30]	PAN	Solution spinning Carbonization 1000 °C	–	140	–
[31]	PAN	Solution spinning Carbonization 2500 °C	–	414	–
[40]	PAN/MAA	Gel spinning Carbonization 1450 °C	5.5–5.8	354–375	–
[42]	PAN/MA	Gel spinning Carbonization 1000–1500 °C	4.3 ± 1.0	361 ± 45	–
[63]	Isotropic pitch	Melt-spinning Carbonization 1100 °C	2.05	54.5	–
[70]	Eucalyptus tar pitches	Melt-spinning Carbonization 1000 °C	0.13	14	–
[79]	Isotropic pitch	Melt-spinning Carbonization 950 °C	0.635	67	–
[94]	Mesophase pitch	Melt-spinning Carbonization 1300–2500 °C	1.87–2.52	366–605	–
[98]	Cellulose	Dry–wet spinning	1.7	44	–
[109]	PAN/pitch/lignin	Electrospinning Carbonization 800 °C	–	–	SCs specific capacitance of 165 F/g at 1 mA/cm^{-2}
[117]	Lignin/PAN	Electrospinning Carbonization 1000 °C	–	–	Batteries discharge capacity of 150 mAh/g
[121]	softwood kraft lignin	Fusion spinning Carbonization 1000 °C	26.4 ± 3.1	3.59 ± 0.43	–
[123]	Lignin	Electrospinning Carbonization 1400 °C	0.089	> 5	–
[126]	P(AN-*co*MHI) MoS_2	Electrospinning Hydrothermal 200 °C Annealed 500 °C	–	–	Batteries capacity of 1168.6 mA h/g at a current density of 5A/g
[127]	P(AN*co*MHI)/F_2MoS_2	Coaxial electrospinning Carbonization 1300 °C Hydrothermal 200 °C	–	–	Batteries capability of 832 mAh/g at a current density of 10 A/g
[128]	P(AN-*co*MHI)	Electrospinning Hydrothermal 200 °C Calcined 600 °C	–	–	Batteries capacity of 586.7 mAh/g after 400 cycles at 1 A/g
[129]	P(AN-*co*MHI)/MnO_2	Electrospinning Carbonization 1150 °C Hydrothermal 200 °C	–	–	Electrode capacity 587.5 F/g at 0.5 A/g

CNT ribbon due to the presence of the capillary action. The diameter ranged from several micrometers to one hundred micrometers was mainly affected by the processing conditions, such as the diameter of the syringe, the flow rate of the injected solution, and the condition of the polymerization coagulation liquid. As a result, CNT-based CBFs showed a plastic behavior, and the tensile strength, elastic modulus and electrical conductivity were 300 MPa, 40 GPa and 10 S/cm, respectively (Fig. 12b–d) [9]. Moreover, the performance of CNT-based CBFs can be further improved by hot-drawing [130]. In the further investigation, the SDS is replaced by lithium dodecyl sulphate (LDS) to prepare composite CNT-based CBFs containing CNTs (60%) and PVA (40%) with a length of 100 m and a diameter of 50 μm [131]. These fibers exhibit excellent mechanical properties that the tensile strength and elastic modulus are 1.8 GPa and 80 GPa, respectively [131]. The presence of PVA can improve the mechanical performance of CNT-based CBFs composites, while the electrical and thermal abilities decrease compared with pure CNT-based CBFs. Therefore, Ericson et al. adopted fuming sulfuric acid to make SWCNTs dispersed in the solution, and followed by conventional spinning to prepare well-aligned macroscopic fibers [132]. The fuming sulfuric acid would charge the SWNTs and promote its orderly arrangement into an aligned phase of individual mobile SWCNTs surrounded by acid anions. Therefore, CNT-based CBFs show the high electricity of 500 S/cm, thermal conductivity of ~ 21 W/mK, tensile strength of 116 ± 10 MPa and elastic modulus of 120 ± 10 GPa [132].

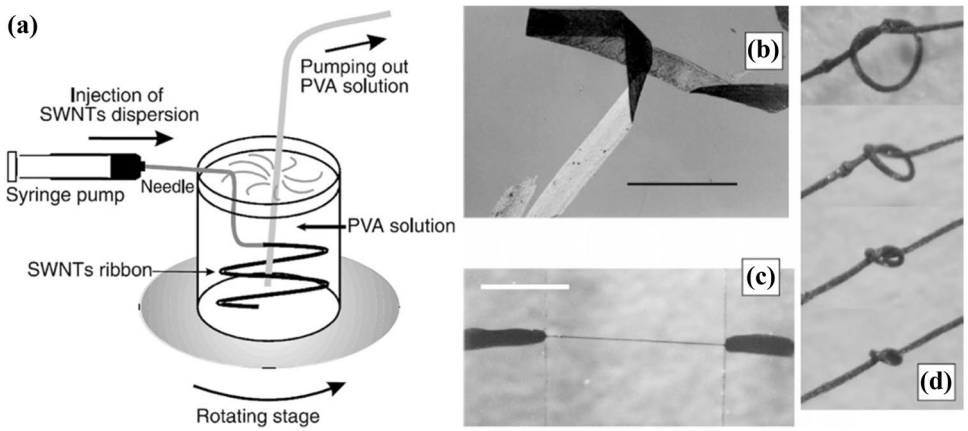

Fig. 12 Schematic of the fabrication process of the CNT ribbons. **a** A single folded ribbon between horizontal and vertical crossed polarizers. (scale bar = 1.5 mm). **b** A freestanding CNT-based CBFs (scale bar = 1 mm). **c** Tying knots [8]. Reproduced with permission from ref. 8. Copyright 2000, The American Association for the Advancement of Science

Kozlov et al. used polymer-free spinning to obtain high purity CNT-based CBFs with ultra-high concentration sulfuric acids as dispersant. The results showed the electrical conductivity of 140 S/cm and the tensile strength of 65 MPa [133]. The concentrated sulfuric acid can be replaced by chlorosulfonic acid to improve the productivity and comprehensive performance [134]. The superacid treatment can functionalize the surface of CNTs, so that CNTs are dispersed in solutions to meet the demand of the wet-spinning. However, indubitably, the super acid will bring some serious problems in industrial production, such as the high demands for equipment and high cost. Some researchers adopted other dispersants to replace the super acid. As an example, Zhang et al. utilized ethylene glycol solution as dispersant to disperse SWCNTs and followed by injecting into ether solution to prepare CNT-based CBFs [135]. The ethylene glycol and ether would diffuse each other during the preparation process, the tensile strength, elastic modulus and electrical conductivity of CNT-based CBFs were 150 ± 60 MPa, 69 ± 41 GPa and 8×10^4 S/m, respectively [135]. Moreover, it was found that the intrinsic parameters of CNTs would cause certain influence on the performance of CNT-based CBFs, including CNT diameter, number of walls, aspect ratio, graphitic character and purity [136]. The tensile strength and conductivity of CNT-based CBFs were improved by assembling high aspect ratio CNTs, which the average tensile strength and room temperature electrical conductivity reached 2.4 GPa and 8.5 MS/m, respectively [136]. In addition, the highly aligned and densified CNT-based CBFs were prepared in rapidly and potentially continuous manner by combining the advantages of the wet spinning and direct spinning methods [137]. The fibers were ultralightweight, strong (specific tensile strength = 4.08 ± 0.25 Ntex^{-1}), stiff (specific tensile modulus = 187.5 ± 7.4 Ntex^{-1}), electrically conductive (2,270 S m^2/kg) and highly flexible (knot efficiency = $48 \pm 15\%$), which were suitable for various fabric-based applications [137].

CNT Arrays

The CNT array drawing has been widely explored to prepare CNT-based CBFs in recent years, which was first proposed by Jiang et al. [10]. The process of array drawing mainly includes the CVD method to grow CNT arrays and spinning. The CNT array is grown vertically on the substrate by the CVD method, and then it is pulled out by using specific machinery so that CNT-based CBFs can be assembled through the intermolecular forces [138]. There are some parameters determining whether the CNT array has spinning capability, such as the pretreatment conditions and the coalescence of catalyst, substrate, temperature, gas flow rates and reaction time. Jiang et al. first prepared a CNT-based CBFs (up to 30 cm) by drawing from super aligned CNT arrays [10], and the twisting process was introduced into the drafting process in the future research [139]. During CVD process, the iron catalyst was deposited on the silicon substrate by the physical vapor deposition (PVD) process to form a stable catalyst layer. The iron layer was placed in the reaction chamber with thickness of 1–3 nm. The argon was added into the chamber to exhaust the air, and then carbon source gas was introduced, such as acetylene and ethylene [138]. The carbon source decomposed to generate carbon atoms at a high temperature. And the carbon atoms reacted with the iron catalyst to form CNTs, which adhered to the catalyst substrate and grow vertically. Eventually, CNTs stopped growing after the deactivation of catalyst [140]. During the spinning process, CNT arrays were pulled from

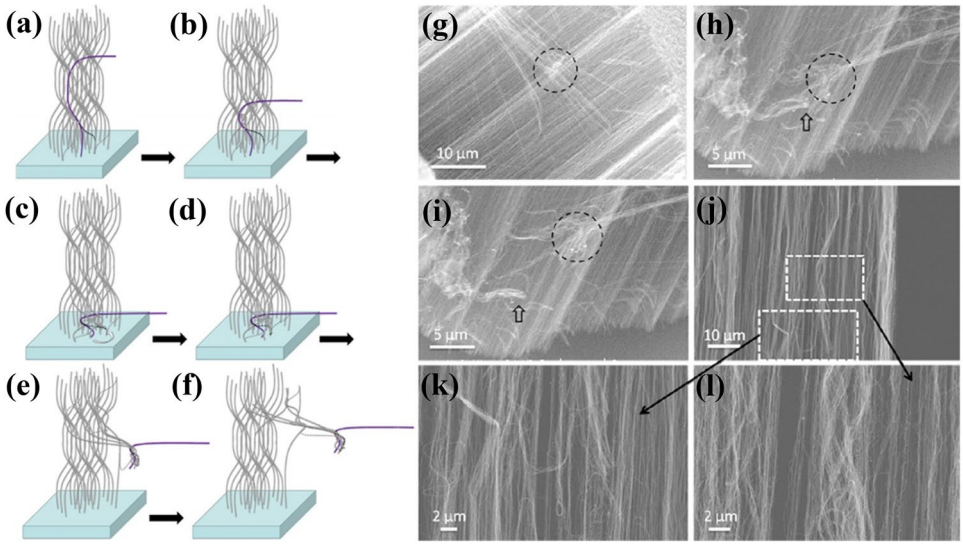

Fig. 13 **a**–**f** Schematic of self-entanglement mechanism for continuous pulling of CNT-based CBFs. The CNT array consists of crossing over (solid gray lines) and branched (dashed gray lines) CNT bundles. **g** SEM image of the pulling process at the top of a CNT array (the junction position is marked by the dashed circle), **h** and **i** at the bottom of a CNT array (two kinds of junctions are marked by the dashed circles and an arrow respectively). **j** CNT-based CBFs took near an entangled structure. **k** and **l** are enlarged images of the areas marked in (**h**) [141]. Reproduced with permission from ref. 141. Copyright 2011, Elsevier Ltd

the substrate under external force, and assembled end-to-end into continuous CNT-based CBFs (Fig. 13a–f) [141]. In the SEM images, it was obvious that the entangled structure appeared at the top and bottom surfaces of the CNT arrays (Fig. 13g–i), while there was no similar structure in the as-grown CNT arrays (Fig. 13j–l). Therefore, it could prove that the entangled structure formed at the bottom or top of the CNT arrays was significant for the continuous pulling process.

In catalyst researches, it is found that the structure and form of catalyst can influence the quality and structure of CNTs [140]. The hierarchical structure of iron/silica can adjust the number of CNT walls below 10 [142], and even to 1 or 2 when aluminum oxide is introduced into iron/silica as a middle layer [139]. Significantly, the mechanical performance of CNT-based CBFs containing CNTs with small diameter and few walls is better than that of CBFs formed by MWCNTs [143]. However, CNT-based CBFs are mainly formed by overlapping a large number of CNTs. Since the height of CNT arrays is relatively low, there are a large number of joint defects inside the fibers. The fiber breakage occurs at the joint under external force, and CNT-based CBFs fracture is mainly completed by the way that the CNT bundle slips off along the joint during the tensile process [144]. Therefore, the tensile performance of CNT-based CBFs is much lower than that of single CNT. Many technologies were explored to improve the mechanical performance of CNT-based CBFs, such as liquid shrinking, polymer infiltration, drawing CNTs from CNT array, and ion irradiation [145–148]. After treatment, the maximum tensile strength and stiffness of CNT-based CBFs reached 3.3 GPa and 263 GPa, respectively [149], and it could remain stable within a few meters [150]. For spinning speed, Alvarez et al. reported a modified dry spinning process. The drawing rate was improved by using spinnable CNT arrays, which were completely detached from the substrate and the corresponding catalyst nanoparticles. Meanwhile, the aligned CNT arrays could detach from the substrate and maintain their integrity [151]. The CNT ribbon of ~ 45 m was fabricated in less than 5 s with a drawing rates of 15.93 m/s [151]. Moreover, array-spun CNT-based CBFs had good conductivity at room temperature [152], while the electrical conductivity was specifically influenced by a large number of pores inside the fibers [153]. Therefore, some feasible methods were used to reduce the pores inside the fibers, such as twisting and acid/oxygen treatment. As an example, Wang et al. prepared a high conductive CNT-based CBFs with an electrical conductivity of 3.2×10^4 S/m after acidification [154]. The acid treatment densifies and functionalizes the surface of the CNT-based CBFs, thereby improving its conductivity.

Floating Catalyst CVD (FCCVD) Spinning

FCCVD spinning is a method of continuously preparing CNT-based CBFs. Unlike other methods, this strategy can convert the carbon source into the aerogel in pyrolysis temperature and followed by directly self-assembling to prepare CNT-based CBFs. Zhu et al. first adopted FCCVD method

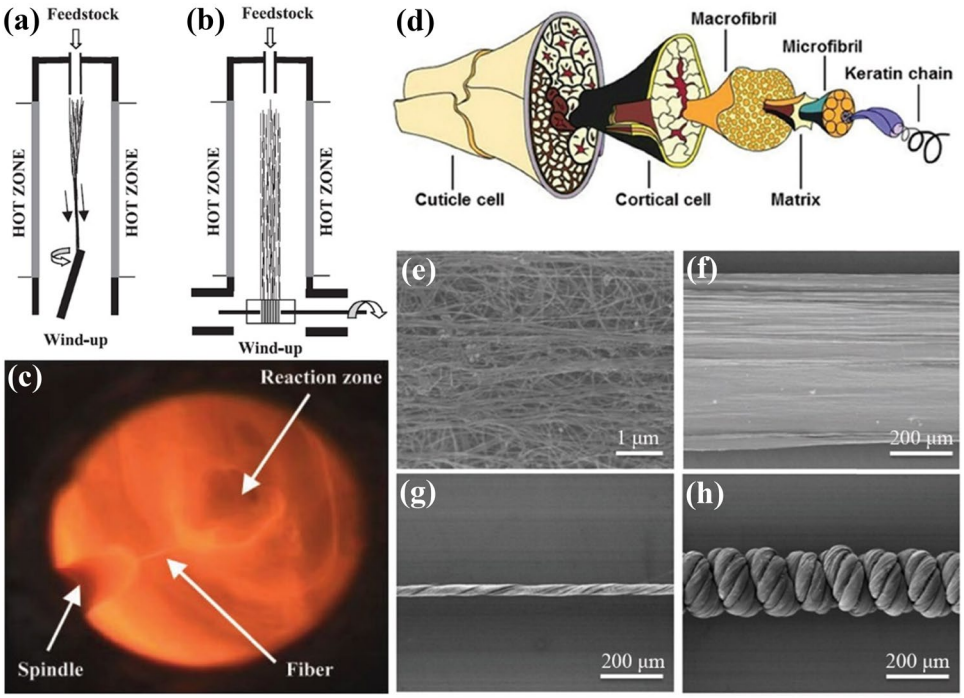

Fig. 14 **a** Schematic of the direct spinning process. **b** Schematic of the clockwork assembly operating at a lower temperature outside the furnace hot zone. **c** The video frame views up the furnace, showing the nanotubes being drawn from the aerogel into the fiber on the spindle [155]. Reproduced with permission from ref. 155. Copyright 2004, American Association for the Advancement of Science. **d** Schematic of the hierarchically helical structure of the wool fiber. **e**, **f** SEM images of CNT ribbon at high and low magnifications, respectively. **g** SEM image of primary CNT-based CBFs. **h** SEM image of the hierarchically helical CNT-based CBFs [162]. Reproduced with permission from ref. 162. Copyright 2017, WILEY–VCH

to prepare CNT-based CBFs with a length of 20 cm in 2002 [11]. During the processing, *n*-hexane was selected as a carbon source and ferrocene/thiophene composition was used as a catalyst, and the prepared fibers showed the tensile strength of ~ 1.2 GPa [11]. Li et al. improved FCCVD method to realize continuous preparation of CNT-based CBFs at the laboratory level in 2004 [155]. The CNT aerogel was mechanically stretched in the gas phase reaction zone, and followed by twisting at a rotating rod to directly obtain pure CNT-based CBFs (Fig. 14a–c). During this process, the number of CNT walls could be adjusted by the sulfur content, carrier gas volume and temperature, resulting in the different performances of CNT-based CBFs. Many methods have been developed to control the number of CNT walls, for example, selecting a carbon source [156], controlling the ratio of thiophene to the catalyst and adding time [157], sulfur doping [158] and adjusting the content of catalyst [159], etc. It was found by Barnard et al. that the SWCNTs with the diameter of 1.1–2.2 nm were easily prepared by using ethanol and toluene as a carbon source, and the high content of DWCNTs with the diameter of 2.2–5.3 nm was obtained by using methanol as a carbon source [156]. Lee et al. investigated the effect of sulfur on the size of iron catalyst particles and synthesized CNTs during the direct spinning of CNT-based CBFs [158]. The DWCNTs with the diameter of 5–10 nm were synthesized from acetone, ferrocene, and thiophene, whereas the single-walled CNTs with the diameter of 1–1.5 nm were obtained from methane, ferrocene, and sulfur, because the anti-agglomeration effects of sulfur atoms [158].

Koziol et al. found that CNT-based CBFs spun from the gas phase had high strength, high axial elastic modulus and high toughness [160]. The orientation and density of CNTs were improved by increasing the speed of winding rates, thereby enhancing the mechanical properties of CNT-based CBFs, therefore, the tensile strength and elastic modulus reached 8.8 GPa and 357 GPa, respectively [160]. Although the method of directly spinning CNT-based CBFs from CNT aerogel is convenient, the obtained fibers tend to contain some impurities including residual catalysts or unreacted carbon, which can adversely affect the performance. Therefore, Lee et al. introduced the esterification of carboxylic acid and 1,5-pentanediol to cross-link between CNTs, thereby improving the mechanical properties of the final fibers [161]. Inspired by wool fibers, Liu et al. designed an aligned CNT-based CBFs with hierarchically helical structure (HHF) (Fig. 14d). It showed excellent mechanical and heating properties because there were many hierarchically

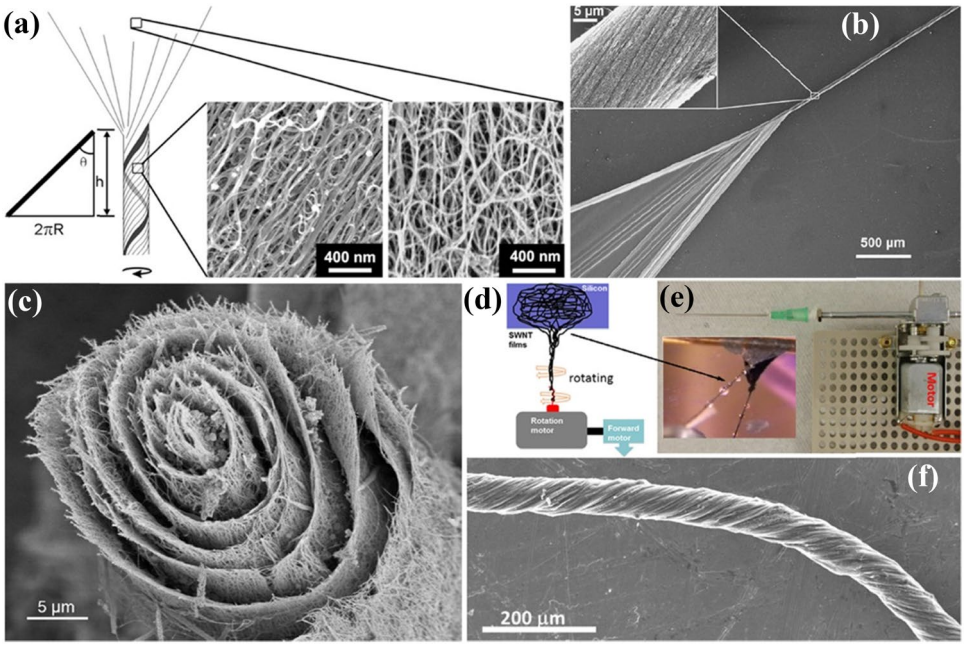

Fig. 15 **a** Schematic of the twisting process and the geometrical elongation for the film near the surface of CNT-based CBF (left), and SEM images of the unstretched and stretched parts of the film (right). **b** SEM image of a CNT-based CBF prepared by twisting a piece of as-grown film with a width of 2 mm and a thickness of 200 nm [12]. Reproduced with permission from ref. 12. Copyright 2009, WILEY–VCH. **c** SEM image of a CNT-based CBF obtained by rolling the double-walled CNT film [165]. Reproduced with permission from ref. 165. Copyright 2010, Elsevier Ltd. **d** Schematics of the spin-fabricating process of CNT-based CBFs. **e** Exhibition of the spinning stage with rotation motor. The inset is a typical image of the fiber spinning process. **f** SEM image of a CNT-based CBF with a diameter of ~ 70 μm [166]. Reproduced with permission from ref. 166. Copyright 2012, Elsevier Ltd

helical voids inside fibers (Fig. 3f and 14e) [162]. The helical primary CNT-based CBFs was fabricated at first (Fig. 14g), followed by bundling these fibers to achieve HHF (Fig. 14h). As a result, it exhibited ultrafast thermal response over 1000 °C/s, low operation voltage of several volts, and high heating stability over 5000 cycles. In addition, for multi-fiber consolidation, Li et al. introduced an adhesion agent of polyethyleneimine into CNT-based CBFs to prepare a robust larger-diameter fiber [163]. The merged fibers exhibited excellent strength retention from the component fibers, high electrical conductivity and stability due to the entanglement action between polyethyleneimine and CNTs.

CNT Films Twisting/Rolling

The CNT films twisting/rolling is a simple and effective method to prepare CNT-based CBFs. Ma et al. first adopted this method to prepare CNT-based CBFs in 2009 [12]. First, CNT films with net structure were prepared by FCCVD, and then cut a piece of CNT tape from CNT films, followed by twisting tape to prepare CNT-based CBFs (Fig. 15a and b). There was a densification procedure before twisting where the films were immersed in acetone to reduce the free volume in fibers. The length and diameter of the fibers were determined by the length and width of an adopted slice of the films. Typically, the length and diameters of the synthesized fibers were 4–8 cm and 30–50 μm, and the tensile strength and elastic modulus were 550–800 MPa and 9–15 GPa, respectively [12]. To improve the mechanical performance, they introduced epoxy and polyvinyl alcohol into CNT-based CBFs to prepare polymer chains-infiltrated composite fibers [164]. The composite fibers exhibited a range of mechanical properties because the volume fraction of CNTs could not be accurately controlled through the infiltration method. As a result, the tensile strength of epoxy and PVA infiltrated fibers were 0.9–1.6 GPa and 0.7–1.3 GPa, respectively, and the corresponding elastic modulus were 30–50 GPa and 20–35 GPa, respectively [164]. In addition, Feng et al. prepared a high-quality DWCNT film in one-step by FCCVD with acetone as a carbon source in an argon flow, then the firm was rolled into a fiber with multiple membrane structure (Fig. 15c) [165]. Interestingly, Song et al. presented a customized technique to spin CNT-based CBFs from SWCNT films by utilizing a motorized pulling/twisting stage [166]. The silicon film was separated from the silicon wafer with a smooth surface, and then the edge of the film was contacted with a custom-made spinning stage with a sharp tip. When the spinning stage was driven using a motor, the fibers were stretched and spun simultaneously (Fig. 15d and e). The diameter of the fiber could be controlled between approximate 30–130 μm by the area initially covered by the film, the speed of spinning/pulling motors and its ratio (Fig. 15f). The

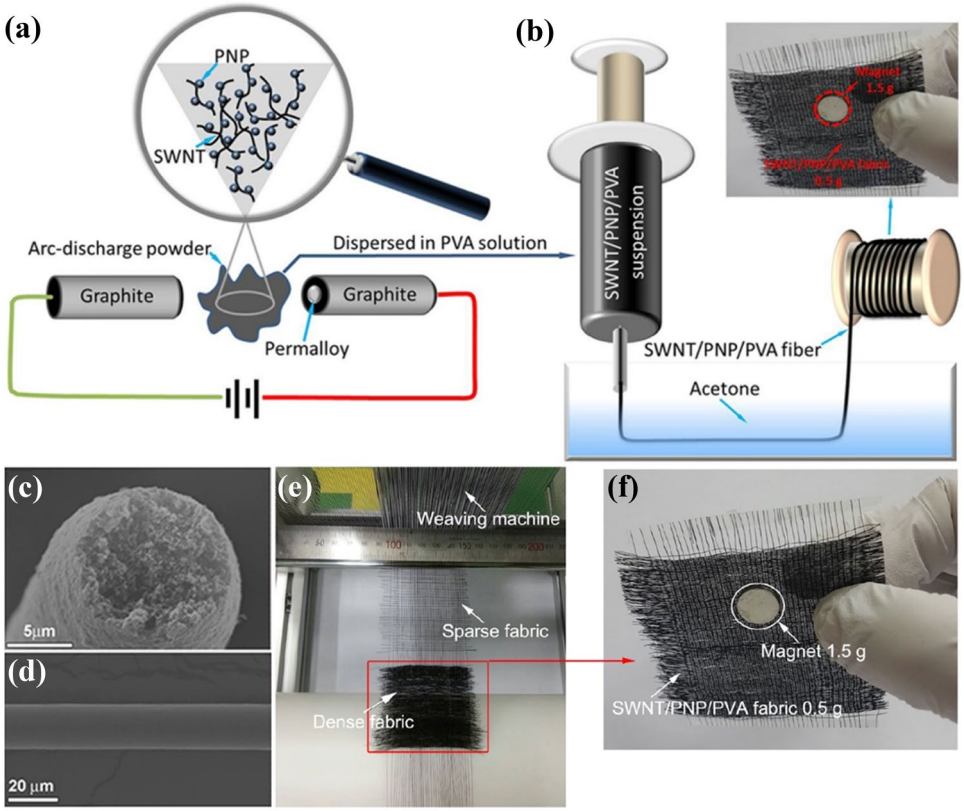

Fig. 16 **a** Schematic of the arc-discharge setup for the fabrication process of SWCNT/PNP: graphite is used as electrodes with permalloy particles embedded in the cathode. **b** Wet spinning process of a SWCNT/PNP/PVA fiber. **c** The cross-sectional morphology and **d** surface morphology of a SWNT/PNP/PVA fiber. **e**, **f** Small magnet is stuck on the fabric [168]. Reproduced with permission from ref. 168. Copyright 2015, American Chemical Society

smaller diameters were achieved by more spinning cycles and slower retraction speed. Although CNT films twisting/rolling can prepare CNT-based CBFs simply, it is not suitable for the production of continuous fibers due to the limitation of the size of CNT films.

CNT-Based CBFs Application

In the past few decades, verious functional devices and composite materials based on CNT-based CBFs have been continuously developed due to the inherent excellent properties of CNT-based CBFs, such as high strength/toughness composite fibers, sensors, actuators transmission lines, supercapacitor, etc. Therefore, the high performance of fibers enhance the development of the tip-fields.

High Strength/Toughness/Conductivity Composite Fibers

CNT-based CBFs with excellent thermal, electrical and mechanical performance are selected to compound with other matrix materials to greatly improve various properties. In the past few decades, verious matrix materials have been adopted to achieve the purpose of enhancing composite fiber properties, such as epoxy resin, PVA, carbon, polyamines, dicyclopentadiene and polydimethylsiloxane. Mora et al. reported CNT-based CBFs-reinforced epoxy matrix composites through the back diffusion of the uncured epoxy into an array of aligned CNT-based CBFs, which was similar to standard composite materials reinforced with commercial fibers in many respects [167]. The tensile strength and stiffness of composite fiber (27% fiber volume fraction) reached 253 MPa and 18.8 GPa, respectively, which was better than that of epoxy (43.0 MPa and 1.2 GPa) [167]. Zhou et al. fabricated high-strength SWCNT/ permalloy nanopowder/PVA multifunctional nanocomposite (SWCNT/PNP/PVA) fibers by wet spinning [168]. The SWCNT/PNP was fabricated by the arc-discharge method with permalloy particles as a catalyst which was embedded in a graphite cathode (Fig. 16a). Then, dispersing SWCNT/PNP in PVA solution to perform wet-spinning to obtain SWCNT/PNP/PVA fibers (Fig. 16b). The composite fiber possessed a smooth and

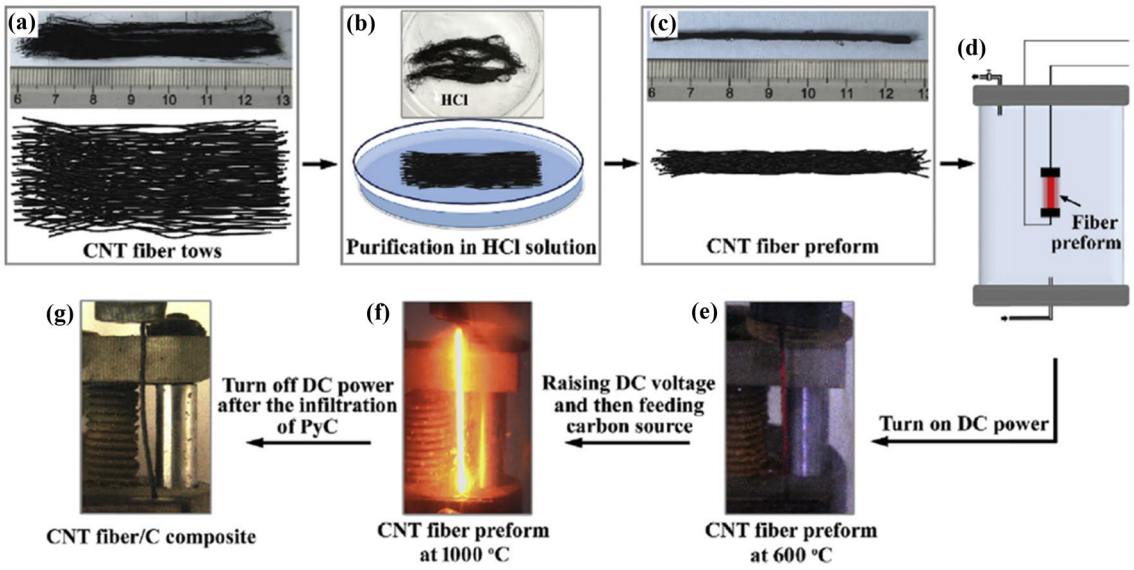

Fig. 17 Overview of the preparation process of CNT-based CBFs/carbon composites by ECVI. **a** Exhibition of CNT-based CBFs tows. **b** Exhibition of the purification of fibers in HCl solution. **c** Exhibition of the CNT-based CBFs preforms. **d** Schematic of equipment for ECVI. **e–g** Exhibition of the fabrication process of CNT-based CBFs/carbon composites [171]. Reproduced with permission from ref. 171. Copyright 2019, Elsevier Ltd

uniform surface with a diameter of 18 μm (Fig. 16c and d), and the failure strength, electrical conductivity and magnetic property (PNP content is 38.0 wt%) were 700 MPa, 96.7 S/m and 24.8 emu/g, respectively. Meanwhile, the fiber could be woven into a piece of fabric by a weaving machine (Fig. 16e), showing a good magnetic property (Fig. 16f). Wu et al. also presented a "layer-by-layer" method to prepare CNT/polymer composite fibers by using PVA as an exemplary polymer [169]. Hollow cylindrical CNTs were continuously produced in a high-temperature reactor, shrank in PVA solution, and deposited on a movable substrate line to obtain composite fibers. The tensile strength and electrical conductivity of composite fibers were 1255 MPa and 1948 S/cm, respectively, which was more than that of PVA matrix (50 MPa and 0 S/cm) [169].

Zhang et al. adopted phenolic resin as a carbon source to prepare CNT-based CBFs/carbon composites, successfully improving the strength and electrical conductivity [170]. During the fabrication process, the polydopamine (PDA) formed on the surface of CNTs through an auto-oxidative reaction, followed by pyrolysis to build the effective physical interlocking and conductive pathways at the interface between CNTs and carbon matrix, resulting in better load transfer and electron transport. The tensile strength and the electrical conductivity of fibers reached 727 MPa and 2.1×10^3 S/cm, respectively [170]. Feng et al. reported a facile and efficient strategy for preparing CNT-based CBFs/carbon composites via electrified preform heating chemical vapor infiltration (ECVI) [171]. CNT-based CBFs were fabricated by FCCVD (Fig. 17a), followed by acid treating to dissolve the metal catalysts and twisting to form unidirectional preforms (Fig. 17b and c). CNT-based CBFs preform was clamped between graphite electrodes, and the voltage was applied to reach the reaction temperature of 1000 °C, followed by adding hexane as a carbon source to prepare CNT-based CBFs /carbon composites (Fig. 17d–g). The performance of the composites could be adjusted by different ECVI times. The optimized CNT-based CBFs/carbon composites exhibited a combination of tensile strength (205 MPa), excellent conductivity (431 S/cm), light weight (1.21 g/cm^3), as well as the fracture strain (21.2%).

Additionally, numbles of metal ions and nanocarbon materials are introduced into CNT-based CBFs to mainly improve the conductivity of the composites, such as copper, silver and graphene. Han et al. reported an effective method to fabricate CNT-based CBFs/Cu composites through PVD and drawing [172]. CNT-based CBFs were fabricated by FCCVD, then the copper film was coated on the surface of the fibers by PVD (Fig. 18a). CNT-based CBFs/Cu composites were drawn through a small die hole to satisfy the densification and alignment (Fig. 18b). The electrical conductivity and ampacity of composite fibers increased from 7.64×10^6 S/m and 5.76×10^3 A/cm^2 to 1.37×10^7 S/m and 1.09×10^4 A/cm^2, respectively, and tensile strength increased from 258 to 515 MPa [172]. Rho et al. reported the preparation of continuous CNT-based CBFs/Cu composites with a high current-carrying capacity due to the existence of Cu nano fibrillar structures [173]. During the early stage of electrodeposition, Cu was electroplated on continuous fibers and Cu fibril structures were embedded in the voids inside the

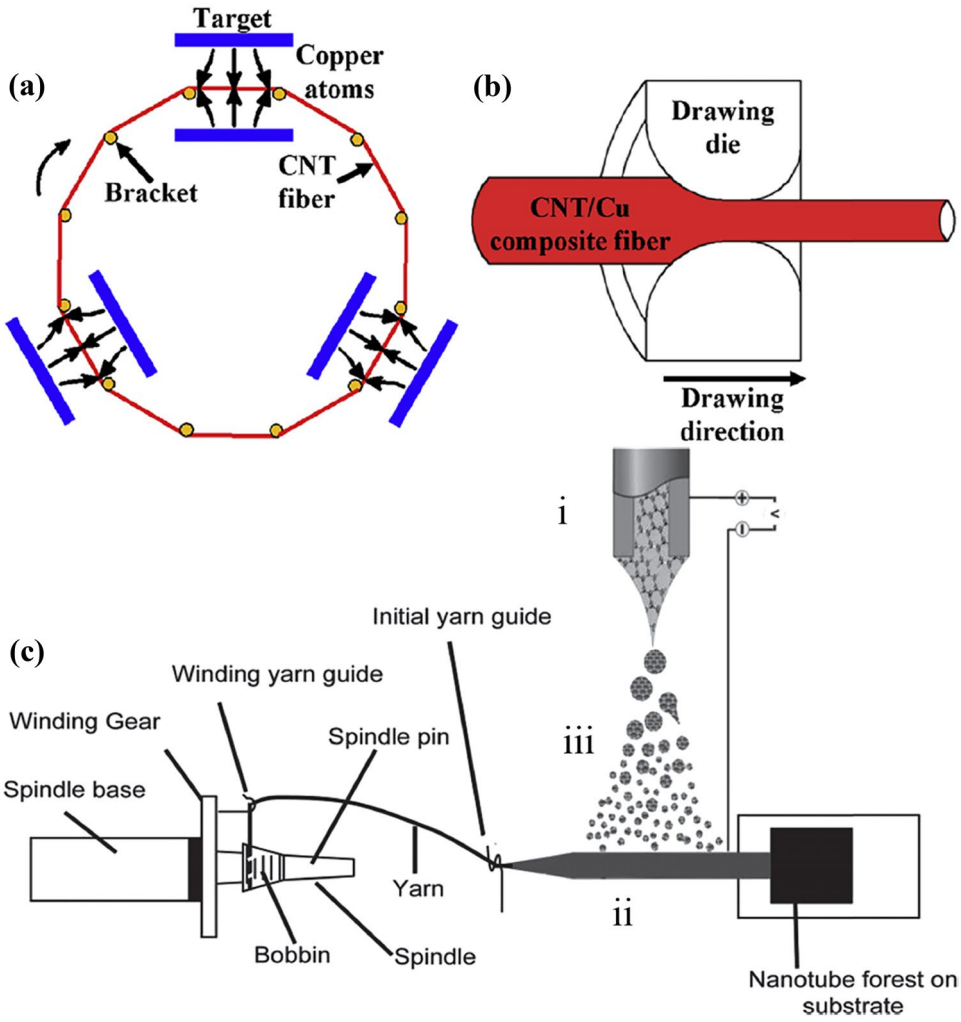

Fig. 18 Schematic of **a** PVD of copper on the CNT-based CBFs, and **b** drawing treatment processing for CNT-based CBFs/Cu composites [172]. Reproduced with permission from ref. 172. Copyright 2017, Elsevier Ltd. **c** Schematic of continuous production of hybrid CNT/graphene fibers. (i) Electrospinning setup used for graphene deposition; (ii) MWCNT sheets drawn from spinnable forest and employed as graphene collector; (iii) graphene dispersion (electrospray) [172]. Reproduced with permission from ref. 176. Copyright 2014, WILEY–VCH

fibers, so that the effective ampacity reached ~ 1×10^7 A/cm^2 [173]. Moreover, silver/polymer can also improve the mechanical and electrical abilities of CNT-based CBFs, and the composite fiber is still flexible after infiltration [174]. The introduction of graphene will greatly enhance the comprehensive performance of composite materials because of the intrinsic properties of graphene. Zhong et al. fabricated DWCNT/graphene multiple-thread fibers by FCCVD and posted-stretching processing [175]. DWCNT bundles wrapped by graphene in the monofilament fibers were highly disordered. The hybrid multiple-thread fibers were twisted to form one fiber, of which tensile strength and electrical conductivity were 300 MPa and 10^5 S/m, respectively [175]. In the further study, Foroughi et al. adopted MWCNTs and graphene to prepare MWCNT/graphene hybrid fibers with excellent electrical conductivity of > 900 S/cm [176]. The arrays of vertically aligned MWCNTs were converted into indefinite long MWCNT sheets by drawing. Then the graphene flakes were deposited onto MWCNT sheets by electrospinning to form a composite structure. Finally, the composites were twisted to fabricate fibers (Fig. 18c). Lepak-Kuc et al. developed a theoretical model to explain the role of CNTs and graphene in the hybrid networks [177]. The graphene was not only effective conductive fillers of CNT networks, but also the effective bridges to introduce additional states at the Fermi level of CNTs.

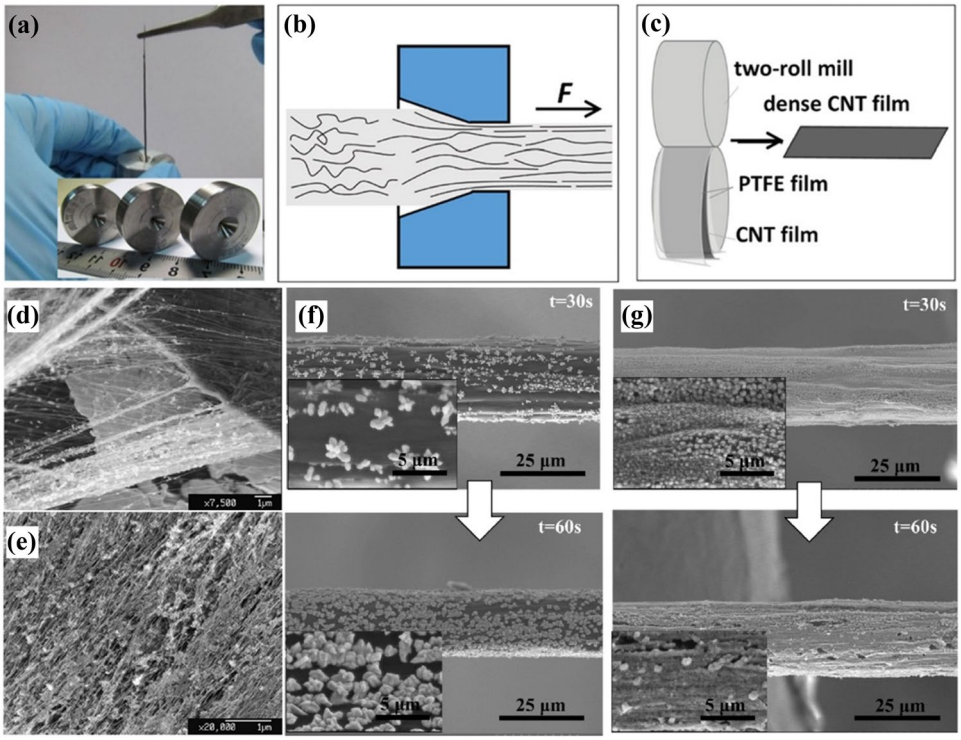

Fig. 19 **a** Exhibition of a CNT-based CBFs was drawn through a diamond wire-drawing die. Inset was optical image of some diamond wire-drawing dies. **b** Schematic of the morphological changes of CNT bundles passing through the dies. **c** Schematic of the fabrication of dense CNT films by rolling [181]. Reproduced with permission from ref. 181. Copyright 2015, IOP Publishing Ltd. **d** SEM images of silver clusters attached to individual CNT bundles and **e** the distribution of silver on the lateral surface of the fiber [182]. Reproduced with permission from ref. 182. Copyright 2014, Elsevier Ltd. **f** SEM images and the insets show the electrodeposition of Cu on as-received CNT wires and **g** Au-sputtered CNT wires in 60 s [183]. Reproduced with permission from ref. 183. Copyright 2019, Elsevier Ltd

Transmission Lines

CNT-based CBFs with excellent conductivity can be selected to fabricate transmission lines. For conductive materials, low resistance and high conductivity are the main evaluation indexs that determine the ability of the wires. The electrical properties of CNTs play a decisive role in the intrinsic conductivity of CNT-based CBFs. Generally, according to their atomic structures, CNTs can be divided into metallic and semiconducting, the electrical conductivity of the former is higher than that of the latter [178]. Therefore, the better conductivity of CNT-based CBFs will be obtained by using metallic CNTs. In addition to the type of the CNTs, many techniques have been developed to improve the conductivity of CNT-based CBFs, such as type enrichment, doping, alignment and densification. Zhao et al. reported the iodine-doped DWCNT cables with an electrical resistivity of ~ 10^{-7} Ω·m and a high current-carrying capacity of 10^4–10^5 A/cm^2 [179]. Moreover, the cables could be connected to arbitrary length and diameter without degrading their electrical properties, and ionic doping was combined with densification to improve the conductivity. Alvarenga et al. adopted a drawing dies to radially densify CNTs sheets into bulk wires, and $KAuBr_4$ doping solution was used to further improve the conductivity during wire drawing [180]. KAuBr4 could significantly reduce the tunneling barrier between individual CNTs and the concomitant doping, meanwhile, the densification process made CNTs closer and lower charge transfer barrier, resulting in enhancing bulk electrical conductivity to 1.3×10^6 S/m [180]. In the further study, the influence of the alignment of the fibers for the conductivity was investigated. Guo et al. fabricated light-weight CNT-based CBFs by drawing macroscopic CNT films through diamond wire-drawing die, and the electrical conductivity was as high as that of stainless steel [181]. The entangled CNT bundles were straightened by tension to improve the alignment (Fig. 19a–c), simultaneously, the intertube space and contact resistance were reduced by the process of diamond wire-drawing dies, leading the conductivity reached 1.6×10^6 S/m [181]. The introduction of metals also significantly improves the conductivity of CNT wires, such as gold, silver and copper. Lekawa-Raus et al. prepared a hybrid CNT-based CBFs/silver conductor by introducing silver nanoparticles into the CNT network [182]. The silver nanoparticles acetone suspension solution with extremely low surface tension and viscosity was uniformly coated on the CNT-based CBFs. The

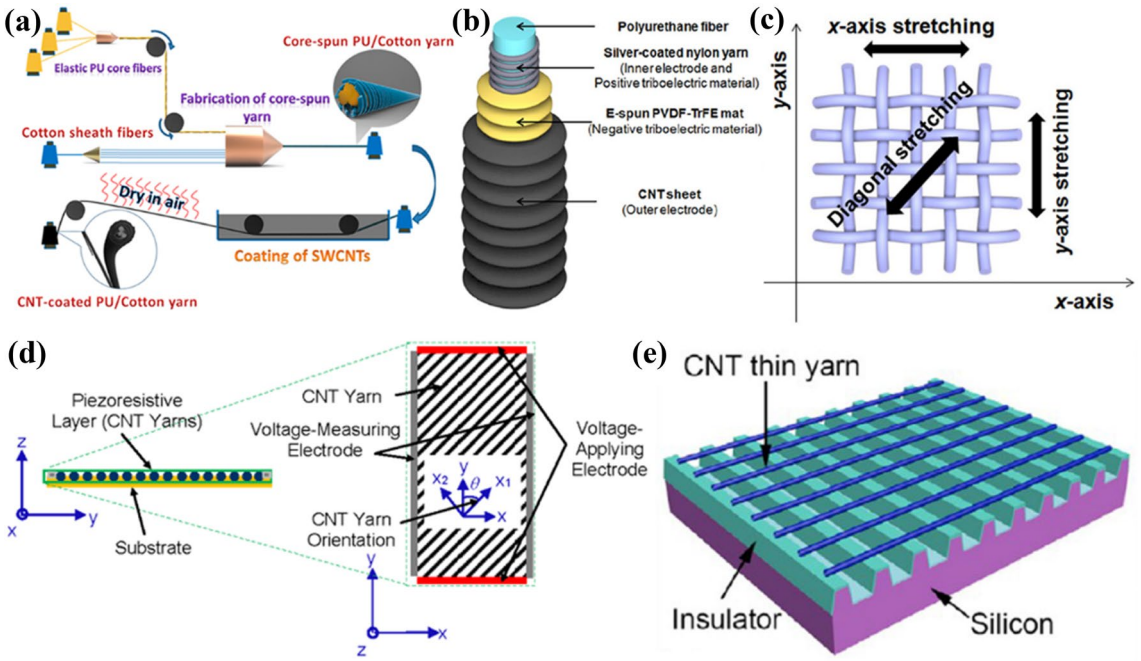

Fig. 20 **a** Schematic of the self-developed fabrication process of the PU/cotton/CNT-based CBFs [188]. Reproduced with permission from ref. 188. Copyright 2016, American Chemical Society. **b** Schematic of stretchable triboelectric structure. **c** Schematic of experimental setup of motion sensing fabric [189]. Reproduced with permission from ref. 189. Copyright 2016, The Authors, published by Springer Nature. **d** Schematic of cross-section of the four-terminal strain gauge sensor comprised of CNT-based CBFs. Inset: top schematic view of the arrangement of the CNT-based CBFs and the electrodes including unidirectional and bidirectional configurations [190]. Reproduced with permission from ref. 190. Copyright 2015, IOP Publishing Ltd. **e** Schematic of the CNT thermoacoustic chip [191]. Reproduced with permission from ref. 191. Copyright 2013, American Chemical Society

nanosilver clusters were adhered to CNT bundles after solvent evaporating, forming an evenly distributed silver phase (Fig. 19d and e). Therefore, the silver doping improved the conductivity of CNT-based CBFs and promoted their applications on transmission lines. Thang et al. synthesized CNT wires by wet-spinning, and made Au and Cu deposite on wires to produce high-performance CNT/Au/Cu composite wires by sputtering and electroplating two-step deposition method [183]. It was found that the deposition of Cu on the CNT wires was more homogeneous due to the improvement of wettability and reactivity of the wire surface (Fig. 19f and g). The tensile strength and electrical conductivity of the composite wires reached 0.74 GPa and 4.65×10^5 S/cm, respectively. Moreover, the composite wires with high CNTs volume fraction were expected to be light-weight, which was a promising candidate to substitute conventional heavy metal wires in the future transmission applications. In addition, some studies have been developed to improve the comprehensive properties of CNT-based CBFs. The poly (dimethyl siloxane) is introduced into CNT-based CBFs to enhance the flexibility of the fiber-based conductor [184], and the polyimide aerogels are used as the dielectric layer for CNT wires to achieve the electrical insulation properties without changing the conductivity [185].

Electronic Sensors

The electronic sensors fabricated by CNT-based CBFs with excellent electric response capability have been developed in recent years, which are generally divided into three types: strain sensors, thermal and potentiometric sensors and biological sensors. Zhao et al. first developed a prototype CNT-based CBFs strain sensor by CNT array spinning and the deposition of aluminum electrodes in 2010 [186]. It showed consistent piezoresistive behavior under repetitive straining and unloading, as well as good resistance stability at temperatures ranging from 77 to 373 K [186]. In further study, the twisting technology was introduced into CNT-based CBFs to improve flexibility [187]. The tensile strain was improved from 1 to 500%, meanwhile, the relative resistance maintained highly stable and reproducible during 100 stretchings (strain 500%) cycles [187]. Moreover, the twisted CNT-based CBFs can be used to fabricate a reusable rotational actuation with energy densities of 8.3 kJ/kg [187]. Elastic polymers, such as polyurethane (PU), can also improve the flexibility of the CNT-based CBFs. Wang et al. used a highly reliable, stretchable and conductive composite fibers as an effective strain sensor through a self-designed coating approach to incorporate highly conductive SWCNTs into

the elastic cotton/PU core-spun fibers (Fig. 20a) [188]. The sensor could reach 300% strain and maintain stability during nearly 300,000 stretching (40% strain) cycles, moreover, it was also able to detect and monitor the movement of human limbs, such as fingers, elbows and even the wink of eyes [188]. In the further research, Sim et al. introduced triboelectric technology into fiber to prepare a self-poared strain sensor, which used the silver-coated nylon/PU as core fiber and the wrinkled polyvinylidene fluoride-co-trifluoroethylene/CNT layer as shell (Fig. 20b) [189]. During tensile deformation, the reversible distance change induced by the Poisson's ratio difference between the core fiber and the shell was the reason for electrical generation. The sensors exhibited 50% resilience and maintained high-performance after 10,000 stretching cycles. Moreover, it was woven into a textile as sensors to detect the magnitude and direction of the motion (Fig. 20c). Jandro et al. presented a foil strain gauge sensor by using CNT-based CBFs as the piezoresistive sensing element (Fig. 20d) [190]. The result of parametric studies is used to design the sensor, which maximize the sensitivity of the sensors to mechanical loading, so that it can detect the deformation and maintain stability during the cycle process. Besides, Wei et al. fabricated thermoacoustic chips with CNT-based CBFs arrays on patterned silicon wafers (Fig. 20e) [191]. They showed excellent mechanical robustness and thermoacoustic effect that could be used at the loudspeakers and earphones.

CNT-based CBFs-based temperature sensors with miniaturized and flexible capabilities have received wide attention. According to researches, the introduction of polymer can improve the performance of temperature sensings, such as epoxy resin and poly (vinylidene fluoride) (PVDF). Sibinski et al. adopted PVDF to prepare a temperature sensor since its sufficient temperature resistance, good flexibility and proper adhesion, therefore, it could be easily integrated into textronic inner garments [192]. Moreover, Guinovart et al. presented a simple and generalized approach to build electrochemical sensors. Interestingly, the commercial cotton fibers were turned into electrical conductors through the dyeing process by using a CNT ink, and then partially coated with a suitable polymeric membrane to build ion-selective electrodes [193]. The sensor could sense the concentration of pH, K^+ and NH_4^+, more importantly, it showed the limits of detection and the linear ranges that were similar to those electrodes obtained with lab-made solid-state ion-selective.

In terms of biological sensors, Schmidt et al. demonstrated a CNT-based CBFs-based sensor to detect electroactive neurotransmitter dynamics in the brain [194]. CNT-based CBFs electrodes coupled with fast-scan cyclic voltammetry (FSCV) are used to discriminately detect rapid neurotransmitter fluctuations in acute brain slices, such as dopamine, adenosine and serotonin. The presence of CNT-based CBFs can improve the selectivity, sensitivity, and spatial resolution of the microelectrode, as well as faster apparent electron transfer kinetics. Moreover, it is found that in the process of characterizing CNT-based CBFs microelectrodes for high-speed measurements with FSCV, the detection of dopamine by CNT-based CBFs microelectrodes can simultaneously achieve high sensitivity, high sampling frequency and high time resolution [195]. Similarly, many technologies have been developed to improve the surface topography of the electrode and increased its selectivity and sensitivity, such as laser treating, oxygen plasma etching, antistatic gun treating, chlorosulfonic acid treating and nafion polymer coating [196–199]. As an example, Yang et al. introduced oxygen plasma etching and antistatic gun treating to modify the surface of CNT-based CBFs microelectrodes [197]. The current for dopamine was increased threefold by single oxygen plasma etching and fourfold by single antistatic

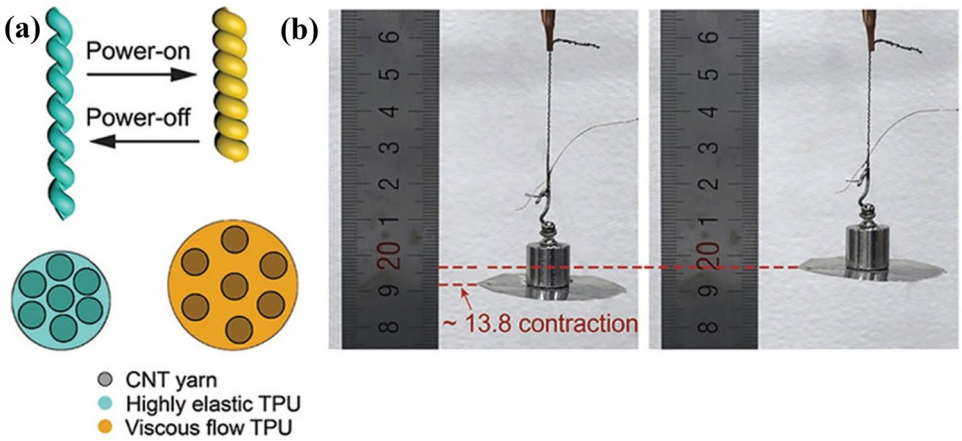

Fig. 21 **a** Actuation mechanism of CNT-based CBFs/TPU composite actuator. **b** Exhibition of a spiral CNT-based CBFs/TPU composite driver [205]. Reproduced with permission from ref. 205. Copyright 2018, Society of Chemistry

gun treating, as well as 12-fold by the combination of above two methods. It is found that oxygen plasma etching will increase surface oxygen content without affecting the surface roughness, while the antistatic gun treating will increase surface roughness without changing oxygen content, so that the sensitivity was improved by both of above two technologies.

Actuators

The intelligent actuators made of CNT-based CBFs usually have the ability to twist and stretch when it is subjected to external stimuli such as chemical, electric and thermal. Foroughi et al. designed a three-electrode electrochemical system by using an electrolyte-filled twist-spun CNT-based CBFs which could provide a reversible 15,000 rotations and 590 revolutions per minute, since the fiber volume was increased by electrochemical double-layer charge injection [200]. In the further study, Lee et al. adopted solid gel to replace electrolyte to prepare all-solid-state CNT-based CBFs muscles with the tensile contraction of 16.5% and the contractile energy conversion efficiency of 5.4% [201]. The tensile contractions of parallel muscles and braided muscles assembled by several fibers were 11.6% and 5%, respectively [201]. Kim et al. demonstrated hierarchically twisted CNT-based CBFs artificial muscles with a contractile work capacity of 3.78 kJ/kg which was 95 times more than the work capacity of mammalian skeletal muscles [202]. Besides, the actuator could be excited without electrochemical infiltrating of polymer, such as paraffin wax, polystyrene (PS), poly(styrene-b-isoprene-b-styrene) (SIS) and polyurethane (PU), etc. Lima et al. designed a paraffin wax-infiltrated, twist-spun CNT-based CBFs as electrolyte-free muscles that could spin a rotor at an average 11,500 revolutions/minute or deliver 3% tensile contraction at 1200 cycles/minute [203]. The volume of paraffin wax could be changed by external stimuli, such as electrical, chemical or photonic excitation, thereby generating torsional rotation and contraction of the fiber. In further study, Kwon et al. compared the effects of different polymers on fiber rotation [204]. The results showed that PS-infiltrated CNT-based CBFs muscles possessed larger rotation (29.7 deg/mm) than that of those

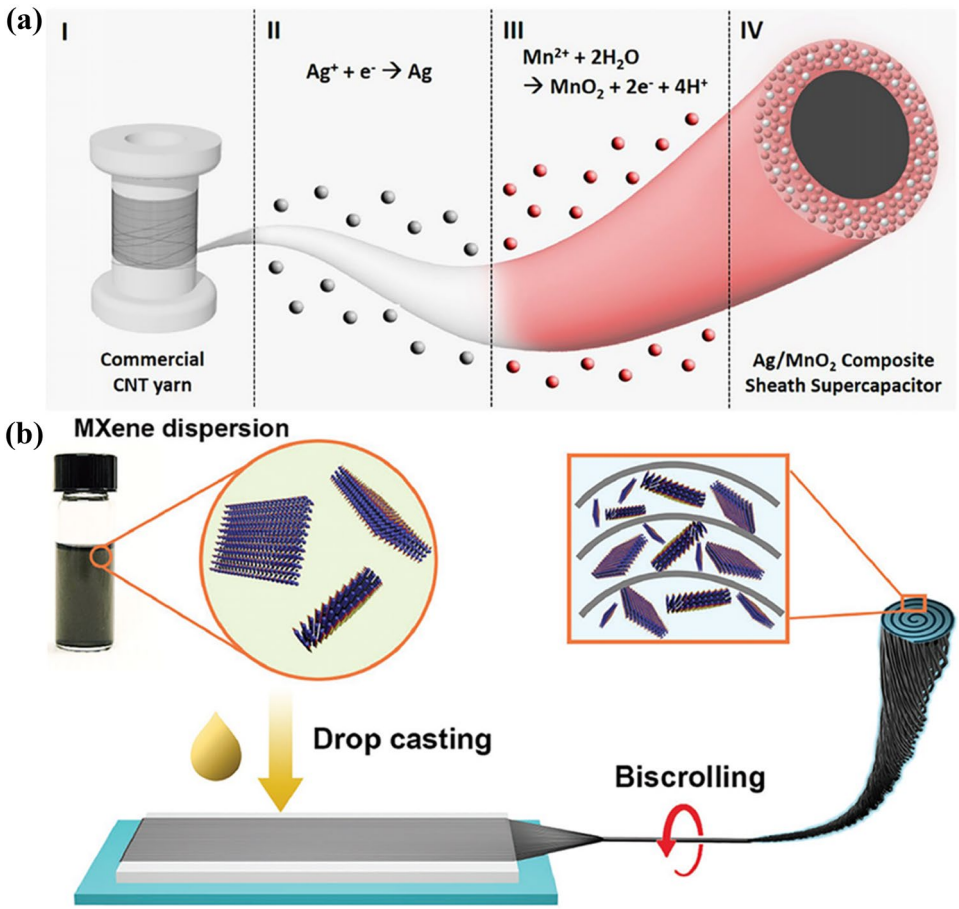

Fig. 22 **a** Schematic of the fabrication process of Ag/MnO_2 composite sheath fibers [210]. Reproduced with permission from ref. 210. Copyright 2018, Nature Publishing Group. **b** Schematic of the fabrication process of MXene/CNT fibers [213]. Reproduced with permission from ref. 213. Copyright 2018, WILEY–VCH

SIS-infiltrated CNT-based CBFs muscles (14.4 deg/mm). Song et al. prepared an electrothermally reversible actuator by using CNT-based CBFs and thermoplastic PU resin (TPU) with excellent shape memory, contraction and stability (Fig. 21a) [205]. A large stretching stroke was obtained within 5 s (about 13.8%) when lifting load was ~ 1905 times more than the weight of the actuator (Fig. 21b). Moreover, the tensile actuation of the actuator was 3.6% when the stress was more than 33 MPa (corresponding to 28 400 times the weight of actuator), which was about 30 times higher than the recovery stress of shape memory polymer.

Supercapacitors (SCs)

SCs with the ability to store electrical energy, have been widely investigated, which possess the better energy density and longer cyclic lifetimes than that of traditional capacitors and lithium batteries. In recent years, CNT-based CBFs with excellent conductivity are used to prepare excellent SCs, and many methods have been developed to improve energy density and intrinsic capacitance of SCs. Lee et al. designed a hybrid nanomembranes with high mechanical strength and flexibility to prepare SCs that are made of densified CNT sheets coated with poly(3,4-ethylenedioxythiophene) [206]. The hybrid nanomembrane attached to a current collector exhibited volumetric capacitance of ~ 40 F/cm^3 at 100 V/s [206]. SCs with diameters of ~ 30 μm were obtained by twisting the hybrid nanomembranes, and its volume energy and power density were ~ 47 mWh/cm^3 and ~ 538 mWh/cm^3, respectively. Moreover, Wang et al. prepared SCs by using two individual CNT-based CBFs infiltrated with polyaniline nanowire arrays [207]. As a result, the prepared SCs had high flexibility and an area capacitance of 38 mF/cm^2, which could be easily woven or knitted into conventional textile fabrics to use in wearable electronics. In further study, the gamma irradiation treatment on the surface of CNTs would improve the area capacitance (43 mF/cm^2) owing to the increase of the carboxyl groups [208].

In addition to the introduction of polymers, some metal oxides are also used to improve the electrochemical performance of SCs. Choi et al. prepared a CNT/MnO_2 composite SCs with CNT-based CBFs electrode prepared by twisting MWCNT sheets to achieve high internal porosity followed by MnO_2 depositing [209]. MnO_2 was effectively trapped in the pores during deposition due to the 3D porosity inside the fibers, followed by forming a well-blended zone with aligned CNT bundles. The all-solid-state SCs with KOH gel as the electrolyte achieved good electrochemical performance that the specific capacitance was 25.4 F/cm^3 at 10 mV/s, and energy and average power density were 3.52 mWh/cm^3 and 127 mW/cm^3, respectively [209]. Next, Kim et al. further introduced the Ag layers into MnO_2-deposited SCs to increase the specific areal capacitance and energy density to 322.2 mF/cm^2 and 18.3 μWh/cm^2, respectively [210]. The Ag interlayers would decrease the solid-state charge diffusion length in the MnO_2, and the generated electrons during the charge/discharge process were rapidly collected by the adjacent Ag layer (Fig. 22a). Su et al. produced high performance asymmetric two-ply fiber SCs consisted of CNT-based CBFs as negative electrode and CNT/MnO_2 composites as positive electrode in aqueous electrolyte [211]. As a result, the energy reached 42.0 Wh/kg at a power density of 483.7 W/kg, and 28.02 Wh/kg at 19.25 kW/kg [211]. Co_3O_4 can also be deposited into SCs with H_2SO_4 gel as the electrolyte to improve electrochemical performance, so that the areal capacitance and energy density reached 52.6 mF/cm^2 and 1.10 μWh/cm^3, respectively [212]. Moreover, transition metal MXenes can be used in SCs due to its high electrical conductivity and hydrophobic surface. As an example, Wang et al. prepared MXene/CNT SCs with the 3 M H_2SO_4

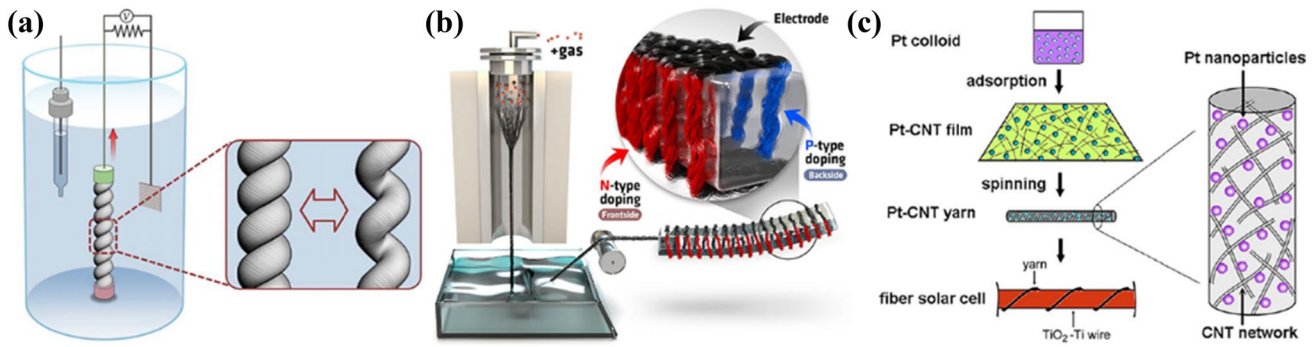

Fig. 23 **a** Schematic of a torsionally tethered coiled harvester electrode and counter and reference electrodes in an electrochemical bath, showing the coiled fibers before and after stretching [220]. Reproduced with permission from ref. 220. Copyright 2017, American Chemical Society. **b** Schematic of the flexible CNT-based thermoelectric generators based on CNT-based CBFs [221]. Reproduced with permission from ref. 221. Copyright 2017, American Chemical Society. **c** Schematic of the preparation processes of Pt-adsorbed hybrid fibers and application as counter electrodes for fiber solar cells [225]. Reproduced with permission from ref. 225. Copyright 2012, American Chemical Society

as the electrolyte by crolling MXene-coated CNT sheets (Fig. 22b) [213]. MXene/CNT SCs with double MXene/CNT electrodes showed the specific capacitance of 1083 F/cm^3, the SCs with Mxene/CNT and RuO_2/CNT electrodes achieved a maximum energy density of 61.6 mWh/cm^3 and a power density of 5428 mW/cm^3, which were suitable for small electronic devices [213].

The metal wires, such as Pt and Cu, are also introduced into SCs to improve the electrochemical performance. Zhang et al. presented core/sheath structured linear SCs through one-step continuous spinning with CNT-based CBFs as sheath and Pt wire as core [214]. Pt wire served as a current collector could make charges produced on the active materials transport efficiently along the length of the SCs. The gravimetric capacitance and areal capacitance of SCs (PVA-H_3PO_4 Gel as the electrolyte) reached 86.2 F/g and 52.5 mF/cm^2, respectively [214]. Kim et al. prepared the SCs by using giant GO sheets and SWCNTs, while it showed relatively low areal capacitance of 2.38 mF/cm^2 in LiCl gel electrolyte [215]. To increase electrochemical performance, Kou et al. prepared two-ply fibers SCs with polyelectrolyte-wrapped graphene/CNT core-sheath fibers as electrodes [216]. The SCs showed capacitance of 269 mF/cm^2 and energy density of 5.91 μWh/cm^2 in the liquid electrolyte (1 M H_2SO_4 solution), as well as 177 mF/cm^2 and 3.84 μWh/cm^2 in a solid electrolyte (PVA-phosphoric acid). Meanwhile, some researchers introduce the elastic matrix into SCs to improve the flexibility, such as polydimethylsiloxane, PU, nylon, rubber and spandex. As an example, Son et al. prepared the fibers with supercoil structure by inserting a giant twist into CNT-wrapped spandex fibers [217]. The fiber exhibited a highly ordered and compact structure along the fiber direction with the elastic deformation up to 1500%. The superelastic SCs were fabricated by incorporating MnO_2 and coating an aqueous PVA/LiCl gel electrolyte on the fibers, and its linear and areal capacitance values were 21.7 mF/cm and 92.1 mF/cm^2, respectively [217]. Moreover, it can be reversibly stretched to 1000% without significant capacitance loss. Similarly, Choi et al. prepared a solid-state SCs with stretchability up to 30% strain, and the fibers electrodes were made by trapping high content (93%) of MnO_2 nanoparticles within the galleries of helically scrolled CNT sheets [218]. Simultaneously, it showed the line capacitance of 60.6 mF/cm, the area capacitance of 888.7 mF/cm^2 and the volumetric capacitance of 154.7 mF/cm^3 [218].

Energy Harvesters

In recent years, energy recovery has attracted increasing attention due to the huge energy demand and the continuous reduction of existing resources. Some new technologies have been developed to transform the external energies into electrical energy which are called "energy harvesters" [219]. For CNT-based CBFs, there are mainly three technologies to realize energy conversion including mechanoelectrical conversion, thermoelectric conversion and photoelectric conversion. Kim et al. reported a CNT-based CBFs harvester that could convert tensile or torsional mechanical energy into electrical energy through electrochemical methods without an external bias voltage (Fig. 23a) [220]. The electric energy generated by the fibers was 250 W/kg as the stretching cycle frequency reached 30 Hz [220]. Moreover, the harvester could be used in the collection of wave energy, respiration sensors and other composite electrical devices.

For thermoelectric conversion, a variety of researchers introduce polymer into individual CNT films to enhance the thermoelectric performance of the final CNT composites, such as polyethylene, poly(vinyl acetate), polyaniline and polyvinylidene fluoride. However, these composite films possess certain limitations in wearable devices. In further research, CNT-based CBFs are selected to fabricate thermoelectric harvesters. Choi et al. proposed a flexible and ultralight thermoelectric generator based on all-carbon CNT-based CBFs without metal electrodes (Fig. 23b) [221].

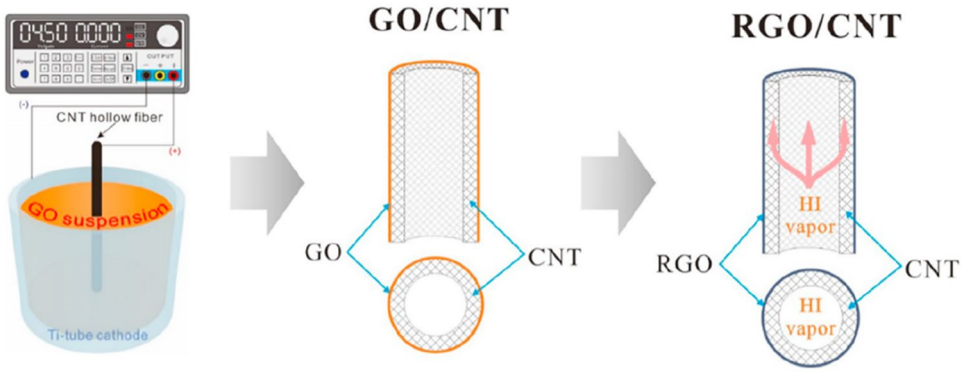

Fig. 24 Schematic of the fabrication process of RGO/hollow CNT-based CBFs membrane [229]. Reproduced with permission from ref. 229. Copyright 2018, Elsevier B.V

Table 2 The various parameters of CBFs prepared by CNTs

References	Precursors	Processing/modification technology	Tensile strength (GPa)	Elastic modulus (GPa)	Conductivity (S/cm)	Applications
[132]	SWCNTs/fuming sulfuric acid	Solution spinning	0.016 ± 0.01	120 ± 10	500	–
[133]	SWCNTs/ultra-high concentration sulfuric acids	Polymer-free spinning	0.065	–	140	–
[135]	SWCNTs/ ethylene glycol	Wet spinning	0.15 ± 0.06	69 ± 41	8×10^4	–
[136]	high aspect ratio CNTs	Wet spinning	2.4	250 ± 60	8.5×10^4	–
[138]	CNTs	CNT arrays	0.564	74	–	–
[144]	MWNTs	CNT arrays	1.068	55	–	–
[146]	CNTs	CNT arrays Polymer Infiltration Curing	2.2 ± 0.15	120 ± 23	–	–
[154]	CNTs	CNT arrays Acidization	1.103	67	3.2×10^4	–
[160]	CNTs	FCCVD Winding	8.8	357	–	–
[164]	CNTs	CNT films twisting/rolling Polymer infiltration	0.9–1.6	30–50	–	–
[169]	CNT/PVA	CNT arrays Solvent shrinking	1.225	15	1948	–
[170]	CNTs/PDA	CNT arrays Auto-oxidative reaction	0.727	–	2.1×10^3	–
[171]	CNTs/graphite	CNT arrays Applied voltage	0.205 ± 0.019	11.2 ± 0.51	431	–
[172]	CNT/Cu	PVD Drawing	0.515 ± 0.011	–	$(1.37 \pm 0.1) \times 10^5$	Ampacity of $(1.09 \pm 0.06) \times 10^4$ A/cm^2
[174]	CNTs/polymer/Silver	CNT arrays Silver-paste liquid infiltration	0.94	24	5.0×10^3	–
[176]	MWCNTs/Grapheme	Electrospinning	0.14 ± 0.01	2.58 ± 0.3	> 900	SCs specific capacitance of > 111 F/g
[183]	CNTs/Au/Cu	Wet-spinning Two-step deposition	0.74	–	4.65×10^5	–
[187]	CNTs	FCCVD CNT films twisting/rolling	0.1	–	–	Rotational actuation energy densities of 8.3 kJ/kg
[188]	SWCNTs/PU/Cotton	Entwining cotton yarns around urethane filament Coating of SWCNTs	–	–	–	Sensors 300% strain and maintain stability during 300,000 stretching cycles
[194]	MWCNTs	CVD Spun into yarns	–	–	–	Microelectrodes enhanced detection of neurotransmitter dynamics in live brain Tissue
[201]	CNT yarn	Opposite direction to the yarn's internal twisting	–	–	–	Artificial muscles tensile contraction of 16.5%

Table 2 (continued)

References	Precursors	Processing/modification technology	Tensile strength (GPa)	Elastic modulus (GPa)	Conductivity (S/cm)	Applications
[206]	CNT sheets/3,4-ethylenedioxythiophene	vapor phase polymerization	0.135	12.6	–	SCs volumetric capacitance of~40 F/cm^3 at 100 V/s
[209]	MWCNTs/MnO_2	MWCNT sheets twisting MnO_2 depositing	–	–	–	Electrolyte specific capacitance of 25.4 F/cm3 at 10 mV/s
[210]	CNT yarn/MnO_2/Ag	Alternating depositions of MnO_2 and Ag layers	–	–	–	SCs specific areal capacitance and energy density of 322.2 mF/cm2 and 18.3 μWh/cm
[212]	CNT yarn/Co_3O_4	Electrodeposition	–	–	–	Two-ply SCs capacitance of 52.6 Mf/cm^2 and energy density of 1.10 $\mu Wh/cm^2$
[218]	CNT yarn/MnO_2	MnO_2 drop casting Biscrolling	–	–	–	Solid-state yarn SCs line capacitance of 60.6 mF/cm
[221]	CNT-based CBFs/polyethyleneimine /FeCl3	n- /p-types doping	–	–	–	Thermoelectric Generators density of 10.85 μW/g and 697 μW/g at a temperature of 5 and 40 K
[226]	CNTs/PTFE/PICNT sheets/Paraffin wax/polyimide	CNT arrays Evaporation Plasma polarization	–	–	–	Fiber-type photoelectric conversion devices output a peak voltage of nearly 150 mV under the light irradiated
[229]	CNT/RGO	Electrophoretic deposition Chemical reduction	–	–	–	Sewage treatment water flux of 22.6 LMH during against DI water feed using 0.5 M NaCl draw solution

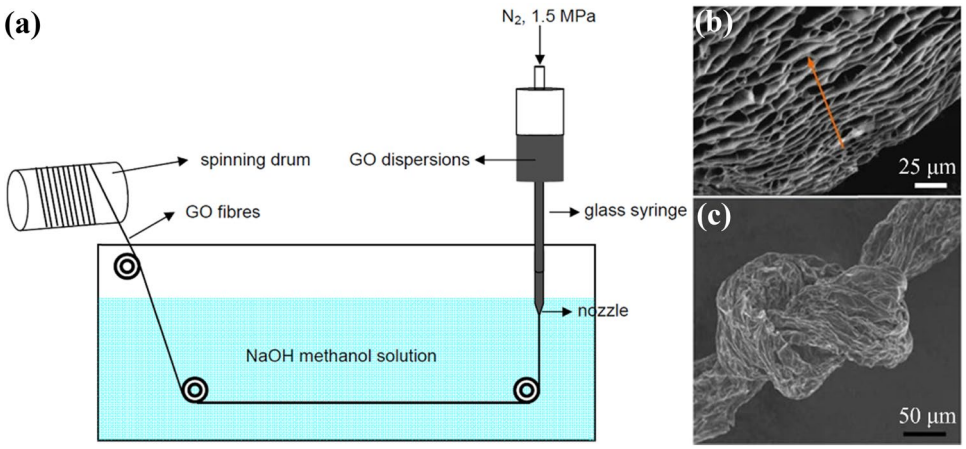

Fig. 25 **a** Schematic of wet-spinning process of GO fibers. **b** Side-view SEM image of assembled GO blocks. **d** The tighten knot of graphene-based CBFs [23]. Reproduced with permission from ref. 23. Copyright 2011, Springer Nature

CNT-based CBFs were alternatively doped into n- and p-types by using polyethyleneimine and $FeCl_3$, respectively, and the highly conductive CNT-based CBFs were used as electrodes between the doped regions to minimize the circuit resistance. The thermoelectric generators based on 60 pairs of n- and p-doped CNT-based CBFs showed the maximum power density of 10.85 μW/g and 697 μW/g at a temperature of 5 and 40 K, respectively [221].

Generally, the photoelectric conversion is used in solar cells, and it is popular for Pt and titanium dioxide (TiO_2) to fabricate solar cells due to the special photoelectric capability [222]. In the past ten years, CNT-based CBFs have been selected to prepare the solar cell for photoelectric conversion. Chen et al. prepared fiber-shaped dye-sensitized solar cells by utilizing CNT-based CBFs and TiO_2 nanoparticles [223]. A CNT-based CBFs incorporated with dye-loaded TiO_2 nanoparticles were used as working electrode and another individual CNT-based CBFs were used as counter electrode, followed by twining to produce the fiber-shaped solar cells with the power conversion efficiency of 2.94% [223]. Liu et al. introduced the semiconducting polymer into fiber-shaped solar cells to improve the flexibility, resulting in power conversion efficiencies from 1.4% to 2.3% [224]. To make the power conversion more efficient, Zhang et al. fabricated TiO_2-based dye-sensitized fiber solar cells with a Pt-CNT hybrid fibers as a counter electrode, and the power conversion efficiency achieved 4.85% under standard illumination (AM1.5, 100 mW/cm^2), which was comparable to the same type of fiber cells with a Pt wire electrode (4.23%) (Fig. 23c) [225]. Besides, Yu et al. presented a novel photoelectric conversion fiber by integrating photomechanical actuation and the electrostatic effect [226]. One electrode was an aligned CNT-based CBF coated with poly(tetrafluoroethylene) to store charges, and the other electrode was made of a bilayer composite strip of CNT sheets/paraffin wax/polyimide for photomechanical actuation. The fiber-type photoelectric conversion device was repeatedly bent and released to change the distance between the strip and the electrodes under the periodical irradiation of visible light, so that the number of induced charges was changed to generate potential differences. As a result, it can output a peak voltage of nearly 150 mV under the light irradiated, as well as exhibiting highly stable and durable properties [226].

Sewage Treatment

In addition to the fields of thermal, electrical and mechanical applications, CNT-based CBFs can also be designed into specific structures for sewage treatment. In recent years, forward osmosis (FO) has become a very popular technology for sewage treatment due to its relatively low hydraulic requirement, simply fouling removal and low energy consumption [227]. Fan et al. first proposed a self-sustained hollow CNT-based CBFs and polyamide thin film composites (CNT TFC-FO) with high porosity, good hydrophilicity and excellent electro-conductivity [228]. In the FO and pressure retarded osmosis modes, the fluxes (against a pure water feed using 2.0 M NaCl draw solution) of the membrane with the thickness of 126 μm was 4.7 and 3.6 times higher than that of the commercial cellulose triacetate TFC-FO membrane, respectively [228]. Moreover, the flux of the membrane increased by about 50% in the process of simulated separation of oil and water at a voltage of 2.0 V [228]. In further research, they adopted reduced GO (RGO) to improve the

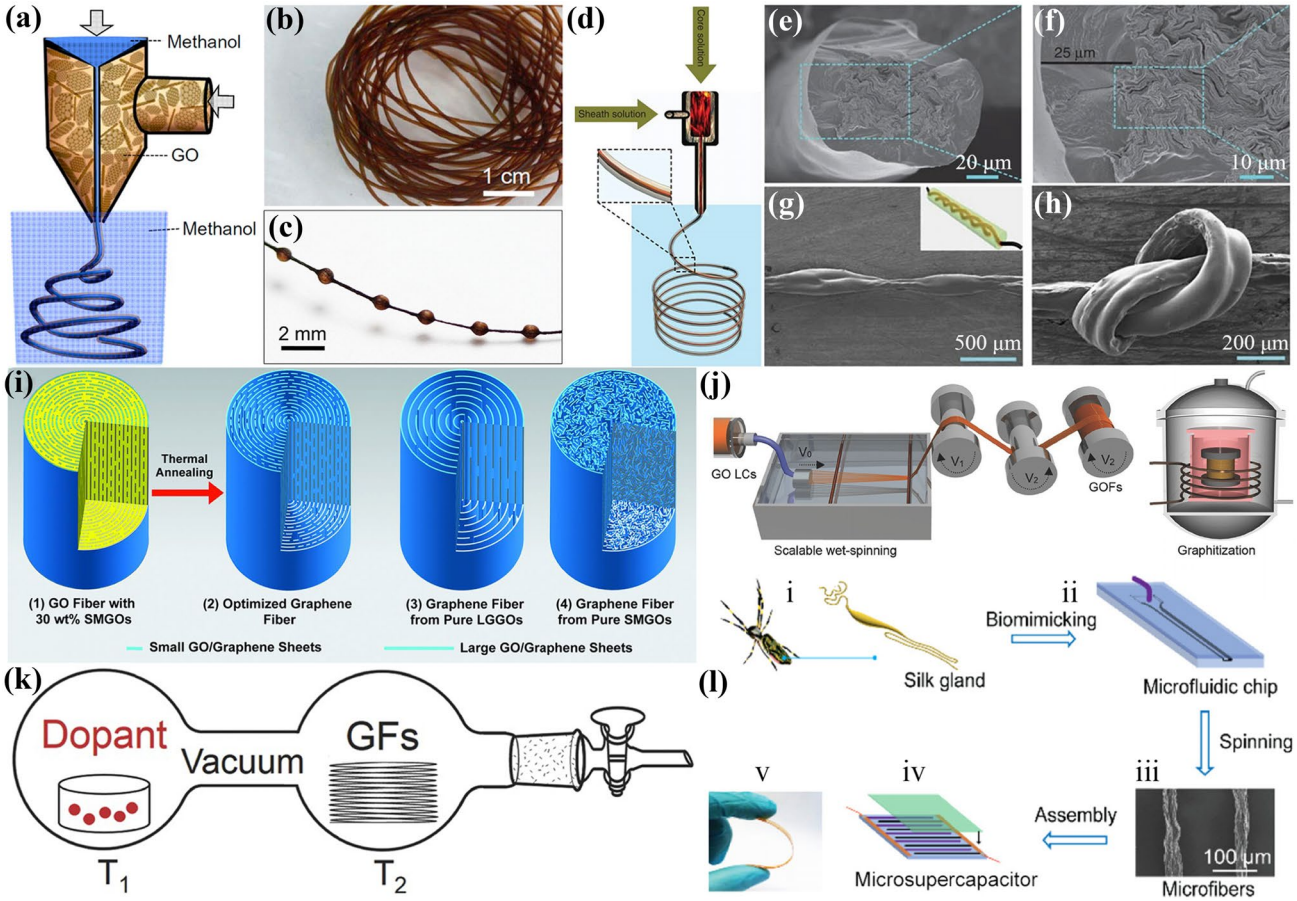

Fig. 26 **a** Schematic of CTCS technology. **b** Photograph of GO hollow fibers. **c** Photograph of GO hollow fibers generated with the air flow rate of 1.0 mL/min [244]. Reproduced with permission from ref. 244. Copyright 2013, American Chemical Society. **d** Schematic of the coaxial spinning process. **e–f** SEM images of GO/sodium carboxymethyl cellulose composite fibers. **g** SEM images of side view of a two-ply SC. **h** SEM image of a two-ply SC knot [216]. Reproduced with permission from ref. 216. Copyright 2014, Springer Nature. **i** Schematic of the "intercalated" structure of the GO fibers and graphene-based CBFs [245]. Reproduced with permission from ref. 245. Copyright 2015, American Association for the Advancement of Science. **j** Schematic of wet-spinning of GO fibers, two-step reduction and thermal annealing [246]. Reproduced with permission from ref. 246. Copyright 2016, Wiley–VCH. **k** Schematic of the preparation of chemically doped graphene-based CBFs via a two-zone vapor transport method [247]. Reproduced with permission from ref. 247. Copyright 2016, Wiley–VCH. **l** (i) Schematic of the biomimicking thought process. (ii) Schematic of the microfluidic channel design and spinning process. (iii) SEM image of the microfibers. (iv) Schematic of the micro SC assembly. (v) Exhibition of the micro SC under bending [248]. Reproduced with permission from ref. 248. Copyright 2018, American Chemical Society

forward osmosis performance [229]. The membranes were fabricated by constructing RGO on a hollow CNT-based CBFs substrates via electrophoretic deposition coupling with chemical reduction processes (Fig. 24). RGO could provide water permeability and ion selectivity due to the ultra-low friction and well-defined interlayer spacing, moreover, its high porosity and good wettability would increase the water flux of CNT hollow fiber substrates. Therefore, the DI water flux of the membrane (0.5 M NaCl draw solution) was 22.6 LMH, which was 3.3 times more than that of the commercial membrane [229]. Eventually, the various parameters of CBFs prepared by CNTs are shown in Table 2.

Graphene-Based CBFs

Graphene-Based CBFs Fabrication

Wet-Spinning with GO LCs

GO LCs are popular substance to fabricate GO fibers explored by Xu et al. [230], and they prepared the first continuous GO fibers by traditional wet-spinning technology in the same year [23]. GO dispersions were injected into NaOH/methanol coagulation bath by using a glass syringe with a nozzle, and GO fibers were wrapped around the spinning drum (Fig. 25a). Eventually, GO fibers were reduced in hydroiodic acid to obtain graphene-based CBFs. The neat

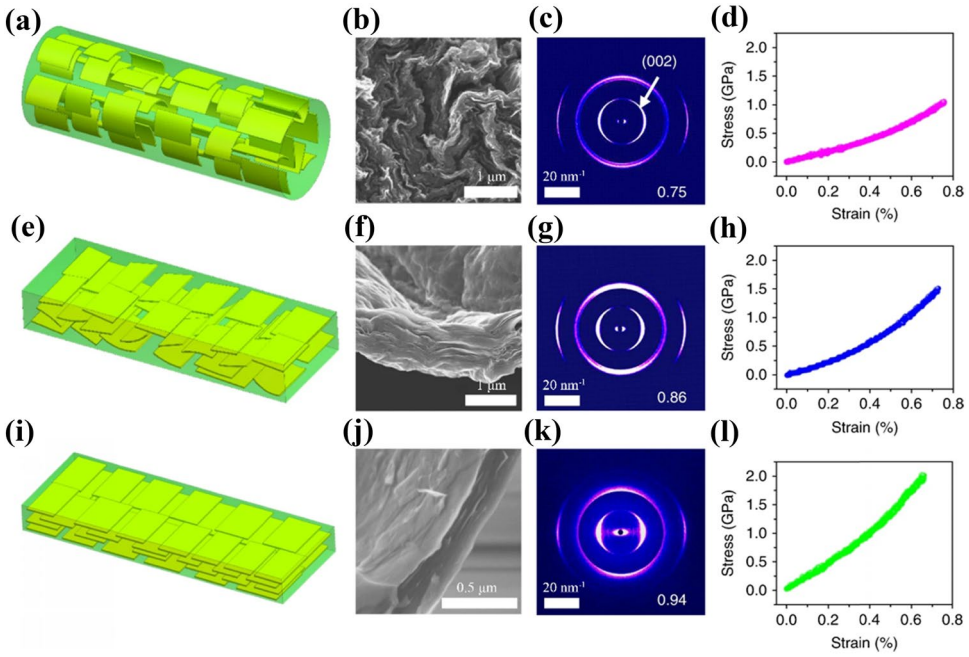

Fig. 27 Schematic of GO sheets flowing in **a** tubular channel, **e** mesophase flat channel, and **i** thinner flat channel. SEM images of **b** wrinkled sheets in the cross-section of the columnar fiber produced from a tubular channel. **f** A layer structure of a graphene belt assembled by a flat channel. **j** A highly ordered and compact structure of a thin graphene belt. **c** Long arc and dispersed intensity of the characteristic (002) reflection on WAXS patterns indicating low sheet orientation along the fiber axis direction. **g** Narrow dispersion of the (002) plane on WAXS patterns indicating enhanced sheet orientation order. **k** A high degree of sheet orientation indicated by the concentrated short arc of the (002) plane on the WAXS pattern. **d**, **h** and **l** are the stress–strain curve of graphene-based CBFs prepared for three different microfluidic channels [24]. Reproduced with permission from ref. 24. Copyright 2019, IOP Publishing Ltd

and tight arrangement of GO sheets have strong interactions between layers (Fig. 25b), which caused high elastic moduli of GO fibers (5.4 GPa) and graphene-based CBFs (7.7 GPa) [23]. Moreover, graphene-based CBFs can be knotted and woven without any break (Fig. 25c). Cong et al. used cetyltrimethyl ammonium bromide (CTAB) to replace NaOH methanol solution to induce the self-assembly of GO sheets because of the electrostatic interaction between CTAB and GO, the tensile strength, elastic modulus and electrical conductivity reached up to 182 MPa, 8.7 GPa and ~ 35 S/cm, respectively [231].

To further improve the mechanical properties of graphene-based CBFs without reduction of the electrical conductivity, the large-scale GO sheets are introduced to fabricate high-strength graphene-based CBFs that the tensile strength and elastic modulus achieve 501.5 MPa and 11.2 GPa, respectively [232]. The fibers possess fewer defects and higher ordered arrangement, leading to better mechanical performance. To investigate the relationship between GO sheets parameters and fibers properties, chen et al. used different kinds of GO sheets to prepare graphene-based CBFs [233]. The results depicted that the performance of graphene-based CBFs was influenced by size, alignment, orientation, inter-sheet interactions, defects and packing density of GO sheets. Moreover, the high-performance graphene-based CBFs were achieved by using large dimension graphene sheets that lead to highly aligned structures and fewer defects [234]. Cao et al. selected GO sheets with two sizes (17 μm and 30 μm) to prepare graphene-based CBFs [235]. It was found that the tensile strength of GO fibers prepared by large GO sheets was higher (267 MPa) than that of the sample prepared by small GO sheets (192 MPa), and the former was improved to 365 MPa after chemical reduction. Wallace et al. prepared the high-performance RGO fibers by the self-assembly of ultralarge GO crystalline dispersions, which showed the elastic modulus of > 29 GPa, the electrical conductivity of 2508 ± 632 S/m, and specific surface area of 2210 m^2/g (2605 m^2/g before reduction), respectively [236]. Besides, various methods can improve the performance of graphene-based CBFs, such as ion-doping [237, 238], coagulation fluid adjusting [239], polymer grafting [240], bionic structure designing [241], etc. Huang et al. used universal GO precursors to prepare graphene-based CBFs by hydrogel-assisted spinning [242]. The rolling process could improve the performance of graphene-based CBFs that the tensile strength, elongation, and average density were 238 MPa, 2%, and 1.7960 g/cm^3, respectively [242]. Chen et al. developed a scalable

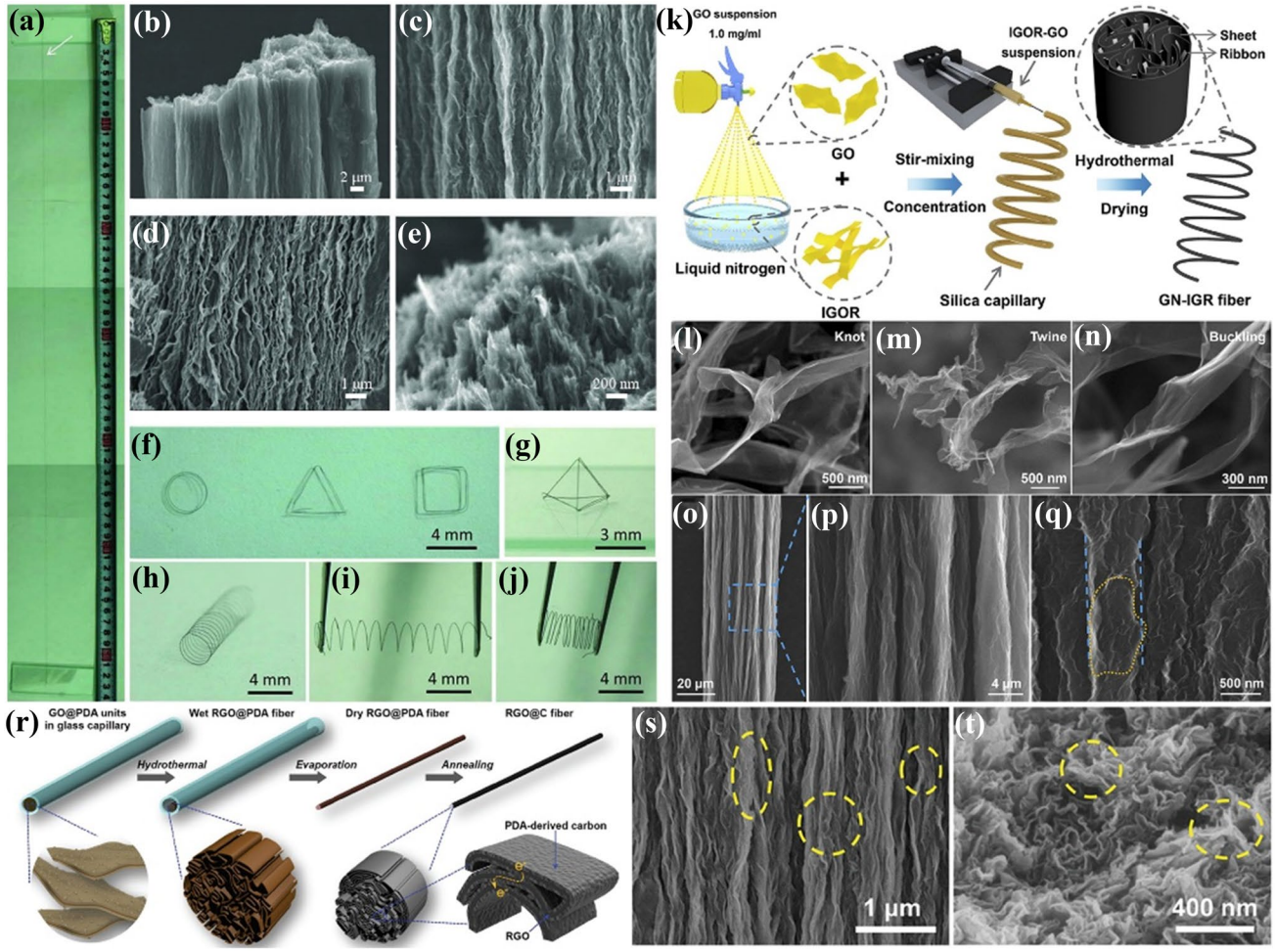

Fig. 28 **a** Exhibition of single graphene-based CBFs with a diameter of ~33 μm and length of 63 cm. **b** SEM image of the cross-section of graphene-based CBFs. **c** and **d** The axial external surface and inner cross-section SEM images of graphene-based CBFs, respectively. **e** The high-resolution SEM image of the cross-section of graphene-based CBFs. **f–j** Shaping and weaving of graphene-based CBFs [25]. Reproduced with permission from ref. 25. Copyright 2012, Wiley–VCH. **k** Schematic for the formation process of graphene sheet/ribbon hybrid fibers. **l–n** SEM images of the IGORs with different structures, such as a knot, twine, and buckling. **o–q** SEM images of the GN-IGR fibers. The graphene ribbons were bound by the sheets (marked by a dotted circle). The width of the bundled ribbons by graphene sheet was ~ 600 nm (marked by parallel dotted lines) [249]. Reproduced with permission from ref. 249. Copyright 2017, Elsevier Ltd. **r** Schematic of the preparation process of the RGO@C fibers. **s** Surface morphology of the RGO@PDA fibers. **t** SEM image of the cross-section of RGO@PDA fibers [250]. Reproduced with permission from ref. 250. Copyright 2018, Wiley–VCH

non-liquid–crystal spinning technology to synthesize continuous graphene-based CBFs with high electrical performance (the capacitance of 279 F/g at a current density of 0.2 A/g) [243].

Inspired by traditional wet-spinning, the coaxial two-capillary spinning (CTCS) technology is further developed. As shown in Fig. 26a, CTCS equipment was designed as a hollow tube structure with a tip. Yang et al. prepared a hollow graphene-based CBFs by CTCS technology and designed the macro morphology of CBFs (Fig. 26b, c) [244]. Similarly, Liang et al. prepared graphene/polymer composite fibers by CTCS. The sodium carboxymethyl cellulose solution was injected into two capillaries with GO suspension as inner fluid, and the as-prepared fibers were called core-sheath fibers (Fig. 26d–f) [216]. SCs were prepared after chemical reduction which could be knotted without damage (Fig. 26g–h). However, there were many defects in graphene-based CBFs, which would effect the mechanical performance. In order to minimize fiber defects, Xin et al. prepared graphene-based CBFs by utilizing large and small GO sheets. The small GO sheets were inserted into the large GO sheets as backbone skeleton (Fig. 26i), the tensile strength was improved to 1080 ± 61 MPa after thermal annealing (1800 °C) [245]. Xu et al. prepared extremely strong graphene-based CBFs via full-scale synergetic defect engineering (Fig. 26j)

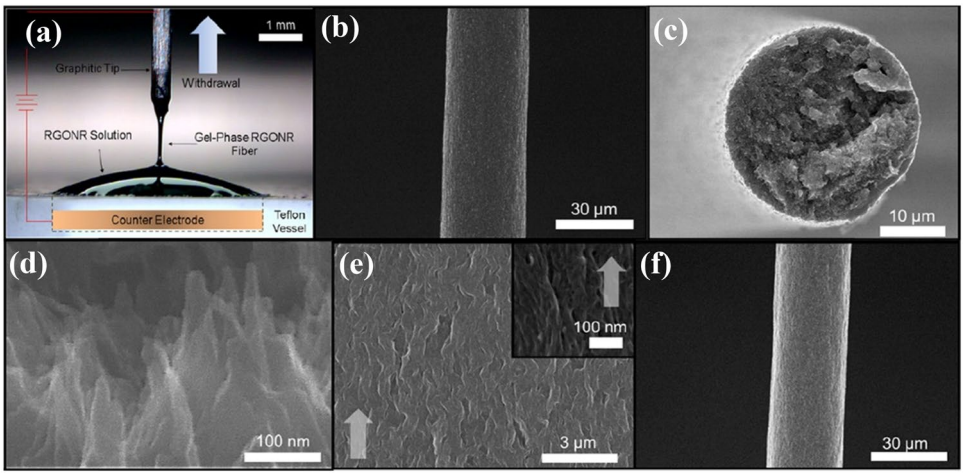

Fig. 29 **a** Schematic of a gel-phase RGONR fiber being formed from chemically reduced GONR solution during the drawing process. **b** A solid RGONR fiber formed by the electrophoretic self-assembly method. **c** Cross-section and **d** side-view images of the fracture surface of the RGONR fiber. **e** The surface texture of the RGONR fiber and the partial alignment of associated features along the direction of the fibers. The magnified image in the inset showed aligned nanoribbons. **f** Image of the as-spun fiber after annealing at 800 °C. Parts **b**–**f** are obtained by SEM [28]. Reproduced with permission from ref. 28. Copyright 2012, IOP Publishing Ltd

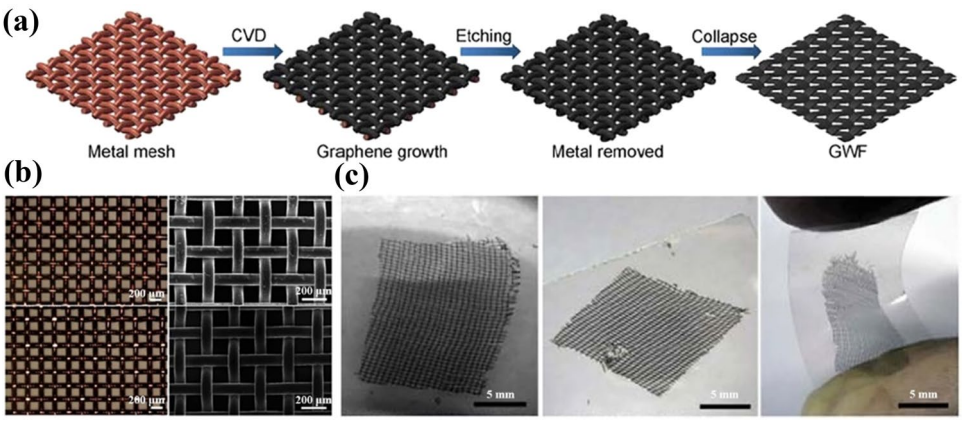

Fig. 30 Fabrication of GWFs by CVD with copper wire meshes as substrates. **a** Schematic of steps for GWF preparation. **b** Macroscopic optical images (left), top-view SEM images (right) of copper meshes before (top) and after (bottom) graphene growth. **c** Optical images of GWF films floating on water and depositing on glass and PET [251]. Reproduced with permission from ref. 251. Copyright 2012, IOP Publishing Ltd

[246]. Undergoing two-step reduction (chemical reduction with hydroiodic acid, thermal reduction at 1300 °C) and thermal annealing (3000 °C), the tensile strength and elastic modulus of graphene-based CBFs reached 1450 MPa and 282 GPa, respectively [246]. Meanwhile, Liu et al. chemically doped (potassium, $FeCl_3$ and Br_2) graphene-based CBFs with superb electrical conductivity by a facile two-zone vapor transport method, making the conductivity reach $(0.77–2.24)\times10^7$ S/m (Fig. 26k) [247]. Also, inspired by the spinning process of spiders (Fig. 26l), Pan et al. designed a spider biomimicking microfluidic channels to prepare micro graphene-based CBFs with excellent flexibility after assembled into micro SCs [248].

To further investigate microfluidics technology, Xin et al. designed several different microfluidics channel models to explore the influence of channel shape on the arrangement and orientation of GO sheets and the mechanical properties of graphene-based CBFs [24]. When GO sheets flowed in a tubular channel (Fig. 27a), a mesophase flat channel (Fig. 27e) and a thinner flat channel (Fig. 27i), there were different arrangement patterns appearing which included curved and distorted of 0.75, arranged of 0.86, and neatly organized of 0.94 (Fig. 27c, g, k). The arrangement of the GO sheets showed the increasingly regular and compact as the channel shape changed from tubular to mesophase flat, thinner flat, and the increaseing degree of orientation (Fig. 27b, f, j). Moreover, the mechanical performance of

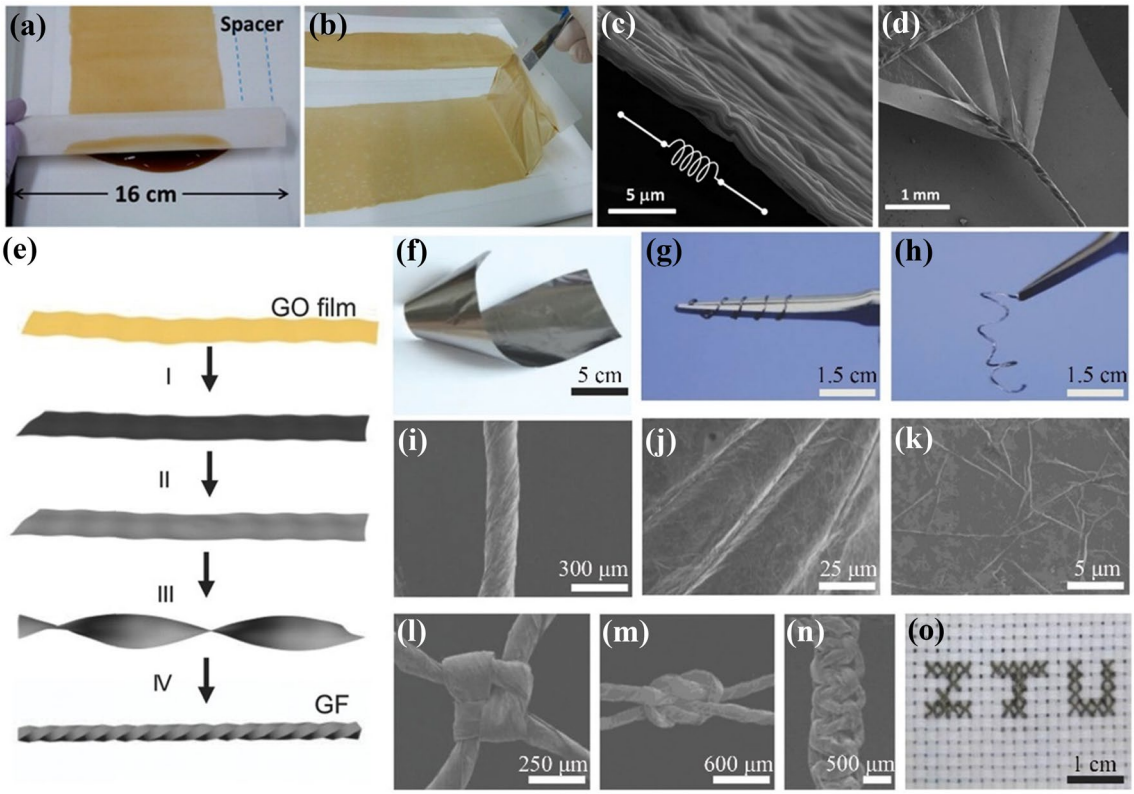

Fig. 31 **a** Fabrication of the 2D GO films. **b** Free-standing thin GO film. **c** SEM image of a GO film. **d** SEM image of a thin GO film being scrolled into a GO fiber [27]. Reproduced with permission from ref. 27. Copyright 2014, American Chemical Society. **e** Schematic of the fabrication process of Graphene-based CBFs. (I) HI reduction; (II) thermal annealing and mechanical press; (III, IV) twist. **f** Optical image of thermally annealed graphene film. **g**, **h** Optical images of graphene-based CBFs. **i–k** SEM images of a single graphene-based CBF in differently magnified views. SEM images of (l) a cross knot, **m** a carrick bend knot, and **n** a flat knot. **o** Photograph of cross-stitch in the pattern of ZJU by woven graphene-based CBFs into cotton cloth [254]. Reproduced with permission from ref. 254. Copyright 2016, Wiley–VCH

graphene-based CBFs was enhanced by adjusting the maximum tensile strength and elastic modulus of fibers (Fig. 27l), which was higher than other graphene-based CBFs fabricated in a tubular and mesophase flat channel (Fig. 27d, h). Therefore, it is proved that the performance of Graphene-based CBFs can be regulatable by designing different microfluidics channel models.

Dimensionally Confined Hydrothermal (DCH) Method

DCH method is an effective process to fabricate shape-confined graphene-based CBFs. Dong et al. prepared single graphene-based CBFs with a diameter of ~ 33 μm and a length of 63 cm by DHC method (Fig. 28a) [25]. GO sheets suspension is poured into a glass tube with an inner diameter of 0.4 mm, followed by hydrothermal treating and drying in air. The shape of graphene-based CBFs is consistent with the glass tube (Fig. 28b–e), which can be designed for different planar and 3D geometric structures (Fig. 28f–j). Sheng et al. prepared graphene composite fibers named GN-IGR fibers using highly interconnected graphene ribbons (IGRs) and graphene nanosheets (GNs) (Fig. 28k) [249]. The interconnected graphene oxide ribbons (IGORs) with different structures (Fig. 28l–n), such as knot, twine, and buckling, are consistent with the prepared GN-IGR fiber structure (Fig. 28o–q). The tensile strength and elongation of GN-IGR fibers reached up to 223 MPa and 22.0%, respectively [249]. Ma et al. prepared carbon-coated RGO composite (RGO@C) fibers by putting polydopamine PDA and GO (GO@PDA) into fibers, and following evaporating and annealing to obtain RGO@C fiber (Fig. 28r) [250]. And the GO@PDA was assembled into flexible fibers with uniform linear morphology, neat arrangement and compact layered organization (Fig. 28s and t).

Electrophoretic Self-Assembly

Electrophoretic self-assembly is an effective method to prepare functional graphene-based CBFs without any polymer or surfactant. Jang et al. fabricated RGO nanoribbon

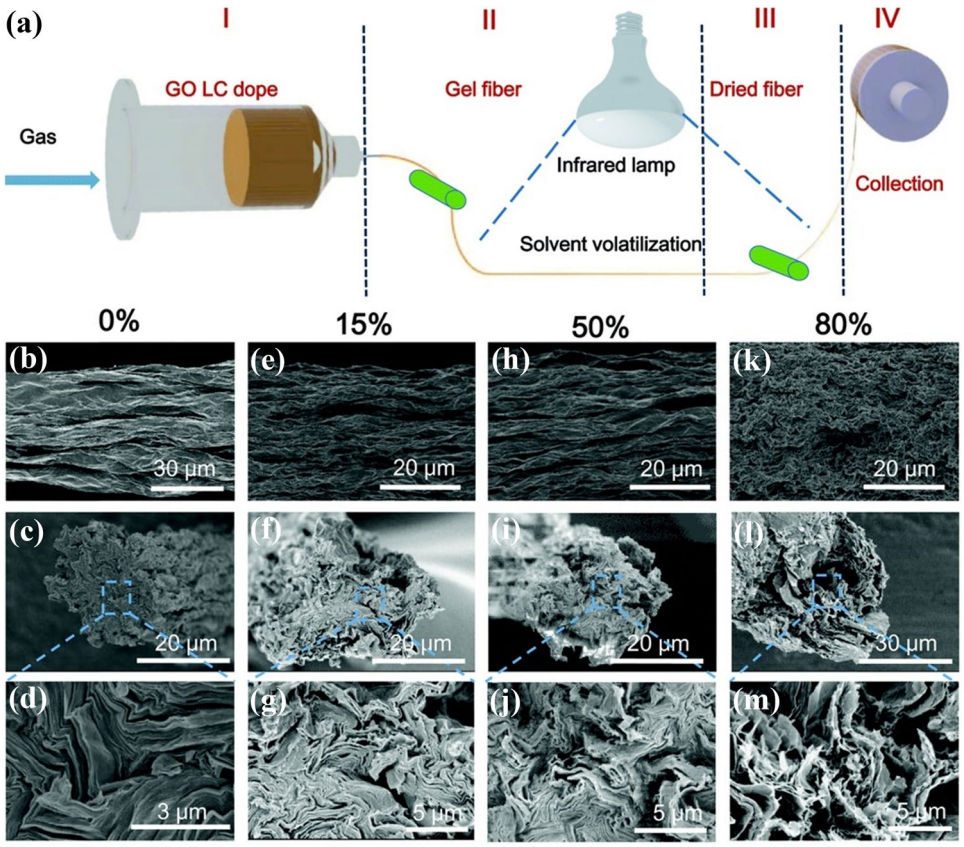

Fig. 32 **a** Schematic of the dry-spinning process of GO sheets with a concentrated organic dispersion. The SEM images of GO fibers with different shrink ratios including **b** 0%, **e** 15%, **h** 50% and **k** 80%. The cross-section of GO fibers with different shrink ratios including **c** 0%, **f** 15%, **i** 50% and **m** 80%. The magnified images of the top SEM images **d**, **g**, **j** and **m**, respectively [29]. Reproduced with permission from ref. 29. Copyright 2017, Royal Society of Chemistry

(RGONR) fibers with electrical and field emission properties by electrophoretic self-assembly [28]. A graphitic tip was immersed into the chemically RGO nanoribbon colloidal solution in a Teflon vessel in which the counter electrode was embedded (Fig. 29a). The distance between the counter electrode and the immersed tip was ~ 5 mm and a constant voltage ranging from 1 to 2 V was applied during the withdrawal process for the graphitic tip. The structure of the prepared RGONR fibers was uniform and the arrangement of nanoribbons was neat and closing along the axial direction of fibers (Fig. 29b–f). And the prepared RGONR fibers showed a low potential for field emission (0.7 V/μm) and field emission currents (400 A/cm^2) after thermal annealing, which maintained excellent durability at a high current level (300 A/cm) during long-term operation [28].

Chemical Vapor Deposition (CVD) Method

CVD methods have been utilized to prepare 1D, 2D and 3D carbon materials including fibers, films and spatial network structure polymers in recent years. Li et al. directly reported self-assembled, porous, and monolithic graphene-based CBFs with the electrical conductivity of ~ 1000 S/m from CVD-grown graphene film [26]. The morphology and pore structure of fibers were controlled by the evaporation of solvents with suitable surface tension. Zhu et al. prepared graphene-based woven fabrics (GWFs) in three steps: CVD-growth, etching, and collapsing (Fig. 30a) [251]. Graphene uniformly and neatly grew on the copper mesh (Fig. 30b), and the GWFs exhibited well-aligned arrays along with the horizontal and vertical directions (Fig. 30c). In addition, Xiao et al. designed 3D Ni scaffolds to prepare 3D graphene with a uniform arrangement structure using CVD methods [252].

2D Films Twisting

2D film twisting method is simple and efficient which can synthesize graphene-based CBFs. Cruz-Silva et al. prepared graphene-based CBFs by twisting the 2D GO film [27]. GO dispersion was evenly spread on the PTFE substrate by a bar (Fig. 31a), forming an ultra-thin (2.9 μm) GO film

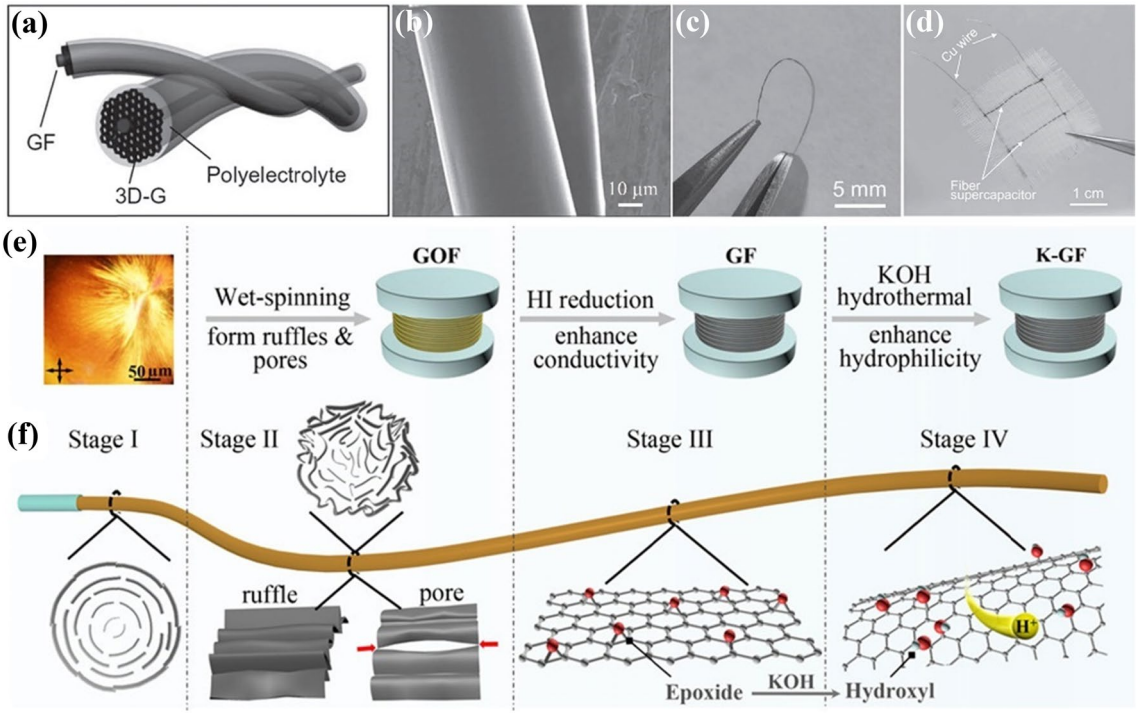

Fig. 33 **a** Schematic of a wire-shaped supercapacitor fabricated from two twined graphene-based CBFs with polyelectrolyte. **b** SEM images of the twined structure of graphene-based CBFs coated with polyelectrolyte. **c** Exhibition of graphene-based CBFs@3D-G fiber SCs in bending state. **d** Exhibition of the textile embedded with two graphene-based CBFs@3D-G fiber CSs [256]. Reproduced with permission from ref. 256. Copyright 2013, Wiley–VCH. **e** Schematic of the fabrication process of K-GF using GO liquid crystal (8 g/L) as the precursor, and **f** the microstructure and surface functional group changes of the fiber during the fabrication process [260]. Reproduced with permission from ref. 260. Copyright 2019, American Chemical Society

(Fig. 31b). The prepared GO film showed a slightly wrinkled structure that can enhance ductility for films (Fig. 31c), GO fiber was fabricated by winding GO film with the elongation of 0.76 (Fig. 31d). Electrical conductivity of as-prepared graphene-based CBFs was 416 S/cm after thermal reduction at 2000 °C. Hua et al. prepared helical GO and RGO fibers by twisting and chemical reduction of GO films [253]. Interestingly, the elongation of GO fibers (20–30%) was lower than that of RGO fibers (40–50%), while the elastic modulus of GO fiber was higher than that of RGO fibers because of the hollow cavities and the stress concentration. Wang et al. synthesized highly stretchable graphene-based CBFs by GO films twisting (Fig. 31e) [254]. After chemical reduction, carbonization and twisting (Fig. 31f–h), graphene-based CBFs possessed a uniform scrolled structure (Fig. 31i–k) which could be knotted in several ways and knitted into the cotton cloth without damage (Fig. 31l–o).

Dry-Spinning

Dry-spinning is a convenient and energy-saving method to prepare graphene-based CBFs. Tian et al. obtained tough graphene-based CBFs by a concentrated organic dispersion of GO sheets without any coagulating baths [29]. The GO LCs dopes were extruded through spinneret tip and followed by drying and infrared irradiation to obtain Graphene-based CBFs (Fig. 32a). The mixed solvents, including methanol, ethanol, acetone, tetrahydrofuran and water, were chosen to promote the balance of surface tension and volatility of the spinning dopes. GO fibers possessed numerous aligned wrinkles along the axial direction of the fibers (Fig. 32b–m), the tensile strength, elongation and electrical conductivity of RGO fibers were 375 ± 20 MPa, 9.4% and 1.32×10^4 S/m, respectively [29]. Additionally, Feng et al. synthesized GO fibers by using highly concentrated GO inks through the dry-spinning method and the average tensile strength, elastic modulus and fracture toughness of GO fibers were 105 MPa, 0.4 GPa and 5 MJ/m^3, respectively [255].

Graphene-Based CBFs Applications

SCs

SCs, with the ability of high capacitance, fast charge/discharge and cycle stability, have potential applications in the field of energy storage. It is suitable to use graphene-based CBFs as an electrode, which can satisfy the requirements

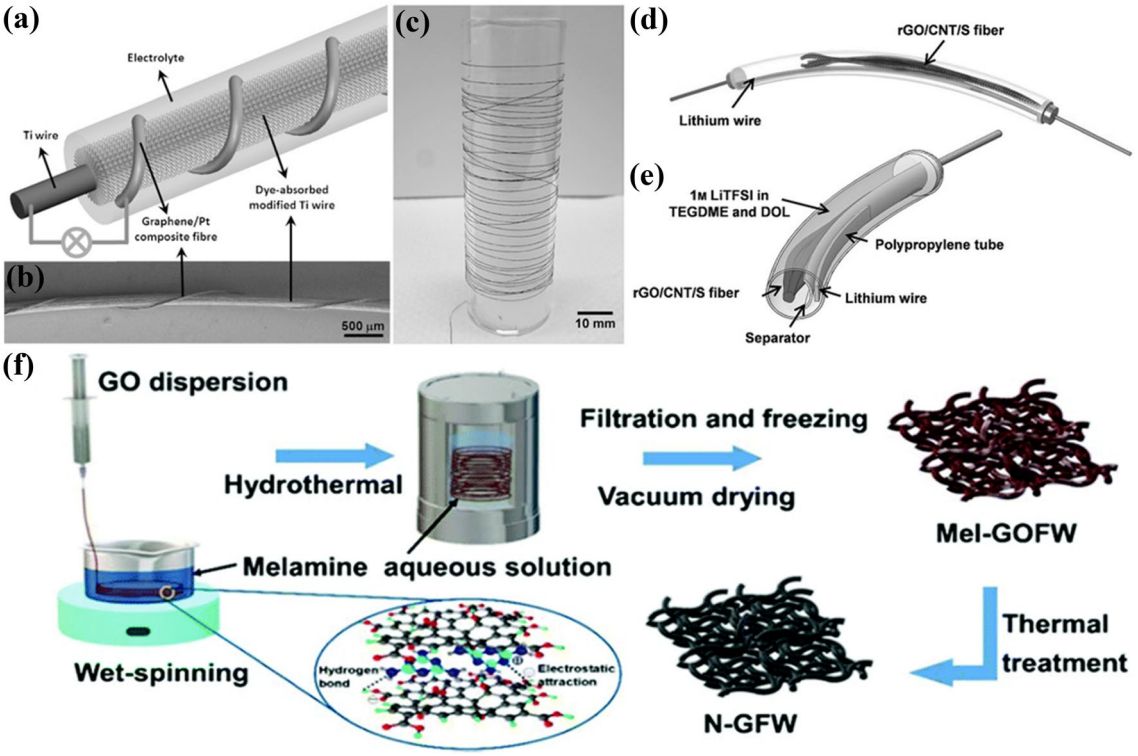

Fig. 34 **a** Schematic of the fabrication of dye-sensitized photovoltaic wire. **b** SEM image of dye-sensitized photovoltaic wire [261]. Reproduced with permission from ref. 261. Copyright 2013, Wiley–VCH. **c** A GO/CNT/S fiber wrapped around a glass cylinder. **d** Schematic of cable LSB. **e** Schematic of the cross-sectional view of cable LSB components [263]. Reproduced with permission from ref. 263. Copyright 2017, Wiley–VCH. **f** Schematic of the fabrication of N-GFWs [264]. Reproduced with permission from ref. 264. Copyright 2019, Royal Society of Chemistry

of novel SCs including portability, lightness and wearable. Meng et al. first prepared graphene-based CBFs SCs in 2013 [256]. Graphene-based CBFs were synthesized via a DCH method and then the 3D porous, core–shell graphene-based CBFs (GF@3D-G) were fabricated by electrochemical deposition and reduction reaction. Eventually, GF@3D-G fiber SCs with excellent flexibility and knittability assembled by GF@3D-G as an electrode and PVA/H_2SO_4 as the gel electrolyte displayed a specific capacitance of 1.7 mF/cm^2 (Fig. 33a–d). Zhao et al. prepared an all-graphene coaxial fiber SCs with graphene-based CBFs as core and dip-coated graphene as sheath [257]. As a result, it exhibited a high specific capacitance of 205 mF/cm^2 (182 F/g) and a high energy density of 104 μW h/cm^2 [257]. The electrical performance of graphene-based CBFs SCs was enhanced by introducing functional materials, such as CNTs [258]. Kou et al. prepared two-ply fiber SCs using polyelectrolyte-wrapped graphene/CNT core-sheath fibers showing an ultra-high capacitance of 269 mF/cm^2 and an energy density of 5.91 μWh/cm^2 [216]. Yu et al. designed a CNT-graphene fiber with a hierarchical structure to assemble SCs, and the specific volumetric capacity reached 305 F/cm^3 [259]. In addition, Guan et al. prepared graphene-based CBFs by wet-spinning which possessed porous and wrinkled structure, hydrophilicity and excellent conductivity obtaining after hydrophilic treating in KOH solutions (Fig. 33e and f) [260]. The SCs based on K-GF showed the capacitance of 145.6 mF/cm^2, an energy density of 3.23 μW h/cm^2 and a power density of 0.017 mW/cm^2, and its angle could be folded from 0° to 180° [260].

Batteries

In the field of energy storage, it is popular that graphene-based CBFs are used as battery electrodes. Yang et al. developed wire-shaped photovoltaic devices based on graphene/Pt composite fibers, which displayed an energy conversion efficiency of 8.45% (Fig. 34a and b) [261]. However, the expensive cost of Pt limits the development of solar batteries. Therefore, Chen et al. developed a dye-sensitized solar battery assembled from the novel graphene-based CBFs electrode without Pt nanoparticles, achieving an energy conversion efficiency reached up to 3.25% [262]. Chong et al. prepared an ultralight and flexible RGO/CNT/sulfur (RGO/

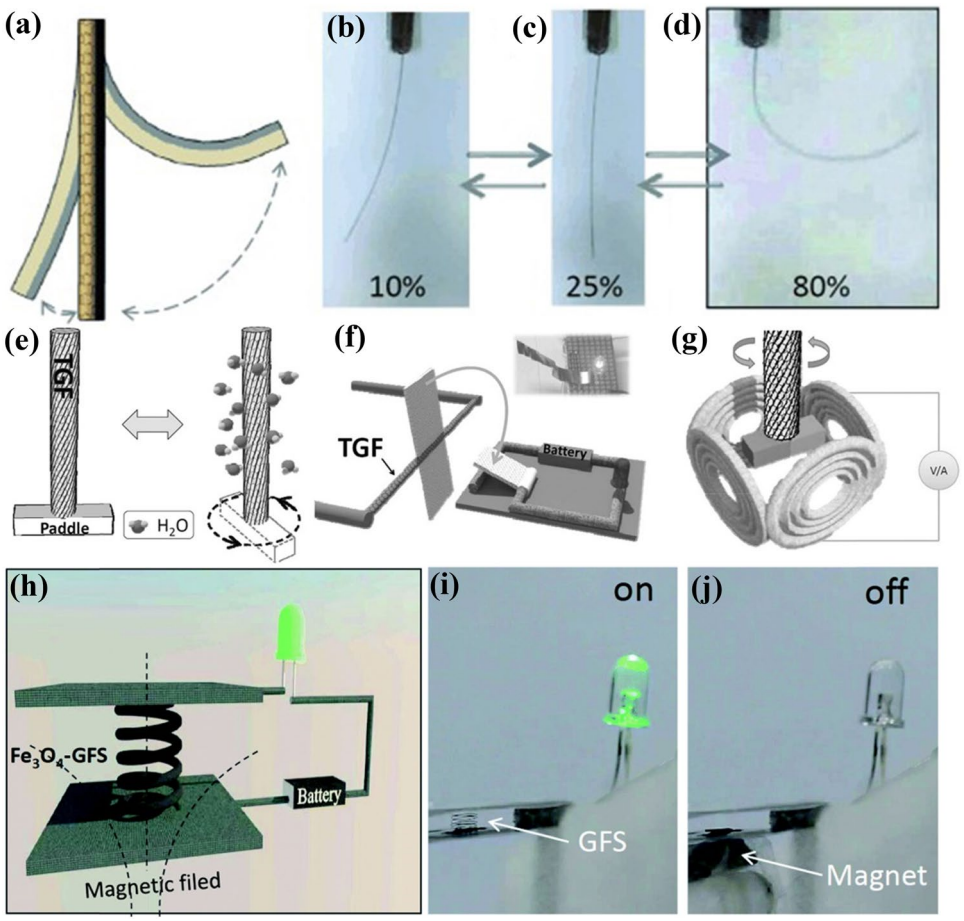

Fig. 35 **a** Schematic illustration of the possible bending of a graphene/GO fiber exposed to different relative humidity. **b–d** Exhibition of a graphene/GO fiber under different relative humidity [265]. Reproduced with permission from ref. 265. Copyright 2013, Wiley–VCH. **e** Schematic rotation of TGF with a paddle at the low (left) and high (right) humidity. **f** and **g** Schematic of the designed humidity switch and the alternating current generator [266]. Reproduced with permission from ref. 266. Copyright 2014, Wiley–VCH. **h** Schematic of Fe_3O_4/graphene-based CBFs spring switch in a circuit, where graphene-based CBFs spring responds to a magnetic field to maintain the **i** "open" and **j** "close" states [267]. Reproduced with permission from ref. 267. Copyright 2014, Royal Society of Chemistry

CNT/S) composite fiber, which was further assembled into a cable lithium-sulfur battery (LSB) with an initial capacity of 1255 mAh/g and areal capacity of 2.49 mAh/cm^2 at C/20 (Fig. 34c–e) [263]. The graphene-based CBFs can be also fabricated as circuit transmissions. Liu et al. prepared the chemically doped ($FeCl_3$, Br_2, and K) graphene-based CBFs with excellent conductivity ($(0.77 \sim 2.2) \times 10^5$ S/cm), which could be used as USB cable and wire [247]. Recently, Chong et al. also synthesized novel highly porous nitrogen-doped graphene-based CBFs webs (N-GFWs) in three main steps: wet-spinning, hydrothermal activation and drying, and thermal reduction (Fig. 34f) [264]. To satisfy the demand for multi-battery charge storage in both lithium-oxygen batteries (LOBs) and lithium-sulfur batteries (LSBs), the atomic structure and electrical conductivity of N-GFWs were designed by adjusting the degree of N-doping and thermal reduction. The maximum area capacity of LOBs was 2 mAh/cm^2, and the capacity retention of LSBs after 200 cycles was up to 99.96% because the abundant oxygenated and nitrogen functional groups were entrapped into electrodes [264].

Intelligent Actuators and Sensors

An intelligent actuator is a device that can adaptively adjust and deform under the stimulation of the external environment such as temperature, humidity, light, current, voltage, etc. Cheng et al. designed a moisture-triggered actuator using graphene/GO composite fibers with asymmetric structure through positioned laser reduction [265]. The actuator could perform complex motion forms such as bending and torsion according to the change of environmental humidity, and made into a humidity-driven robot hand and crawling device (Fig. 35a–d). In further research, they also fabricated twisted GO fibers (TGF) with spiral structure by rotating the

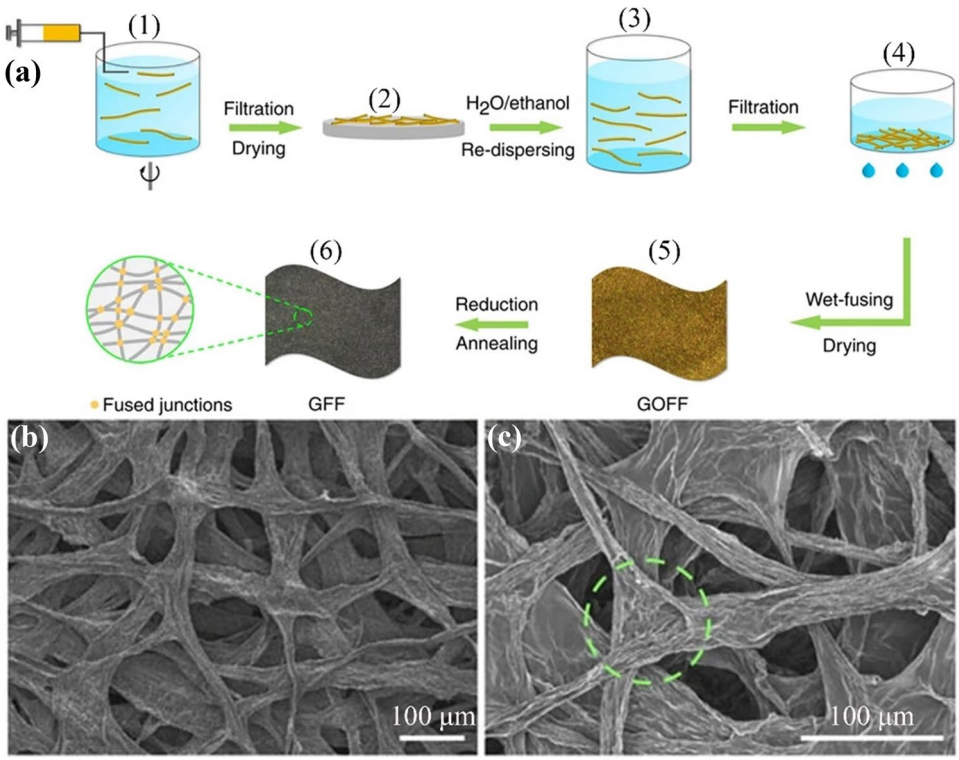

Fig. 36 **a** Schematic of the fabrication of graphene-based CBFs fabrics. **b** SEM images of GO fiber fabrics and **c** graphene-based CBFs fabrics [271]. Reproduced with permission from ref. 271. Copyright 2016, Nature Publishing Group

Table 3 The various parameters of CBFs prepared by graphene and GO

References	Precursors	Processing/modification technology	Tensile strength (GPa)	Elastic modulus (GPa)	Conductivity (S/cm)	Applications
[23]	GO	GO LCs wet-spinning HI acid reduction	0.14	7.7	–	–
[26]	Graphene	CVD Directly drawing graphene films	–	–	~1000	SCs capacitance of 0.6–1.4 mF/cm^2
[27]	GO	GO films twisting/rolling Thermal reduction	0.085	–	416	Batteries current densities of 5.3 A/cm^2
[28]	GO	Electrophoretic self-assembly Hydrazine monohydrate	–	–	–	Batteries current densities of 300 A/cm^2
[29]	GO	Dry spinning HI acid reduction	0.375 ± 0.02	11.6	132	–
[231]	GO/CTAB	Self-assembly Wet-spinning HI acid reduction	0.182	8.7	~35	–
[232]	Large-scale GO sheets	GO LCs wet-spinning HI acid reduction	0.501	11.2	410	–

Table 3 (continued)

References	Precursors	Processing/modification technology	Tensile strength (GPa)	Elastic modulus (GPa)	Conductivity (S/cm)	Applications
[236]	GO	GO LCs wet-spinning Annealing reduction	~0.05	>29	25.08 ± 6.32	Energy Storage Textiles charge storage capacity of 409 F/g at 1 A/g
[243]	GO	Non-liquid–crystal spinning HI acid reduction	0.15 ± 0.05	7.5 ± 0.28	44.2 ± 1.3	SCs capacitance of 279 F/g at a current density of 0.2 A/g
[246]	GO	Full scale defect engineering	1.45	282	8×10^3	Batteries ampacity of 2.3×10^{10} A/m^2
[250]	GO	DCH method Annealing reduction	~0.724	~37	~660	–
[255]	GO	Dry-spinning HI acid/annealing reduction	0.105	0.4	–	–
[259]	GO/SWCNTs	DCH method Annealing reduction	0.084	–	102	SCs specific volumetric capacity of 305 F/cm^3 in sulphuric acid
[264]	GO/melamine	Wet-spinning Hydrothermal Thermal reduction	–	–	0.951	LOBs areal capacity of 2 mAh/cm^2 at 0.2 mA/cm^2
[265]	Graphene/GO	DCH method Positioned laser reduction	–	–	–	Humidity-driven actuator humidity-driven robot hand and crawling device
[269]	GO/ZIF-67/pyrrole	Wet-spinning Electrodeposition Annealing reduction	–	–	–	Adrenaline (Ad) non-enzymatic detection sensitivity of 44.6 mA/(mM·cm^2) and 11.0 mA/(mM·cm^2) at Ad in the range of 0.06–95 μM and 95.0–5900 μM
[271]	GO	Wet-spinning Hydrazine vapour/ Annealing reduction	0.6×10^{-3}	0.0299 ± 0.064	~280	Non-woven fabrics thermal conductivity of ~301.5 W/(m·K)

gel fibers [266]. Interestingly, when the environment humidity increased, the fibers would rotate at a high speed and return to the initial state after the humidity drops (Fig. 35e). Additionally, fibers were further used to make humidity-responsive control switches and humidity generators (Fig. 35f and g). The magnetic nanoparticles (Fe_3O_4) were introduced into graphene-based CBFs to assemble magnetic actuators (Fig. 35h) [267]. The elasticity of the spring was adjusted by applying a magnetic field to realize the switching control of the circuit (Fig. 35i abd j).

The excellent deformation response of intelligent sensor can be prepared from graphene-based CBFs. You et al. fabricated graphene-based CBFs sensors with high stretchability and sensitivity by direct extrusion of ink [268]. The results showed that the resistance would change accordingly during the bending, twisting, compressing, and stretching of the fibers [268]. Zeng et al. fabricated novel zeolitic imidazolate frameworks entrapped 3D graphene-based CBFs by electrodeposition technology [269]. The prepared fibers were used as electrodes at adrenaline (Ad) non-enzymatic detection, which showed high sensitivity of 44.6 mA/(mM·cm^2) and 11.0 mA/(mM·cm^2) corresponding to the concentration of Ad in the range of 0.06–95 μM and 95.0–5900 μM, respectively [269]. Moreover, the sensitivity of the sensor exhibited excellent repeatability at extremely low Ad concentration (0.02 Mm) [269].

Table 4 The various parameters of CBFs prepared by different precursors

Precursor	Processing	Heat treatment temperature (°C)	Carbon yield	Tensile modulus	Tensile strength
PE [272]	Melt-spinning	600–3000	75%	139 GPa	2.5 GPa
UHWMPE [273]	–	2000–3000	–	150 g/d	8(J/g)
LLDPE [118]	Melt-spinning	–	65%	134 GPa	1.54 GPa
PVDC/PVC [274]	Thermal decomposition	2500	–	28 GPa	0.24 GPa
At-PBD [275]	Melt-spinning	3000	70%	70 GPa	1.2 GPa
St-PBD [276]	Melt-spinning	3000	82%	4010 t/cm^2	20 t/cm^2
PVA [277]	Heating	1000	–	–	5800 kg/cm^2
Phenol-hexamine [278]	Melt-spinning	2800	–	69 GPa	2.1 GPa
PA-resin [279]	Thermal treatment	2500–3000	–	69 GPa	0.7 GPa
phenolic resin [280]	Thermal treatment	900	56%	–	0.35 GPa
PBZT [281]	Dry-jet wet spinning	850–1600	–	196 GPa	0.93 GPa
PBO [282]	Dry-jet wet spinning	700–2000	–	175 GPa	0.6 GPa
Polyacetylene [283]	Melt-spinning	2500–3000	–	390 GPa	2.3 GPa
PI (S35) [118]	–	–	–	120 GPa	3.5 GPa

Multifunctional Fabrics

Fiber fabrics play a significant role in various fields such as wearable device and energy. Cao et al. prepared nonwoven, nonknitted, graphene-based networks with excellent mechanical properties by programmable writing technique [235]. The GO dispersions were programmed into a cross-network structure and followed by thermal or chemical reduction fuyu to endow fiber with mechanical properity and electrical conductivity. Moreover, graphene-based CBFs with a cross-net structure which showed mechanical stimuli properity. Seyedin et al. introduced highly flexible and tough GO fibers which could be knitted by textile machinery [270]. Graphene-based CBFs were fabricated by dry–wet spinning technology, followed by co-knitting with commercial nylon fibers to achieve the mechanical weaving of graphene-based CBFs for the first time [270]. Li et al. reported non-woven graphene-based CBFs fabrics which composed of randomly oriented and interfused fibers with strong inter-fiber bonding (Fig. 36a) [271]. The overlapping structures of fabrics (Fig. 36b and c) showed the electrical conductivity of 28,000 S/m and thermal conductivity of 301 W/mK, respectively [271]. Eventually, the various parameters of CBFs prepared by graphene and GO are shown in Table 3.

Other CBFs Precursors

Except for the aforementioned CBFs precursors, there are some precursor materials including polyethylene (PE), UHWMPE, LLDPE, poly(vinylidenechloride)-poly(vinyl chloride) (PVDC/PVC), atactic and syndiotactic poly(butadiene) (at-PBD and st-PBD), polyvinyl alcohol (PVA), phenol-hexamine, polyamide(PA)-resin, phenolic resin, poly(p-phenylene benzobisthiazole) (PBZT), poly(p-phenylenebenzobisoxazole) (PBO), polyacetylene, polyimide (PI), etc. The main information about these precursors is shown in Table 4.

Summary

In this review, we mainly summarize the fabrication, characterization and application of CBFs based on the different precursors, mainly including PAN, pitch, cellulose, lignin, CNTs, graphene. Among them, PAN-based CBFs with outstanding mechanical performances have already occupied the most of the fiber materials markets in modern life. There are still some significant challenges for CBFs prepared by PAN, pitch, cellulose, lignin, especially in terms of structure control (arrangement, orientation, crystallinity, crystallite size, defect, sp^2 and sp^3 hybrid) and performances improvement (tensile strength, Young's modulus and electrical conductivity). The development of CBFs prepared by carbon units is only two decades, but their unprecedented characteristics make them have great potential in practical applications, such as batteries, supercapacitors, sensors, etc. At present, the performances of CNTs and graphene-based CBFs fibers are far from the theoretical values, which mainly face the problems of insufficient raw material preparation technology, high cost and limited production scale. In addition. the concept of green sustainable development is also one of the most significant factors that must be considered in protecting the environment. Green, sustainable,

recyclable, and simply available CBFs precursors prepared by lignin have attracted more and more attention. Therefore, the green and low-cost materials will play their unique advantages in various fields in the future.

Acknowledgements This work was supported by Key Support Project of State Key Laboratory for Modification of Chemical Fibers and Polymer Materials (No. 21M1060212), Open project of Shanghai Key Laboratory of Lightweight Structural Composite Materials (No. 2232019A4-02) and National Natural Science Foundation of China (No. 51503086). We dedicated the review to professor Ding Pan on the occasion of his 78th birthday.

Declarations

Conflict of Interest The authors declare that there are no conflicts of interest.

References

1. Newcomb BA. Processing, structure, and properties of carbon fibers. *Compos Pt A-Appl Sci Manuf* **2016**;*91*:262–82.
2. Das S, Warren J, West D, Schexnayder SM. Global carbon fiber composites supply chain competitiveness analysis. Knoxville: Oak Ridge National Laboratory, The University of Tennessee; **2016**.
3. Jang Y, Kim SM, Spinks GM, Kim SJ. Carbon nanotube yarn for fiber-shaped electrical sensors, actuators, and energy storage for smart systems. *Adv Mater* **2020**;*32*(5):1902670.
4. Iijima S. Helical microtubles of graphitic carbon. *Nature* **1991**;*354*:56–8.
5. Yu M-F, Files BS, Arepalli S, Ruoff RS. Tensile loading of ropes of single wall carbon nanotubes and their mechanical properties. *Phys Rev Lett* **2000**;*84*(24):5552–5.
6. Wei BQ, Vajtai R, Ajayan PM. Reliability and current carrying capacity of carbon nanotubes. *Appl Phys Lett* **2001**;*79*(8):1172–4.
7. Li QW, Li Y, Zhang XF, Chikkannanavar SB, Zhao YH, Dangelewicz AM, Zheng LX, Doorn SK, Jia QX, Peterson DE, Arendt PN, Zhu YT. Structure-dependent electrical properties of carbon nanotube fibers. *Adv Mater* **2007**;*19*(20):3358.
8. Vigolo B, Penicaud A, Coulon C, Sauder C, Pailler R, Journet C, Bernier P, Poulin P. Macroscopic fibers and ribbons of oriented carbon nanotubes. *Science* **2000**;*290*(5495):1331–4.
9. Launois P, Marucci A, Vigolo B, Bernier P, Derre A, Poulin P. Structural characterization of nanotube fibers by X-ray scattering. *J Nanosci Nanotechnol* **2001**;*1*(2):125–8.
10. Jiang K, Li Q, Fan S. Spinning continuous carbon nanotube yarns. *Nature* **2002**;*419*(6909):801–801.
11. Zhu HW, Xu CL, Wu DH, Wei BQ, Vajtai R, Ajayan PM. Direct synthesis of long single-walled carbon nanotube strands. *Science* **2002**;*296*(5569):884–6.
12. Ma W, Liu L, Yang R, Zhang T, Zhang Z, Song L, Ren Y, Shen J, Niu Z, Zhou W, Xie S. Monitoring a micromechanical process in macroscale carbon nanotube films and fibers. *Adv Mater* **2009**;*21*(5):603–8.
13. Brodie BCXIII. On the atomic weight of graphite. *Philos Trans R Soc Lond* **1859**;*149*:249–59.
14. Novoselov KS, Geim AK, Morozov SV, Jiang D, Zhang Y, Dubonos SV, Grigorieva IV, Firsov AA. Electric field effect in atomically thin carbon films. *Science* **2004**;*306*(5696):666–9.
15. Meyer JC, Geim AK, Katsnelson MI, Novoselov KS, Booth TJ, Roth S. The structure of suspended graphene sheets. *Nature* **2007**;*446*(7131):60–3.
16. Liu F, Ming PM, Li J. Ab initio calculation of ideal strength and phonon instability of graphene under tension. *Phys Rev B* **2007**;*76*(6):064120.
17. Lee C, Wei XD, Kysar JW, Hone J. Measurement of the elastic properties and intrinsic strength of monolayer graphene. *Science* **2008**;*321*(5887):385–8.
18. Chen JH, Jang C, Xiao SD, Ishigami M, Fuhrer MS. Intrinsic and extrinsic performance limits of graphene devices on SiO_2. *Nat Nanotechnol* **2008**;*3*(4):206–9.
19. Balandin AA, Ghosh S, Bao WZ, Calizo I, Teweldebrhan D, Miao F, Lau CN. Superior thermal conductivity of single-layer graphene. *Nano Lett* **2008**;*8*(3):902–7.
20. Nair RR, Blake P, Grigorenko AN, Novoselov KS, Booth TJ, Stauber T, Peres NMR, Geim AK. Fine structure constant defines visual transparency of graphene. *Science* **2008**;*320*(5881):1308–1308.
21. Dreyer DR, Park S, Bielawski CW, Ruoff RS. The chemistry of graphene oxide. *Chem Soc Rev* **2010**;*39*(1):228–40.
22. Bagri A, Mattevi C, Acik M, Chabal YJ, Chhowalla M, Shenoy VB. Structural evolution during the reduction of chemically derived graphene oxide. *Nat Chem* **2010**;*2*(7):581–7.
23. Xu Z, Gao C. Graphene chiral liquid crystals and macroscopic assembled fibres. *Nat Commun* **2011**;*2*(1):571.
24. Xin GQ, Zhu WG, Deng YX, Cheng J, Zhang LT, Chung AJ, De S, Lian J. Microfluidics-enabled orientation and microstructure control of macroscopic graphene fibres. *Nat Nanotechnol* **2019**;*14*(2):168.
25. Dong ZL, Jiang CC, Cheng HH, Zhao Y, Shi GQ, Jiang L, Qu LT. Facile fabrication of light, flexible and multifunctional graphene fibers. *Adv Mater* **2012**;*24*(14):1856–61.
26. Li XM, Zhao TS, Wang KL, Yang Y, Wei JQ, Kang FY, Wu DH, Zhu HW. Directly drawing self-assembled, porous, and monolithic graphene fiber from chemical vapor deposition grown graphene film and its electrochemical properties. *Langmuir* **2011**;*27*(19):12164–71.
27. Cruz-Silva R, Morelos-Gomez A, Kim HI, Jang HK, Tristan F, Vega-Diaz S, Rajukumar LP, Elias AL, Perea-Lopez N, Suhr J, Endo M, Terrones M. Super-stretchable graphene oxide macroscopic fibers with outstanding knotability fabricated by dry film scrolling. *ACS Nano* **2014**;*8*(6):5959–67.
28. Jang EY, Carretero-Gonzalez J, Choi A, Kim WJ, Kozlov ME, Kim T, Kang TJ, Baek SJ, Kim DW, Park YW, Baughman RH, Kim YH. Fibers of reduced graphene oxide nanoribbons. *Nanotechnology* **2012**;*23*(23):235601.
29. Tian QS, Xu Z, Liu YJ, Fang B, Peng L, Xi JB, Lia Z, Gao C. Dry spinning approach to continuous graphene fibers with high toughness. *Nanoscale* **2017**;*9*(34):12335–42.
30. Osaka. Studies on Graphite Fiber. Report of the Government Industrial Research Institute. 1961.
31. Watt W. The effect of length changes during the oxidation of polyacrylonitrile fibers on the young's modulus of carbon fibers. Appl Polym Symposia. **1967**;9:215–227.
32. Ju A, Guang S, Xu H. Effect of comonomer structure on the stabilization and spinnability of polyacrylonitrile copolymers. *Carbon* **2013**;*54*:323–35.
33. Liu C, Ni X, Chen H, Yu H, Ju A. High molecular weight poly(acrylonitrile-co-3-aminocarbonyl-3-butenoic acid methyl ester) prepared by mixed solvent polymerization I. effect of monomer feed ratios on polymerization and stabilization. *J Polym Res* **2019**;*26*(12):276.
34. Frank E, Hermanutz F, Buchmeiser MR. Carbon fibers: precursors, manufacturing, and properties. *Macromol Mater Eng* **2012**;*297*(6):493–501.

35. Tsai JS, Lin CH. Effect of comonomer composition on the properties of polyacrylonitrile precursor and resulting carbon fiber. *J Appl Polym Sci* **1991**;*43*(4):679–85.
36. Ziabicki A. Fundamentals of fibre formation. *Nihon Rinsho Jpn J Clin Med* **1976**;*48*(33):165–72.
37. Wade B, Knorr R. Polymerization. 1995.
38. Gabrielyan GA, Rogovin ZA. Synthesis of analogues of polyacrylonitrile containing thio-amide groups. *Polym Sci USSR* **1964**;*6*(5):843–4.
39. Frushour BG. Melting behavior of polyacrylonitrile copolymers. *Polym Bull* **1984**;*11*(4):375–82.
40. Chae HG, Newcomb BA, Gulgunje PV, Liu Y, Gupta KK, Kamath MG, Lyons KM, Ghoshal S, Pramanik C, Giannuzzi L, Şahin K, Chasiotis I, Kumar S. High strength and high modulus carbon fibers. *Carbon* **2015**;*93*:81–7.
41. Morris EA, Weisenberger MC, Bradley SB, Abdallah MG, Mecham SJ, Pisipati P, McGrath JE. Synthesis, spinning, and properties of very high molecular weight poly(acrylonitrile-co-methyl acrylate) for high performance precursors for carbon fiber. *Polymer* **2014**;*55*(25):6471–82.
42. Morris EA, Weisenberger MC, Abdallah MG, Vautard F, Grappe H, Ozcan S, Paulauskas FL, Eberle C, Jackson D, Mecham SJ, Naskar AK. High performance carbon fibers from very high molecular weight polyacrylonitrile precursors. *Carbon* **2016**;*101*:245–52.
43. Sawai D, Fujii Y, Kanamoto T. Development of oriented morphology and tensile properties upon superdawing of solution-spun fibers of ultra-high molecular weight poly(acrylonitrile). *Polymer* **2006**;*47*(12):4445–53.
44. Ingildeev D, Hermanutz F, Bredereck K, Effenberger F. Novel cellulose/polymer blend fibers obtained using ionic liquids. *Macromol Mater Eng* **2012**;*297*(6):585–94.
45. Minus ML, Kumar S. The processing, properties, and structure of carbon fibers. *Jom* **2005**;*57*(2):52–8.
46. Ko TH. The influence of pyrolysis on physical properties and microstructure of modified PAN fibers during carbonization. *J Appl Polym Sci* **1991**;*43*(3):589–600.
47. William J, William W. Production of carbon fibres and compositions containing said fibres. Google Patents. No. 3412062, **1968**-11-19.
48. Rašković V, Marinković S. Temperature dependence of processes during oxidation of PAN fibres. *Carbon* **1975**;*13*(6):535–8.
49. White SA, Spruiell JE, Paulauskas FL. Fundamental studies of stabilization of polyacrylonitrile precursor, part 1: Effects of thermal and environmental treatments. International SAMPE Symposium and Exhibition (Proceedings). 2006;51.
50. Paulauskas FL, Spruiell JE. Structure and properties of carbon fibers produced using microwave-assisted plasma technology. Part 1. *Int SAMPE Tech Conf* **2004**;*40*:203–16.
51. Dietrich J, Hirt P, Herlinger H. Electron-beam-induced cyclisation to obtain C-fibre precursors from polyacrylonitrile homopolymers. *Eur Polymer J* **1996**;*32*(5):617–23.
52. Goodhew PJ, Clarke AJ, Bailey JE. A review of the fabrication and properties of carbon fibres. *Mater Sci Eng* **1975**;*17*(1):3–30.
53. Tsai JS. Effect of nitrogen atmosphere on the structure and properties of a PAN-based carbon fiber. *Text Res J* **1994**;*64*:772–4.
54. Rašković V, Marinković S. Processes in sulfur dioxide treatment of PAN fibers. *Carbon* **1978**;*16*(5):351–7.
55. Wangxi Z, Jie L, Gang W. Evolution of structure and properties of PAN precursors during their conversion to carbon fibers. *Carbon* **2003**;*41*(14):2805–12.
56. Guigon M, Oberlin A. Heat-treatment of high tensile strength PAN-based carbon fibres: microtexture, structure and mechanical properties. *Compos Sci Technol* **1986**;*27*(1):1–23.
57. Matsumoto T. Mesophase pitch and its carbon fibers. *Pure and Applied Chemistry - PURE APPL CHEM* **1985**;*57*:1553–62.
58. Zhou G, Liu Y, He L, Guo Q, Ye H. Microstructure difference between core and skin of T700 carbon fibers in heat-treated carbon/carbon composites. *Carbon* **2011**;*49*(9):2883–92.
59. Ōtani S. On the carbon fiber from the molten pyrolysis products. *Carbon* **1965**;*3*(1):31–8.
60. Brooks JD, Taylor GH. The formation of graphitizing carbons from the liquid phase. *Carbon* **1965**;*3*(2):185–93.
61. Özsin G, Pütün AE. Pitch based carbon fiber production. *J Facult Eng Arch Gazi Univ* **2018**;*33*(4):1433–44.
62. Chand S. Review carbon fibers for composites. *J Mater Sci* **2000**;*35*(6):1303–13.
63. Kim B-J, Kotegawa T, Eom Y, An J, Hong I-P, Kato O, Nakabayashi K, Miyawaki J, Kim BC, Mochida I, Yoon S-H. Enhancing the tensile strength of isotropic pitch-based carbon fibers by improving the stabilization and carbonization properties of precursor pitch. *Carbon* **2016**;*99*:649–57.
64. Pérez M, Granda M, Santamaría R, Morgan T, Menéndez R. A thermoanalytical study of the co-pyrolysis of coal-tar pitch and petroleum pitch. *Fuel* **2004**;*83*(9):1257–65.
65. Zeng SM, Maeda T, Tokumitsu K, Mondori J, Mochida I. Preparation of isotropic pitch precursors for general purpose carbon fibers (GPCF) by air blowing—II. Air blowing of coal tar, hydrogenated coal tar, and petroleum pitches. *Carbon* **1993**;*31*(3):413–9.
66. Angier D J, Barnum H W. Neomesophase formation. Google Patents. No. 4184942, **1980**-1-22.
67. Diefendorf R J, Riggs D M. Forming optically anisotropic pitches. Google Patents. No. 4208267, **1980**-6-17.
68. Yamada Y, Imamura T, Shibata M, Arita S, Honda H. Method for the preparation of pitches for spinning carbon fibers. Google Patents. No. 4606808, **1986**-8-19.
69. Seo I, Oono T, Murakami Y. Catalytic process for producing raw material pitch for carbon materials from naphthalene. Google Patents. No. 5066779, **1991**-11-19.
70. Prauchner MJ, Pasa VMD, Otani S, Otani C. Biopitch-based general purpose carbon fibers: processing and properties. *Carbon* **2005**;*43*(3):591–7.
71. Fan Z, Cao M, Yang WB, Zhu SP, Feng ZH. The evolution of microstructure and thermal conductivity of mesophase pitch-based carbon fibers with heat treatment temperature. *New Carbon Mater* **2019**;*34*(1):38–43.
72. Edie DD. The effect of processing on the structure and properties of carbon fibers. *Carbon* **1998**;*36*(4):345–62.
73. Liu J, Shimanoe H, Nakabayashi K, Miyawaki J, Ko S, Jeon Y-P, Yoon S-H. Preparation of isotropic pitch precursor for pitch-based carbon fiber through the co-carbonization of ethylene bottom oil and polyvinyl chloride. *J Ind Eng Chem* **2018**;*67*:276–83.
74. Mochida I, Toshima H, Korai Y, Matsumoto T. A microscopic study on the oxidative stabilization of a coal-tar-based mesophase pitch and its blends with PVC pitch. *J Mater Sci* **1989**;*24*(6):2191–8.
75. Mochida I, Toshima H, Korai Y, Matsumoto T. Control of molecular orientations in mesophase pitch-based carbon fibre by blending PVC pitch. *J Mater Sci* **1989**;*24*(1):57–62.
76. Mochida I, Shimizu K, Korai Y, Sakai Y, Fujiyama S, Toshima H, Hono T. Mesophase pitch catalytically prepared from anthracene with HF/BF3. *Carbon* **1992**;*30*(1):55–61.
77. Lu S, Blanco C, Rand B. Large diameter carbon fibres from mesophase pitch. *Carbon* **2002**;*40*(12):2109–16.
78. Krumpfer J, Giebel E, Frank E, Müller A, Ackermann L-M, Tironi C, Mourgas G, Unold J, Klapper M, Buchmeiser M, Müllen K. Poly(Methyl Vinyl Ketone) as a potential carbon fiber precursor. *Chem Mater* **2016**;*29*:780–8.

79. Özsin G, Pütün AE, Nakabayashi K, Miyawaki J, Yoon S-H. Environmental-friendly production of carbon fiber from isotropic hybrid pitches synthesized from waste biomass and polystyrene with ethylene bottom oil. *J Clean Prod* **2019**;*239*:118025.
80. Korai Y, Nakamura M, Mochida I, Sakai Y, Fujiyama S. Mesophase pitches prepared from methylnaphthalene by the aid of HFBF3. *Carbon* **1991**;*29*(4):561–7.
81. Mochida I, Inaba T, Korai Y, Takeshita K. Carbonization properties of carbonaceous substances oxidized by air blowing—II: acid-catalyzed modification of oxidized residual oil for better anisotropic development. *Carbon* **1983**;*21*(6):553–8.
82. Díez N, Álvarez P, Santamaría R, Blanco C, Menéndez R, Granda M. Optimisation of the melt-spinning of anthracene oil-based pitch for isotropic carbon fibre preparation. *Fuel Process Technol* **2012**;*93*(1):99–104.
83. Tagawa T, Miyata T. Size effect on tensile strength of carbon fibers. *Mater Sci Eng A* **1997**;*238*(2):336–42.
84. Yoon S-H, Korai Y, Mochida I, Kato I. The flow properties of mesophase pitches derived from methylnaphthalene and naphthalene in the temperature range of their spinning. *Carbon* **1994**;*32*(2):273–80.
85. Cato AD, Edie DD. Flow behavior of mesophase pitch. *Carbon* **2003**;*41*(7):1411–7.
86. Park SH, Kim C, Yang KS. Preparation of carbonized fiber web from electrospinning of isotropic pitch. *Synth Met* **2004**;*143*(2):175–9.
87. Mochida I, Yoon SH, Korai Y. Control of transversal texture in circular mesophase pitch-based carbon fibre using non-circular spinning nozzles. *J Mater Sci* **1993**;*28*(9):2331–6.
88. Gerard LJ. Chemical reactions in the stabilization of mesophase pitch-based carbon fiber. *Carbon* **1992**;*30*(3):351–7.
89. Drbohlav J, Stevenson WTK. The oxidative stabilization and carbonization of a synthetic mesophase pitch, part I: the oxidative stabilization process. *Carbon* **1995**;*33*(5):693–711.
90. Drbohlav J, Stevenson WTK. The oxidative stabilization and carbonization of a synthetic mesophase pitch, part II: the carbonization process. *Carbon* **1995**;*33*(5):713–31.
91. Prauchner MJ, Pasa VMD, Molhallem NDS, Otani C, Otani S, Pardini LC. Structural evolution of Eucalyptus tar pitch-based carbons during carbonization. *Biomass Bioenerg* **2005**;*28*(1):53–61.
92. Goma J, Oberlin M. Graphitization of thin carbon films. *Thin Solid Films* **1980**;*65*(2):221–32.
93. Mora E, Blanco C, Prada V, Santamaría R, Granda M, Menéndez R. A study of pitch-based precursors for general purpose carbon fibres. *Carbon* **2002**;*40*(14):2719–25.
94. Qin X, Lu Y, Xiao H, Wen Y, Yu T. A comparison of the effect of graphitization on microstructures and properties of polyacrylonitrile and mesophase pitch-based carbon fibers. *Carbon* **2012**;*50*(12):4459–69.
95. Edison T A, Electric lamp. Google Patents. No. 223898, **1880**-1-27.
96. Bacon R, Schalamon WA. High strength and high modulus carbon fibers. *Carbon* **1968**;*6*(2):211.
97. Chegolya A, Grinshpan DD, Burd E. Production of regenerated cellulose fibers without carbon disulfide. *Text Res J* **1989**;*59*:501–6.
98. Northolt MG, Boerstoel H, Maatman H, Huisman R, Veurink J, Elzerman H. The structure and properties of cellulose fibres spun from an anisotropic phosphoric acid solution. *Polymer* **2001**;*42*(19):8249–64.
99. Bredereck K, Hermanutz F. Man–made cellulosics. *Rev Prog Color Relat Top* **2005**;*35*(1):59–75.
100. Ingildeev D, Effenberger F, Bredereck K, Hermanutz F. Comparison of direct solvents for regenerated cellulosic fibers via the lyocell process and by means of ionic liquids. *J Appl Polym Sci* **2013**;*128*(6):4141–50.
101. Tang MM, Bacon R. Carbonization of cellulose fibers—I. Low temperature pyrolysis. *Carbon* **1964**;*2*(3):211–20.
102. Bacon R, Tang M M J C. Carbonization of cellulose fibers—II. Physical property study. Carbon. 1964;2(3):221,IN3,223–222,IN4,225.
103. Brunner PH, Roberts PV. The significance of heating rate on char yield and char properties in the pyrolysis of cellulose. *Carbon* **1980**;*18*(3):217–24.
104. Tomlinson JB, Theocharis CR. Studies of steam-activated viscose rayon chars. *Carbon* **1992**;*30*(6):907–11.
105. Villaine P, Janin C. Anistropic compositions of cellulose esters; processes for obtaining such compositions; fibers of cellulose esters or cellulose. Google Patents. No. 4839113, **1989**-6-13
106. Souto F, Calado V, Pereira N Jr. Lignin-based carbon fiber: a current overview. *Mater Res Express* **2018**;*5*(7):072001.
107. Sakakibara A. A structural model of softwood lignin. *Wood Sci Technol* **1980**;*14*(2):89–100.
108. Upton BM, Kasko AM. Strategies for the conversion of lignin to high-value polymeric materials: review and perspective. *Chem Rev* **2016**;*116*(4):2275–306.
109. Yun SI, Kim SH, Kim DW, Kim YA, Kim B-H. Facile preparation and capacitive properties of low-cost carbon nanofibers with ZnO derived from lignin and pitch as supercapacitor electrodes. *Carbon* **2019**;*149*:637–45.
110. Roman J, Neri W, Derré A, Poulin P. Electrospun lignin-based twisted carbon nanofibers for potential microelectrodes applications. *Carbon* **2019**;*145*:556–64.
111. Saito T, Brown RH, Hunt MA, Pickel DL, Pickel JM, Messman JM, Baker FS, Keller M, Naskar AK. Turning renewable resources into value-added polymer: development of lignin-based thermoplastic. *Green Chem* **2012**;*14*(12):3295–303.
112. Lora JH, Glasser WG. Recent industrial applications of lignin: a sustainable alternative to nonrenewable materials. *J Polym Environ* **2002**;*10*(1–2):39–48.
113. Braun JL, Holtman KM, Kadla JF. Lignin-based carbon fibers: oxidative thermostabilization of kraft lignin. *Carbon* **2005**;*43*(2):385–94.
114. Otani S, Fukuoka Y, Igarashi B, Sasaki K. Method for producing carbonized lignin fiber. Google Patents. No. 3461082, **1969**-8-12.
115. Fang W, Yang S, Wang XL, Yuan TQ, Sun RC. Manufacture and application of lignin-based carbon fibers (LCFs) and lignin-based carbon nanofibers (LCNFs). *Green Chem* **2017**;*19*(8):1794–827.
116. Seo DK, Jeun JP, Kim HB, Kang PH. Preoaration and characterization of the carbon nanofiber mat produced from electrospun PAN/lignin precursors by electron beam irradiation. *Rev Adv Mater Sci* **2011**;*28*(1):31–4.
117. Choi DI, Lee JN, Song J, Kang PH, Park JK, Lee YM. Fabrication of polyacrylonitrile/lignin-based carbon nanofibers for high-power lithium ion battery anodes. *J Solid State Electrochem* **2013**;*17*(9):2471–5.
118. Frank E, Steudle LM, Ingildeev D, Spörl JM, Buchmeiser MR. Carbon fibers: precursor systems, processing, structure, and properties. *Angew Chem Int Ed* **2014**;*53*(21):5262–98.
119. Thunga M, Chen K, Grewell D, Kessler MR. Bio-renewable precursor fibers from lignin/polylactide blends for conversion to carbon fibers. *Carbon* **2014**;*68*:159–66.
120. Nowak AP, Hagberg J, Leijonmarck S, Schweinebarth H, Baker D, Uhlin A, Tomani P, Lindbergh G. Lignin-based carbon fibers for renewable and multifunctional lithium-ion battery electrodes. *Holzforschung* **2018**;*72*(2):81–90.
121. Kubo S, Uraki Y, Sano Y. Preparation of carbon fibers from softwood lignin by atmospheric acetic acid pulping. *Carbon* **1998**;*36*(7–8):1119–24.

122. Norberg I, Nordstrom Y, Drougge R, Gellerstedt G, Sjoholm E. A new method for stabilizing softwood kraft lignin fibers for carbon fiber production. *J Appl Polym Sci* **2013**;*128*(6):3824–30.
123. Dai Z, Shi XJ, Liu H, Li HM, Han Y, Zhou JH. High-strength lignin-based carbon fibers via a low-energy method. *RSC Adv* **2018**;*8*(3):1218–24.
124. Sagues W, Jain A, Brown D, Aggarwal S, Suarez A, Kollman M, Park S, Argyropoulos D. Are lignin-derived carbon fibers graphitic enough? *Green Chem* **2019**;*21*:4253–65.
125. Yang YC, Wang TJ, Wang SD, Cong X, Zhang SL, Zhang M, Luan JS, Wang GB. Strong interface construction of carbon fiber-reinforced PEEK composites: an efficient method for modifying carbon fiber with crystalline PEEK. *Macromol Rapid Commun* **2020**;*41*(24):2000001.
126. Ni X, Chen H, Liu C, Zeng F, Yu H, Ju A. A freestanding nitrogen-doped carbon nanofiber/MoS2 nanoflowers with expanded interlayer for long cycle-life lithium-ion batteries. *J Alloys Comp* **2020**;*818*:152835.
127. Ni X, Cui Z, Jiang N, Chen H, Wu Q, Ju A, Zhu M. Hollow multi-nanochannel carbon nanofiber/MoS2 nanoflower composites as binder-free lithium-ion battery anodes with high capacity and ultralong-cycle life at large current density. *J Mater Sci Technol* **2021**;*77*:169–77.
128. Ni X, Cui Z, Luo H, Chen H, Liu C, Wu Q, Ju A. Hollow multi-nanochannel carbon nanofibers@MoSe2 nanosheets composite as flexible anodes for high performance lithium-ion batteries. *Chem Eng J* **2021**;*404*:126249.
129. Raza F, Ni X, Wang J, Liu S, Jiang Z, Liu C, Chen H, Farooq A, Ju A. Ultrathin honeycomb-like MnO2 on hollow carbon nanofiber networks as binder-free electrode for flexible symmetric all-solid-state supercapacitors. *J Energy Storage* **2020**;*30*:101467.
130. Yue Y, Liu K, Li M, Hu X. Thermal manipulation of carbon nanotube fiber by mechanical stretching. *Carbon* **2014**;*77*:973–9.
131. Dalton AB, Collins S, Razal J, Munoz E, Ebron VH, Kim BG, Coleman JN, Ferraris JP, Baughman RH. Continuous carbon nanotube composite fibers: properties, potential applications, and problems. *J Mater Chem* **2004**;*14*(1):1–3.
132. Ericson LM, Fan H, Peng HQ, Davis VA, Zhou W, Sulpizio J, Wang YH, Booker R, Vavro J, Guthy C, Parra-Vasquez ANG, Kim MJ, Ramesh S, Saini RK, Kittrell C, Lavin G, Schmidt H, Adams WW, Billups WE, Pasquali M, Hwang WF, Hauge RH, Fischer JE, Smalley RE. Macroscopic, neat, single-walled carbon nanotube fibers. *Science* **2004**;*305*(5689):1447–50.
133. Kozlov ME, Capps RC, Sampson WM, Ebron VH, Ferraris JP, Baughman RH. Spinning solid and hollow polymer-free carbon nanotube fibers. *Adv Mater* **2005**;*17*(5):614.
134. Behabtu N, Young CC, Tsentalovich DE, Kleinerman O, Wang X, Ma AWK, Bengio EA, ter Waarbeek RF, de Jong JJ, Hoogerwerf RE, Fairchild SB, Ferguson JB, Maruyama B, Kono J, Talmon Y, Cohen Y, Otto MJ, Pasquali M. Strong, light, multifunctional fibers of carbon nanotubes with ultrahigh conductivity. *Science* **2013**;*339*(6116):182–6.
135. Zhang SJ, Koziol KKK, Kinloch IA, Windle AH. Macroscopic fibers of well-aligned carbon nanotubes by wet spinning. *Small* **2008**;*4*(8):1217–22.
136. Tsentalovich DE, Headrick RJ, Mirri F, Hao JL, Behabtu N, Young CC, Pasquali M. Influence of carbon nanotube characteristics on macroscopic fiber properties. *ACS Appl Mater Interfaces* **2017**;*9*(41):36189–98.
137. Lee J, Lee DM, Jung Y, Park J, Lee HS, Kim YK, Park CR, Jeong HS, Kim SM. Direct spinning and densification method for high-performance carbon nanotube fibers. *Nat Commun* **2019**;*10*(1):2962.
138. Zhang XB, Jiang KL, Teng C, Liu P, Zhang L, Kong J, Zhang TH, Li QQ, Fan SS. Spinning and processing continuous yarns from 4-inch wafer scale super-aligned carbon nanotube arrays. *Adv Mater* **2006**;*18*(12):1505.
139. Zhang M, Atkinson KR, Baughman RH. Multifunctional carbon nanotube yarns by downsizing an ancient technology. *Science* **2004**;*306*(5700):1358–61.
140. Li QW, Zhang XF, DePaula RF, Zheng LX, Zhao YH, Stan L, Holesinger TG, Arendt PN, Peterson DE, Zhu YT. Sustained growth of ultralong carbon nanotube arrays for fiber spinning. *Adv Mater* **2006**;*18*(23):3160.
141. Zhu C, Cheng C, He YH, Wang L, Wong TL, Fung KK, Wang N. A self-entanglement mechanism for continuous pulling of carbon nanotube yarns. *Carbon* **2011**;*49*(15):4996–5001.
142. Inoue Y, Kakihata K, Hirono Y, Horie T, Ishida A, Mimura H. One-step grown aligned bulk carbon nanotubes by chloride mediated chemical vapor deposition. *Appl Phys Lett* **2008**;*92*(21):213113.
143. Jia JJ, Zhao JN, Xu G, Di JT, Yong ZZ, Tao YY, Fang CO, Zhang ZG, Zhang XH, Zheng LX, Li QW. A comparison of the mechanical properties of fibers spun from different carbon nanotubes. *Carbon* **2011**;*49*(4):1333–9.
144. Ghemes A, Minami Y, Muramatsu J, Okada M, Mimura H, Inoue Y. Fabrication and mechanical properties of carbon nanotube yarns spun from ultra-long multi-walled carbon nanotube arrays. *Carbon* **2012**;*50*(12):4579–87.
145. Liu K, Sun YH, Zhou RF, Zhu HY, Wang JP, Liu L, Fan SS, Jiang KL. Carbon nanotube yarns with high tensile strength made by a twisting and shrinking method. *Nanotechnology* **2010**;*21*(4):045708.
146. Ryu S, Lee Y, Hwang JW, Hong S, Kim C, Park TG, Lee H, Hong SH. High-strength carbon nanotube fibers fabricated by infiltration and curing of mussel-inspired catecholamine polymer. *Adv Mater* **2011**;*23*(17):1971–5.
147. Kuznetsov AA, Fonseca AF, Baughman RH, Zakhidov AA. Structural model for dry-drawing of sheets and yarns from carbon nanotube forests. *ACS Nano* **2011**;*5*(2):985–93.
148. O'Brien NP, McCarthy MA, Curtin WA. Improved inter-tube coupling in CNT bundles through carbon ion irradiation. *Carbon* **2013**;*51*:173–84.
149. Zhang XF, Li QW, Holesinger TG, Arendt PN, Huang JY, Kirven PD, Clapp TG, DePaula RF, Liao XZ, Zhao YH, Zheng LX, Peterson DE, Zhu YT. Ultrastrong, stiff, and lightweight carbon-nanotube fibers. *Adv Mater* **2007**;*19*(23):4198.
150. Fang C, Zhao JN, Jia JJ, Zhang ZG, Zhang XH, Li QW. Enhanced carbon nanotube fibers by polyimide. *Appl Phys Lett* **2010**;*97*(18):181906.
151. Alvarez NT, Miller P, Haase M, Kienzle N, Zhang L, Schulz MJ, Shanov V. Carbon nanotube assembly at near-industrial natural-fiber spinning rates. *Carbon* **2015**;*86*:350–7.
152. Atkinson KR, Hawkins SC, Huynh C, Skourtis C, Dai J, Zhang M, Fang SL, Zakhidov AA, Lee SB, Aliev AE, Williams CD, Baughman RH. Multifunctional carbon nanotube yarns and transparent sheets: fabrication, properties, and applications. *Physica B* **2007**;*394*(2):339–43.
153. Miao MH. Electrical conductivity of pure carbon nanotube yarns. *Carbon* **2011**;*49*(12):3755–61.
154. Wang K, Li M, Liu YN, Gu YZ, Li QW, Zhang ZG. Effect of acidification conditions on the properties of carbon nanotube fibers. *Appl Surf Sci* **2014**;*292*:469–74.
155. Li YL, Kinloch IA, Windle AH. Direct spinning of carbon nanotube fibers from chemical vapor deposition synthesis. *Science* **2004**;*304*(5668):276–8.
156. Barnard JS, Paukner C, Koziol KK. The role of carbon precursor on carbon nanotube chirality in floating catalyst chemical vapour deposition. *Nanoscale* **2016**;*8*(39):17262–70.

157. Sundaram RM, Koziol KKK, Windle AH. Continuous direct spinning of fibers of single-walled carbon nanotubes with metallic chirality. *Adv Mater* **2011**;*23*(43):5064–8.
158. Lee SH, Park J, Kim HR, Lee J, Lee KH. Synthesis of high-quality carbon nanotube fibers by controlling the effects of sulfur on the catalyst agglomeration during the direct spinning process. *RSC Adv* **2015**;*5*(52):41894–900.
159. Motta M, Li YL, Kinloch I, Windle A. Mechanical properties of continuously spun fibers of carbon nanotubes. *Nano Lett* **2005**;*5*(8):1529–33.
160. Koziol K, Vilatela J, Moisala A, Motta M, Cunniff P, Sennett M, Windle A. High-performance carbon nanotube fiber. *Science* **2007**;*318*(5858):1892–5.
161. Im YO, Lee SH, Kim T, Park J, Lee J, Lee KH. Utilization of carboxylic functional groups generated during purification of carbon nanotube fiber for its strength improvement. *Appl Surf Sci* **2017**;*392*:342–9.
162. Liu P, Li YM, Xu YF, Bao LK, Wang L, Pan J, Zhang ZT, Sun XM, Peng HS. Stretchable and energy-efficient heating carbon nanotube fiber by designing a hierarchically helical structure. *Small* **2018**;*14*(4):1702926.
163. Li WY, Zhao JN, Xue Y, Ren XQ, Zhang XH, Li QW. Merge multiple carbon nanotube fibers into a robust yarn. *Carbon* **2019**;*145*:266–72.
164. Ma WJ, Liu LQ, Zhang Z, Yang R, Liu G, Zhang TH, An XF, Yi XS, Ren Y, Niu ZQ, Li JZ, Dong HB, Zhou WY, Ajayan PM, Xie SS. High-strength composite fibers: realizing true potential of carbon nanotubes in polymer matrix through continuous reticulate architecture and molecular level couplings. *Nano Lett* **2009**;*9*(8):2855–61.
165. Feng J-M, Wang R, Li Y-L, Zhong X-H, Cui L, Guo Q-J, Hou F. One-step fabrication of high quality double-walled carbon nanotube thin films by a chemical vapor deposition process. *Carbon* **2010**;*48*(13):3817–24.
166. Song L, Toth G, Vajtai R, Endo M, Ajayan PM. Fabrication and characterization of single-walled carbon nanotube fiber for electronics applications. *Carbon* **2012**;*50*(15):5521–4.
167. Mora RJ, Vilatela JJ, Windle AH. Properties of composites of carbon nanotube fibres. *Compos Sci Technol* **2009**;*69*(10):1558–63.
168. Zhou G, Wang YQ, Byun JH, Yi JW, Yoon SS, Cha HJ, Lee JU, Oh Y, Jung BM, Moon HJ, Chou TW. High-strength single-walled carbon nanotube/permalloy nanoparticle/poly(vinyl alcohol) multifunctional nanocomposite fiber. *ACS Nano* **2015**;*9*(11):11414–21.
169. Le Wu M, Chen Y, Zhang L, Zhan H, Qjang L, Wang JN. High-performance carbon nanotube/polymer composite fiber from layer-by-layer deposition. *ACS Appl Mater Interfaces* **2016**;*8*(12):8137–44.
170. Zhang SL, Hao A, Nguyen N, Oluwalowo A, Liu Z, Dessureault Y, Park JG, Liang R. Carbon nanotube/carbon composite fiber with improved strength and electrical conductivity via interface engineering. *Carbon* **2019**;*144*:628–38.
171. Feng L, Fu QG, Song Q, Yang YL, Zuo Y, Suo GQ, Hou XJ, Zhang L, Ye XH. A novel continuous carbon nanotube fiber/carbon composite by electrified preform heating chemical vapor infiltration. *Carbon* **2020**;*157*:640–8.
172. Han BS, Guo EY, Xue X, Zhao ZY, Luo LS, Qu HT, Niu T, Xu YJ, Hou HL. Fabrication and densification of high performance carbon nanotube/copper composite fibers. *Carbon* **2017**;*123*:593–604.
173. Rho H, Park M, Park M, Park J, Han J, Lee A, Bae S, Kim TW, Ha JS, Kim SM, Lee DS, Lee SH. Metal nanofibrils embedded in long free-standing carbon nanotube fibers with a high critical current density. *NPG Asia Mater* **2018**;*10*:146–55.
174. Zhong XH, Wang R, Wen YY. Effective reinforcement of electrical conductivity and strength of carbon nanotube fibers by silver-paste-liquid infiltration processing. *Phys Chem Chem Phys* **2013**;*15*(11):3861–5.
175. Zhong XH, Wang R, Wen YY, Li YL. Carbon nanotube and graphene multiple-thread yarns. *Nanoscale* **2013**;*5*(3):1183–7.
176. Foroughi J, Spinks GM, Antiohos D, Mirabedini A, Gambhir S, Wallace GG, Ghorbani SR, Peleckis G, Kozlov ME, Lima MD, Baughman RH. Highly conductive carbon nanotube-graphene hybrid yarn. *Adv Func Mater* **2014**;*24*(37):5859–65.
177. Lepak-Kuc S, Milowska KZ, Boncel S, Szybowicz M, Dychalska A, Jozwik I, Koziol KK, Jakubowska M, Lekawa-Raus A. Highly conductive doped hybrid carbon nanotube-graphene wires. *ACS Appl Mater Interfaces* **2019**;*11*(36):33207–20.
178. Bernholc J, Brenner D, Nardelli MB, Meunier V, Roland C. Mechanical and electrical properties of nanotubes. *Ann Rev Mater Res* **2002**;*32*(1):347–75.
179. Zhao Y, Wei JQ, Vajtai R, Ajayan PM, Barrera EV. Iodine doped carbon nanotube cables exceeding specific electrical conductivity of metals. *Sci Rep* **2011**;*1*(1):83.
180. Alvarenga J, Jarosz PR, Schauerman CM, Moses BT, Landi BJ, Cress CD, Raffaelle RP. High conductivity carbon nanotube wires from radial densification and ionic doping. *Appl Phys Lett* **2010**;*97*(18):182106.
181. Guo FM, Li C, Wei JQ, Xu RQ, Zhang ZL, Cui X, Wang KL, Wu DH. Fabrication of highly conductive carbon nanotube fibers for electrical application. *Mater Res Express* **2015**;*2*(9):095604.
182. Lekawa-Raus A, Haladyj P, Koziol K. Carbon nanotube fiber-silver hybrid electrical conductors. *Mater Lett* **2014**;*133*:186–9.
183. Tran TQ, Lee JKY, Chinnappan A, Jayathilaka W, Ji DX, Kumar VV, Ramakrishna S. Strong, lightweight, and highly conductive CNT/Au/Cu wires from sputtering and electroplating methods. *J Mater Sci Technol* **2020**;*40*:99–106.
184. Zu M, Li QW, Wang GJ, Byun JH, Chou TW. Carbon nanotube fiber based stretchable conductor. *Adv Func Mater* **2013**;*23*(7):789–93.
185. Guo H, Dewey O, McCorkle L, Meador M, Pasquali M. Polyimide aerogels as lightweight dielectric insulators for carbon nanotube cables. *ACS Appl Polymer Mater* **2019**;*1*:1680–8.
186. Zhao HB, Zhang YY, Bradford PD, Zhou QA, Jia QX, Yuan FG, Zhu YT. Carbon nanotube yarn strain sensors. *Nanotechnology* **2010**;*21*(30):305502.
187. Li YB, Shang YY, He XD, Peng QY, Du SY, Shi EZ, Wu ST, Li Z, Li PX, Cao AY. Overtwisted, resolvable carbon nanotube yarn entanglement as strain sensors and rotational actuators. *ACS Nano* **2013**;*7*(9):8128–35.
188. Wang ZF, Huang Y, Sun JF, Huang Y, Hu H, Jiang RJ, Gai WM, Li GM, Zhi CY. Polyurethane/cotton/carbon nanotubes core-spun yarn as high reliability stretchable strain sensor for human motion detection. *ACS Appl Mater Interfaces* **2016**;*8*(37):24837–43.
189. Sim HJ, Choi C, Kim SH, Kim KM, Lee CJ, Kim YT, Lepro X, Baughman RH, Kim SJ. Stretchable triboelectric fiber for self-powered kinematic sensing textile. *Sci Rep* **2016**;*6*:35153.
190. Abot JL, Kiyono CY, Thomas GP, Silva ECN. Strain gauge sensors comprised of carbon nanotube yarn: parametric numerical analysis of their piezoresistive response. *Smart Mater Struct* **2015**;*24*(7):075018.
191. Wei Y, Lin XY, Jiang KL, Liu P, Li QQ, Fan SS. Thermoacoustic chips with carbon nanotube thin yarn arrays. *Nano Lett* **2013**;*13*(10):4795–801.
192. Sibinski M, Jakubowska M, Sloma M. Flexible temperature sensors on fibers. *Sensors* **2010**;*10*(9):7934–46.
193. Guinovart T, Parrilla M, Crespo GA, Rius FX, Andrade FJ. Potentiometric sensors using cotton yarns, carbon nanotubes and polymeric membranes. *Analyst* **2013**;*138*(18):5208–15.
194. Schmidt AC, Wang X, Zhu Y, Sombers LA. Carbon nanotube yarn electrodes for enhanced detection of neurotransmitter dynamics in live brain tissue. *ACS Nano* **2013**;*7*(9):7864–73.

195. Jacobs CB, Ivanov IN, Nguyen MD, Zestos AG, Venton BJ. High temporal resolution measurements of dopamine with carbon nanotube yarn microelectrodes. *Anal Chem* **2014**;*86*(12):5721–7.
196. Yang C, Trikantzopoulos E, Nguyen MD, Jacobs CB, Wang Y, Mahjouri-Samani M, Ivanov IN, Venton BJ. Laser treated carbon nanotube yarn microelectrodes for rapid and sensitive detection of dopamine in vivo. *Acs Sensors* **2016**;*1*(5):508–15.
197. Yang C, Wang Y, Jacobs CB, Ivanov IN, Venton BJ. O-2 plasma etching and antistatic gun surface modifications for CNT yarn microelectrode improve sensitivity and antifouling properties. *Anal Chem* **2017**;*89*(10):5605–11.
198. Yang C, Trikantzopoulos E, Jacobs CB, Venton BJ. Evaluation of carbon nanotube fiber microelectrodes for neurotransmitter detection: correlation of electrochemical performance and surface properties. *Anal Chim Acta* **2017**;*965*:1–8.
199. Al-Graiti W, Yue Z, Foroughi J, Huang X-F, Wallace G, Baughman R, Chen J. Probe sensor using nanostructured multi-walled carbon nanotube yarn for selective and sensitive detection of dopamine. *Sensors* **2017**;*17*(4):884.
200. Foroughi J, Spinks GM, Wallace GG, Oh J, Kozlov ME, Fang SL, Mirfakhrai T, Madden JDW, Shin MK, Kim SJ, Baughman RH. Torsional carbon nanotube artificial muscles. *Science* **2011**;*334*(6055):494–7.
201. Lee JA, Li N, Haines CS, Kim KJ, Lepro X, Ovalle-Robles R, Kim SJ, Baughman RH. Electrochemically powered, energy-conserving carbon nanotube artificial muscles. *Adv Mater* **2017**;*29*(31):1700870.
202. Kim KJ, Hyeon JS, Kim H, Mun TJ, Haines CS, Li N, Baughman RH, Kim SJ. Enhancing the work capacity of electrochemical artificial muscles by coiling plies of twist-released carbon nanotube yarns. *ACS Appl Mater Interfaces* **2019**;*11*(14):13533–7.
203. Lima MD, Li N, de Andrade MJ, Fang SL, Oh J, Spinks GM, Kozlov ME, Haines CS, Suh D, Foroughi J, Kim SJ, Chen YS, Ware T, Shin MK, Machado LD, Fonseca AF, Madden JDW, Voit WE, Galvao DS, Baughman RH. Electrically, chemically, and photonically powered torsional and tensile actuation of hybrid carbon nanotube yarn muscles. *Science* **2012**;*338*(6109):928–32.
204. Kwon CH, Chun K-Y, Kim SH, Lee J-H, Kim J-H, Lima MD, Baughman RH, Kim SJ. Torsional behaviors of polymer-infiltrated carbon nanotube yarn muscles studied with atomic force microscopy. *Nanoscale* **2015**;*7*(6):2489–96.
205. Song YH, Zhou SS, Jin KY, Qiao J, Li D, Xu C, Hu DM, Di JT, Li M, Zhang ZG, Li QW. Hierarchical carbon nanotube composite yarn muscles. *Nanoscale* **2018**;*10*(8):4077–84.
206. Lee JA, Shin MK, Kim SH, Kim SJ, Spinks GM, Wallace GG, Ovalle-Robles R, Lima MD, Kozlov ME, Baughman RH. Hybrid nanomembranes for high power and high energy density supercapacitors and their yarn application. *ACS Nano* **2012**;*6*(1):327–34.
207. Wang K, Meng QH, Zhang YJ, Wei ZX, Miao MH. High-performance two-ply yarn supercapacitors based on carbon nanotubes and polyaniline nanowire arrays. *Adv Mater* **2013**;*25*(10):1494–8.
208. Su F, Miao M, Niu H, Wei Z. Gamma-irradiated carbon nanotube yarn as substrate for high-performance fiber supercapacitors. *ACS Appl Mater Interfaces* **2014**;*6*(4):2553–60.
209. Choi C, Lee JA, Choi AY, Kim YT, Lepro X, Lima MD, Baughman RH, Kim SJ. Flexible supercapacitor made of carbon nanotube yarn with internal pores. *Adv Mater* **2014**;*26*(13):2059–65.
210. Kim JH, Choi C, Lee JM, de Andrade MJ, Baughman RH, Kim SJ. Ag/MnO2 composite sheath-core structured yarn supercapacitors. *Sci Rep* **2018**;*8*:13309.
211. Su FH, Miao MH. Asymmetric carbon nanotube-MnO2 two-ply yarn supercapacitors for wearable electronics. *Nanotechnology* **2014**;*25*(13):135401.
212. Su FH, Lv XM, Miao MH. High-performance two-ply yarn supercapacitors based on carbon nanotube yarns dotted with Co_3O_4 and NiO nanoparticles. *Small* **2015**;*11*(7):854–61.
213. Wang ZY, Qin S, Seyedin S, Zhang JZ, Wang JT, Levitt A, Li N, Haines C, Ovalle-Robles R, Lei WW, Gogotsi Y, Baughman RH, Razal JM. High-performance biscrolled MXene/carbon nanotube yarn supercapacitors. *Small* **2018**;*14*(37):1802225.
214. Zhang DH, Miao MH, Niu HT, Wei ZX. Core-spun carbon nanotube yarn supercapacitors for wearable electronic textiles. *ACS Nano* **2014**;*8*(5):4571–9.
215. Kim KM, Lee JA, Sim HJ, Kim KA, Jalili R, Spinks GM, Kim SJ. Shape-engineerable composite fibers and their supercapacitor application. *Nanoscale* **2016**;*8*(4):1910–4.
216. Kou L, Huang TQ, Zheng BN, Han Y, Zhao XL, Gopalsamy K, Sun HY, Gao C. Coaxial wet-spun yarn supercapacitors for high-energy density and safe wearable electronics. *Nat Commun* **2014**;*5*(1):3754.
217. Son W, Chun S, Lee JM, Lee Y, Park J, Suh D, Lee DW, Jung H, Kim YJ, Kim Y, Jeong SM, Lim SK, Choi C. Highly twisted supercoils for superelastic multi-functional fibres. *Nat Commun* **2019**;*10*:11.
218. Choi C, Kim KM, Kim KJ, Lepro X, Spinks GM, Baughman RH, Kim SJ. Improvement of system capacitance via weavable superelastic biscrolled yarn supercapacitors. *Nat Commun* **2016**;*7*(1):13811.
219. Zheng Q, Shi BJ, Li Z, Wang ZL. Recent progress on piezoelectric and triboelectric energy harvesters in biomedical systems. *Adv Sci* **2017**;*4*(7):1700029.
220. Kim SH, Haines CS, Li N, Kim KJ, Mun TJ, Choi C, Di JT, Oh YJ, Oviedo JP, Bykova J, Fang SL, Jiang N, Liu ZF, Wang R, Kumar P, Qiao R, Priya S, Cho K, Kim M, Lucas MS, Drummy LF, Maruyama B, Lee DY, Lepro X, Gao EL, Albarq D, Ovalle-Robles R, Kim SJ, Baughman RH. Harvesting electrical energy from carbon nanotube yarn twist. *Science* **2017**;*357*(6353):773–8.
221. Choi J, Jung Y, Yang SJ, Oh JY, Oh J, Jo K, Son JG, Moon SE, Park CR, Kim H. Flexible and robust thermoelectric generators based on all-carbon nanotube yarn without metal electrodes. *ACS Nano* **2017**;*11*(8):7608–14.
222. Zhang WM, Minett AI, Gao M, Zhao J, Razal JM, Wallace GG, Romeo T, Chen J. Integrated high-efficiency Pt/carbon nanotube arrays for PEM fuel cells. *Adv Energy Mater* **2011**;*1*(4):671–7.
223. Chen T, Qiu LB, Cai ZB, Gong F, Yang ZB, Wang ZS, Peng HS. Intertwined aligned carbon nanotube fiber based dye-sensitized solar cells. *Nano Lett* **2012**;*12*(5):2568–72.
224. Liu DY, Zhao MY, Li Y, Bian ZQ, Zhang LH, Shang YY, Xia XY, Zhang S, Yun DQ, Liu ZW, Cao AY, Huang CH. Solid-state, polymer-based fiber solar cells with carbon nanotube electrodes. *ACS Nano* **2012**;*6*(12):11027–34.
225. Zhang S, Ji CY, Bian ZQ, Yu PR, Zhang LH, Liu DY, Shi EZ, Shang YY, Peng HT, Cheng Q, Wang D, Huang CH, Cao AY. Porous, platinum nanoparticle-adsorbed carbon nanotube yarns for efficient fiber solar cells. *ACS Nano* **2012**;*6*(8):7191–8.
226. Yu XH, Pan J, Deng J, Zhou J, Sun XM, Peng HS. A novel photoelectric conversion yarn by integrating photomechanical actuation and the electrostatic effect. *Adv Mater* **2016**;*28*(48):10744.
227. Linares RV, Li Z, Sarp S, Bucs SS, Amy G, Vrouwenvelder JS. Forward osmosis niches in seawater desalination and wastewater reuse. *Water Res* **2014**;*66*:122–39.
228. Fan XF, Liu YM, Quan X, Chen S. Highly permeable thin-film composite forward osmosis membrane based on carbon nanotube hollow fiber scaffold with electrically enhanced fouling resistance. *Environ Sci Technol* **2018**;*52*(3):1444–52.
229. Fan XF, Liu YM, Quan X. A novel reduced graphene oxide/carbon nanotube hollow fiber membrane with high forward osmosis performance. *Desalination* **2019**;*451*:117–24.
230. Xu Z, Gao C. Aqueous liquid crystals of graphene oxide. *ACS Nano* **2011**;*5*(4):2908–15.

231. Cong HP, Ren XC, Wang P, Yu SH. Wet-spinning assembly of continuous, neat, and macroscopic graphene fibers. *Sci Rep* **2012**;*2*(1):613.
232. Xu Z, Sun HY, Zhao XL, Gao C. Ultrastrong fibers assembled from giant graphene oxide sheets. *Adv Mater* **2013**;*25*(2):188–93.
233. Chen L, He YL, Chai SG, Qiang H, Chen F, Fu Q. Toward high performance graphene fibers. *Nanoscale* **2013**;*5*(13):5809–15.
234. Xiang CS, Young CC, Wang X, Yan Z, Hwang CC, Cerioti G, Lin J, Kono J, Pasquali M, Tour JM. Large flake graphene oxide fibers with unconventional 100% knot efficiency and highly aligned small flake graphene oxide fibers. *Adv Mater* **2013**;*25*(33):4592–7.
235. Cao J, Zhang YY, Men CL, Sun YY, Wang ZN, Zhang XT, Li QW. Programmable writing of graphene oxide/reduced graphene oxide fibers for sensible networks with in situ welded junctions. *ACS Nano* **2014**;*8*(5):4325–33.
236. Aboutalebi SH, Jalili R, Esrafilzadeh D, Salari M, Gholamvand Z, Yamini SA, Konstantinov K, Shepherd RL, Chen J, Moulton SE, Innis PC, Minett AI, Razal JM, Wallace GG. High-performance multifunctional graphene yarns: toward wearable all-carbon energy storage textiles. *ACS Nano* **2014**;*8*(3):2456–66.
237. Ma WG, Liu YJ, Yan S, Miao TT, Shi SY, Xu Z, Zhang X, Gao C. Chemically doped macroscopic graphene fibers with significantly enhanced thermoelectric properties. *Nano Res* **2018**;*11*(2):741–50.
238. Wu G, Tan PF, Wu XJ, Peng L, Cheng HY, Wang CF, Chen W, Yu ZY, Chen S. High-performance wearable micro-supercapacitors based on microfluidic-directed nitrogen-doped graphene fiber electrodes. *Adv Func Mater* **2017**;*27*(36):1702493.
239. Jalili R, Aboutalebi SH, Esrafilzadeh D, Shepherd RL, Chen J, Aminorroaya-Yamini S, Konstantinov K, Minett AI, Razal JM, Wallace GG. Scalable one-step wet-spinning of graphene fibers and yarns from liquid crystalline dispersions of graphene oxide: towards multifunctional textiles. *Adv Func Mater* **2013**;*23*(43):5345–54.
240. Kou L, Gao C. Bioinspired design and macroscopic assembly of poly(vinyl alcohol)-coated graphene into kilometers-long fibers. *Nanoscale* **2013**;*5*(10):4370–8.
241. Zhang YY, Peng JS, Li MZ, Saiz E, Wolf SE, Cheng QF. Bioinspired supertough graphene fiber through sequential interfacial interactions. *ACS Nano* **2018**;*12*(9):8901–8.
242. Huang GJ, Hou CY, Shao YL, Wang HZ, Zhang QH, Li YG, Zhu MF. Highly strong and elastic graphene fibres prepared from universal graphene oxide precursors. *Sci Rep* **2014**;*4*(1):4248.
243. Chen SH, Ma WJ, Cheng YH, Weng Z, Sun B, Wang L, Chen WP, Li F, Zhu MF, Cheng HM. Scalable non-liquid-crystal spinning of locally aligned graphene fibers for high-performance wearable supercapacitors. *Nano Energy* **2015**;*15*:642–53.
244. Zhao Y, Jiang CC, Hu CG, Dong ZL, Xue JL, Meng YN, Zheng N, Chen PW, Qu LT. Large-scale spinning assembly of neat, morphology-defined, graphene-based hollow fibers. *ACS Nano* **2013**;*7*(3):2406–12.
245. Xin GQ, Yao TK, Sun HT, Scott SM, Shao DL, Wang GK, Lian J. Highly thermally conductive and mechanically strong graphene fibers. *Science* **2015**;*349*(6252):1083–7.
246. Xu Z, Liu YJ, Zhao XL, Peng L, Sun HY, Xu Y, Ren XB, Jin CH, Xu P, Wang M, Gao C. Ultrastiff and strong graphene fibers via full-scale synergetic defect engineering. *Adv Mater* **2016**;*28*(30):6449.
247. Liu YJ, Xu Z, Zhan JM, Li PG, Gao C. Superb electrically conductive graphene fibers via doping strategy. *Adv Mater* **2016**;*28*(36):7941–7.
248. Pan H, Wang DW, Peng QF, Ma J, Meng X, Zhang YP, Ma YN, Zhu SM, Zhang D. High-performance microsupercapacitors based on bioinspired graphene microfibers. *ACS Appl Mater Interfaces* **2018**;*10*(12):10157–64.
249. Sheng LZ, Wei T, Liang Y, Jiang LL, Qu LT, Fan ZJ. Ultra-high toughness all graphene fibers derived from synergetic effect of interconnected graphene ribbons and graphene sheets. *Carbon* **2017**;*120*:17–22.
250. Ma T, Gao HL, Cong HP, Yao HB, Wu L, Yu ZY, Chen SM, Yu SH. A bioinspired interface design for improving the strength and electrical conductivity of graphene-based fibers. *Adv Mater* **2018**;*30*(15):1706435.
251. Li X, Sun PZ, Fan LL, Zhu M, Wang KL, Zhong ML, Wei JQ, Wu DH, Cheng Y, Zhu HW. Multifunctional graphene woven fabrics. *Sci Rep* **2012**;*2*(1):395.
252. Xiao M, Kong T, Wang W, Song Q, Zhang D, Ma QQ, Cheng GS. Interconnected graphene networks with uniform geometry for flexible conductors. *Adv Func Mater* **2015**;*25*(39):6165–72.
253. Hua CF, Shang YY, Li XY, Hu XY, Wang Y, Wang XC, Zhang YJ, Li XJ, Duan HL, Cao AY. Helical graphene oxide fibers as a stretchable sensor and an electrocapillary sucker. *Nanoscale* **2016**;*8*(20):10659–68.
254. Wang R, Xu Z, Zhuang JH, Liu Z, Peng L, Li Z, Liu YJ, Gao WW, Gao C. Highly stretchable graphene fibers with ultrafast electrothermal response for low-voltage wearable heaters. *Adv Electron Mater* **2017**;*3*(2):1600425.
255. Feng LC, Chang Y, Zhong J, Jia DC. Dry spin graphene oxide fibers: mechanical/electrical properties and microstructure evolution. *Sci Rep* **2018**;*8*(1):10803.
256. Meng YN, Zhao Y, Hu CG, Cheng HH, Hu Y, Zhang ZP, Shi GQ, Qu LT. All-graphene core-sheath microfibers for all-solid-state, stretchable fibriform supercapacitors and wearable electronic textiles. *Adv Mater* **2013**;*25*(16):2326–31.
257. Zhao XL, Zheng BN, Huang TQ, Gao C. Graphene-based single fiber supercapacitor with a coaxial structure. *Nanoscale* **2015**;*7*(21):9399–404.
258. Zheng BN, Huang TQ, Kou L, Zhao XL, Gopalsamy K, Gao C. Graphene fiber-based asymmetric micro-supercapacitors. *J Mater Chem A* **2014**;*2*(25):9736–43.
259. Yu DS, Goh K, Wang H, Wei L, Jiang WC, Zhang Q, Dai LM, Chen Y. Scalable synthesis of hierarchically structured carbon nanotube-graphene fibres for capacitive energy storage. *Nat Nanotechnol* **2014**;*9*(7):555–62.
260. Guan TX, Shen LM, Bao NZ. Hydrophilicity improvement of graphene fibers for high-performance flexible supercapacitor. *Ind Eng Chem Res* **2019**;*58*(37):17338–45.
261. Yang ZB, Sun H, Chen T, Qiu LB, Luo YF, Peng HS. Photovoltaic wire derived from a graphene composite fiber achieving an 84.5% energy conversion efficiency. *Angew Chem-Int Edit* **2013**;*52*(29):7545–8.
262. Chen T, Dai LM. Macroscopic graphene fibers directly assembled from CVD-grown fiber-shaped hollow graphene tubes. *Angew Chem-Int Edit* **2015**;*54*(49):14947–50.
263. Chong WG, Huang JQ, Xu ZL, Qin XY, Wang XY, Kim JK. Lithium-sulfur battery cable made from ultralight, flexible graphene/carbon nanotube/sulfur composite fibers. *Adv Func Mater* **2017**;*27*(4):1604815.
264. Chong WG, Xiao F, Yao SS, Cui J, Sadighi Z, Wu JX, Ihsan-Ul-Haq M, Shao MH, Kim JK. Nitrogen-doped graphene fiber webs for multi-battery energy storage. *Nanoscale* **2019**;*11*(13):6334–42.
265. Cheng HH, Liu J, Zhao Y, Hu CG, Zhang ZP, Chen N, Jiang L, Qu LT. Graphene fibers with predetermined deformation as moisture-triggered actuators and robots. *Angew Chem-Int Edit* **2013**;*52*(40):10482–6.
266. Cheng HH, Hu Y, Zhao F, Dong ZL, Wang YH, Chen N, Zhang ZP, Qu LT. Moisture-activated torsional graphene-fiber motor. *Adv Mater* **2014**;*26*(18):2909–13.

267. Cheng HH, Liang Y, Zhao F, Hu Y, Dong ZL, Jiang L, Qu LT. Functional graphene springs for responsive actuation. *Nanoscale* **2014**;*6*(19):11052–6.
268. You X, Yang JS, Wang MM, Huh JB, Ding YS, Zhang XY, Dong SM. Graphene-based fiber sensors with high stretchability and sensitivity by direct ink extrusion. *2D Mater* **2020**;*7*(1):015025.
269. Zeng JF, Xu RY, Jiao L, Wang YZ, Chen LW, Windle CD, Ding XT, Zhang ZP, Han Q, Qu LT. A 3D-graphene fiber electrode embedded with nitrogen-rich-carbon-coated ZIF-67 for the ultrasensitive detection of adrenaline. *J Mat Chem B* **2019**;*7*(35):5291–5.
270. Seyedin S, Romano MS, Minett AI, Razal JM. Towards the knittability of graphene oxide fibres. *Sci Rep* **2015**;*5*(1):14946.
271. Li Z, Xu Z, Liu Y, Wang R, Gao C. Multifunctional nonwoven fabrics of interfused graphene fibres. *Nat Commun* **2016**;*7*(1):13684.
272. Horikiri S, Iseki J, Minobe M. Process for production of carbon fiber. Google Patents. No. 4070446, **1978**-1-24.
273. Dunbar J J, Tan C B, Weedon G C, Tam T Y, Cutrone A L, Bledsoe E S. Entangled high strength yarn. Google Patents. No. 5579628, **1996**-12-3.
274. Boucher EA, Cooper RN, Everett DH. Preparation and structure of Saran-carbon fibres. *Carbon* **1970**;*8*(5):597–605.
275. Nagasaka A, Ashitaka H, Kusuki Y, Oda D, Yoshinaga T. Process for producing carbon fiber. Google Patents. No. 4131644, **1978**-12-26.
276. Ashitaka H, Kusuki Y, Yamamoto S, Ogata Y, Nagasaka A. Preparation of carbon fibers from syndiotactic 1,2-polybutadiene. *J Appl Polym Sci* **1984**;*29*:2763–76.
277. Shindo A, Fujii R, Souma I. Producing method of carbon or carbonaceous material. Google Patents. No. 3427120, **1969**-2-11.
278. Kawamura K, Jenkins GM. A new glassy carbon fibre. *J Mater Sci* **1970**;*5*(3):262–7.
279. Santangelo JG. Graphitization of fibrous polyamide resinous materials. Google Patents. No. 3547584, **1970**-12-15.
280. Oya A, Yoshida S, Abe Y, Iizuka T, Makiyama N. Antibacterial activated carbon fiber derived from phenolic resin containing silver nitrate. *Carbon* **1993**;*31*(1):71–3.
281. Jiang H, Desai P, Kumar S, Abhiraman AS. Carbon fibers from poly (p-phenylene benzobisthiazole) (pbzt) fibers: conversion and morphological aspects. *Carbon* **1991**;*29*(4):635–44.
282. Newell JA, Rogers DK, Edie DD, Fain CC. Direct carbonization of PBO fiber. *Carbon* **1994**;*32*(4):651–8.
283. Krutchen C. Melt extrudable polyacetylene copolymer blends. Google Patents. No. 3852235, **1974**-12-3.

Kunming Li received his Master degree from Changchun University of Technology in 2020. He is a Ph.D. candidate in College of Materials Science and Engineering, Donghua University currently, under the supervision of Prof. Anqi Ju. His research interests focus on preparation and properties of phenolic resin-based carbon xerogels.

Xuepeng Ni received his Master degree from Donghua University in 2020. He is a Ph.D. candidate in College of Materials Science and Engineering, Donghua University currently, under the supervision of Prof. Anqi Ju. His research interests focus on preparation and application of carbon fiber papers.

Qianqian Wu Wu joined Donghua university as a master's student in 2020 under the supervision of Prof. Anqi Ju. Her research interest is preparation and application of electrocatalyst.

Chunshun Yuan is a graduate student at College of Materials Science and Engineering, Donghua University, under the supervision of Prof. Anqi Ju. Her research interest is Si anode for lithium-ion battery based on functionalized carbon nanofibers.

Changlei Li obtained Doctor of Engineering from Tiangong University. He is now working at Weifang Xinlong Biomaterials Co., Ltd. as the director of the Research Institute of the Technology Center. He is mainly engaged in the research development and production of functional regenerated cellulose fibers.

Dong Li joined Donghua university as a master's student in 2020 and has just started his doctoral study in 2022 under the supervision of Prof. Anqi Ju. His research interest is preparation and application of electrocatalyst.

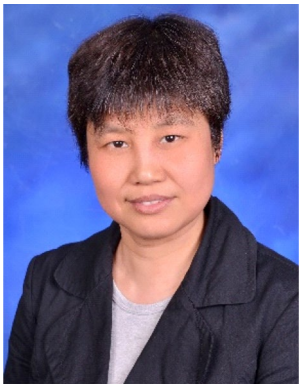

Huifang Chen is a researcher and professor of material processing at the School of Materials Science and Engineering, Donghua University. She is mainly engaged in the research of carbon fiber and carbon materials, especially in PAN-based, viscose-based carbon fiber and its precursors. She presided, participated in and completed more than ten scientific research projects, such as the State Science and Technology Commission, the Ministry of Science and Technology, the Natural Science Foundation, and the Aerospace Department.

Yonggen Lv received his Ph.D. from Institute of Coal Chemistry, Chinese Academy of Sciences. He now is a professor and researcher in Materials Science and Engineering, Donghua University, the Deputy Director, Key Laboratory of High-Performance Fibers and Products, Ministry of Education, Editorial board member of "New Carbon Materials", member of the polymer base branch of China Composites Society. He is mainly engaged in carbon fiber research including the development of mesophase pitch-based and polyacrylonitrile-based carbon fiber technology.

Anqi Ju received his Ph.D. from Donghua University; He now is a researcher and professor at the School of Materials Science and Engineering, Donghua University, secretary-general of the Reinforcement Branch of the China Composites Society, and a permanent member of the State Key Laboratory of Fiber Material Modification. He is mainly engaged in the preparation and industrialization of high-performance/ablation-resistant carbon fibers, and the preparation and properties of carbon fiber functional composites. He has participated in more than ten scientific research projects of the National Key Research and development Program.